International Telecommunication Union

ITU-R

Radiocommunication Sector of ITU

Report ITU-R M.2284-0
(12/2013)

Compatibility of radio-navigation satellite service (space-to-Earth) systems and radars operating in the frequency band 1 215-1 300 MHz

M Series

Mobile, radiodetermination, amateur and related satellite services

International Telecommunication Union

Foreword

The role of the Radiocommunication Sector is to ensure the rational, equitable, efficient and economical use of the radio-frequency spectrum by all radiocommunication services, including satellite services, and carry out studies without limit of frequency range on the basis of which Recommendations are adopted.

The regulatory and policy functions of the Radiocommunication Sector are performed by World and Regional Radiocommunication Conferences and Radiocommunication Assemblies supported by Study Groups.

Policy on Intellectual Property Right (IPR)

ITU-R policy on IPR is described in the Common Patent Policy for ITU-T/ITU-R/ISO/IEC referenced in Annex 1 of Resolution ITU-R 1. Forms to be used for the submission of patent statements and licensing declarations by patent holders are available from http://www.itu.int/ITU-R/go/patents/en where the Guidelines for Implementation of the Common Patent Policy for ITU-T/ITU-R/ISO/IEC and the ITU-R patent information database can also be found.

Series of ITU-R Reports

(Also available online at http://www.itu.int/publ/R-REP/en)

Series	Title
BO	Satellite delivery
BR	Recording for production, archival and play-out; film for television
BS	Broadcasting service (sound)
BT	Broadcasting service (television)
F	Fixed service
M	**Mobile, radiodetermination, amateur and related satellite services**
P	Radiowave propagation
RA	Radio astronomy
RS	Remote sensing systems
S	Fixed-satellite service
SA	Space applications and meteorology
SF	Frequency sharing and coordination between fixed-satellite and fixed service systems
SM	Spectrum management

***Note**: This ITU-R Report was approved in English by the Study Group under the procedure detailed in Resolution ITU-R 1.*

Electronic Publication
Geneva, 2014

REPORT ITU-R M.2284-0

Compatibility of radio-navigation satellite service (space-to-Earth) systems and radars operating in the frequency band 1 215-1 300 MHz

(2013)

TABLE OF CONTENTS

Page

1 Introduction 3

2 Applicable performance metrics 3

3 Assumptions 4

3.1 Radio-navigation satellite service 4

3.2 Radar 4

4 Protection criteria for radiodetermination radars 10

4.1 Protection criteria 10

4.2 Relation between acceptable interference level and radar performance 10

4.3 Consideration of statistical aspects of interference to radars from radio-navigation satellite systems 14

5 Simulation/estimation results 14

5.1 Time/amplitude characteristics of the global positioning system signals as viewed by a radar 14

5.2 Estimation of effect from interference caused by the GLONASS System on the performance of radiodetermination radars operating in the frequency band 1 215-1 260 MHz using alternative radar protection criteria 21

6 Radar/radio-navigation satellite service compatibility measurements 30

6.1 System 2 – Generic radio-navigation satellite service system test 30

6.2 System 5 – GALILEO/Compass test 33

6.3 System 5 – GALILEO/Primary Surveillance Radar Test 33

7 Technical and operational methods for reduction of interference to radars 34

7.1 Reduction of interference by techniques used by primary radar 34

7.2 Operational techniques using multiple systems 36

7.3 Characteristics of radio-navigation satellite service systems to improve compatibility with radar 37

7.4 Consideration of statistical aspects of interference to radars from radio-navigation satellite service systems 38

Page

Annex 1 – References 38

Annex 2 – System 2 – Generic radio-navigation satellite service system test 40

1 Description of long-range l-band radar 40

1.1 General description of the radar 40

1.2 Receiver processing 40

1.3 Antenna characteristics 41

2 Test set-up 41

2.1 Desired signals 41

2.2 Undesired signals 42

2.3 Live target tests 43

3 Test results 44

3.1 Simulated targets with single channel operation 44

3.2 Simulated targets with dual channel operation 44

3.3 Results of live sky tests 45

4 Conclusions 47

Annex 3 – Undesired signal calibration and IF selectivity 48

Annex 4 – Radar technical characteristics 49

Annex 5 – Radio-navigation satellite service system emission signal plots 50

Annex 6 – System 5 – GALILEO/Compass test 52

1.1 Description of radar/radio-navigation satellite service system interference test 52

1.2 Test set-up 52

1.3 Test data 55

1.4 Conclusions 66

Annex 7 – Calculation of probability of detection and probability of false alarm 66

Annex 8 – System 5 – GALILEO/Radar Test 68

1 System 5 – GALILEO/Radar Test 68

1.1 Description 68

2 Test set-up 69

2.1 Overview 69

Page

2.2 Characteristics of the used test equipment 70

3 Test results 80

4 Conclusion 82

1 Introduction

The frequency band 1 215-1 300 MHz is allocated to the radiolocation service, and some parts of the frequency band are allocated to the radio-navigation service on a primary basis. Prior to 2003, only the frequency band 1 215-1 260 MHz was shared with the radio-navigation satellite service (RNSS). An additional RNSS allocation in the frequency band 1 260-1 300 MHz was adopted at WRC-03 with conditions contained in RR No. **5.329**. This ITU-R Report summarizes tests and studies concerned with RNSS impact on radiolocation and radio-navigation radars in the frequency band 1 215-1 300 MHz.

2 Applicable performance metrics

The forms of performance degradation that could be inflicted on radars operating in the radio-navigation or radiolocation service fall into several categories:

– degradation of probability of detection (P_D);
– degradation of the track mechanism;
– generation of false target detections or the higher probability of false alarm (P_{FA});
– reduction in detection range;
– occurrence of extraneous strobes[1];
– loss in resistance to electronic countermeasures;
– harmful interference from adjacent radar sites due to the loss of available spectrum.

The first three effects can be thought of as a general decrease in probability of detection and an increase in probability of false alarms, respectively. However, the main reduction, in probability of detection, affects those targets at long ranges first. This is caused by a desensitization of the radar receiver and predominantly affects small, and/or distant targets.

The generation of strobes is based on methods and algorithms specific to each category of radars, not all radars are capable of producing strobes, and performance loss can occur at interference power levels below the selected threshold. False jamming strobes reduce the operator's ability to detect the presence of electronic countermeasures. Loss of spectrum reduces the radar's ability to avoid or reject jammers and increases the probability of interference with other users of the frequency band (possibly causing jamming strobes). Loss of spectrum also indirectly reduces the radar's probability of detection by reducing the number of independent target detections and reducing sensitivity due to a general increase in the noise floor.

[1] For the purpose of this ITU-R Report, strobes, jamming strobes, or search strobes all refer a radar system's function of indicating to an operator that the performance of the radar has degraded below an operator-selectable threshold.

3 Assumptions

3.1 Radio-navigation satellite service

The description of systems and networks in the RNSS and technical characteristics of transmitting space stations which are operating, or expect to operate, in the frequency band 1 215-1 300 MHz may be found in Recommendation ITU-R M.1787.

3.2 Radar

The characteristics and protection criteria for classes of radars operating in the radiodetermination service in the frequency band 1 215-1 400 MHz are listed in Recommendation ITU-R M.1463.

For each of these classes, models are needed which emulate the signal processing flow of these systems, which are considered in this section.

3.2.1 Receive signal model

The received signal is comprised of the target echo (if present), receiver noise, and RNSS interference. All signals are modelled after filtering and down-conversion using their respective equivalent baseband complex representations.

3.2.1.1 Noise

The noise is modelled as a complex zero-mean Gaussian process having variance:

$$N = \mathrm{k} T_s \mathrm{B} \tag{1}$$

where:

k: Boltzmann's constant (m^2kg/s^2K)

T_S: radar system noise temperature (K)

B: receiver filter bandwidth (Hz).

3.2.1.2 Radionavigation satellite service system signal

The total interference at baseband in the k-th channel due to N_{SAT} satellites operating within the radar field of view is given by:

$$I_{\text{Total},k}(t) = \sum_{\eta=1}^{N_{SAT}} I_{\eta,k}(\mathrm{t}) \tag{2}$$

where, $I_{\eta,\mathrm{k}}(t)$ is the RNSS interference signal from η-th satellite. The $I_{\eta,k}(t)$ are modelled using the complex zero-mean Gaussian process (independent of receiver noise) having variance:

$$Var\{I_{\eta,k}\} = P_{r,\eta} G_r L_{a,\eta}(\varphi,\theta) L_p L_{b,k}(f) \tag{3}$$

where:

$P_{r,\eta}$: incident power from the n-th satellite

G_r = receive antenna gain

$L_{a,\eta}$ = one-way beam-shape loss

$L_{b,k}(f)$ = portion of RNSS power in the k-th channel receiver band

L_p = polarization mismatch loss.

The maximum (that is, worst-case) RNSS power flux-density has been used in all simulations. The $L_{a,\eta}$ compensates for the loss in RNSS power when the satellite is not aligned to the peak of the radar's main beam. Note that a good approximation of the radar's antenna beam pattern is required to compute this value. The $L_{b,k}(f)$ accounts for the reduction in RNSS power due to bandwidth mismatch, where f is the centre frequency of the radar channel. This loss may be significant because RNSS spread spectrum signals typically occupy a much greater bandwidth than the radar receiver bandwidth. This reduction is directly related to the type of spreading waveform and can be estimated from proper modelling of the power spectral density of the RNSS signals. Finally, the polarization mismatch loss accounts for loss due to the mismatch between the radar receive polarization and RNSS signals polarization. For example, if a radar's antenna is vertically polarized and the RNSS signal is right hand circularly polarised (RHCP), then about 3 dB must be deducted to account for the mismatch between these two signals.

The noise and RNSS signals are independent complex zero-mean Gaussian processes, so their sum is a zero-mean Gaussian process with real and imaginary parts having equal variance given by:

$$\sigma_k^2 = \frac{1}{2}\left(Var\left\{I_{\text{Total,k}}\right\} + \mathrm{k}T_S B\right) \tag{4}$$

3.2.1.3 Target signal

The target (desired) signal level A^2 is calculated as:

$$A^2 = \frac{P_t G_t G_r}{(4\pi R^2)^2} \frac{\lambda^2}{4\pi} \frac{p_r \sigma_t}{L_a L_o} \tag{5}$$

where:

- P_t: transmit power
- G_t: transmit antenna gain
- G_r: receive antenna gain
- R: range to the target
- p_r: processing gain from pulse compression
- σ_t: target radar cross section (RCS)
- L_a: two-way beam-shape loss
- L_o: atmospheric loss.

3.2.1.4 Multiple beam processing

In case of detection based on data collected from multiple receive beams, the probability of detection is computed for each beam and the overall P_D is computed using the following equation:

$$P_D = 1 - \prod_{m=1}^{M} (1 - p_{D,m}) \tag{6}$$

where:

- $p_{D,m}$: estimated probability of detection in the m-th elevation beam
- M: total number of elevation beams in coverage.

3.2.1.5 Detection logic model

The understanding of the implemented detection logic model is critical in radar system impact study. In general, multiple constant false alarm rate (CFAR) tests are built into a typical radar system, all with the aim of keeping P_{FA} close to the desired value. The test against noise is considered for further discussion to determine interference impact relative to the noise. In practical implementation, the σ_k^2 are not known *a priori* and must be estimated. The estimate $\overline{n}$ used to set the CFAR threshold is given by:

$$\overline{n} = \frac{1}{2M}\sum_{k=1}^{2}\sum_{m=1}^{M} n_{k,m} \tag{7}$$

where $n_{k,m}$ denotes receive samples in *k*-th receive channel and *m*-th range bin obtained while the transmitter is off. The $n_{k,m}$ will sample both noise and RNSS interference. In this model, the noise-plus-interference is sampled at baseband prior to non-coherent integration so that:

$$E\{\overline{n}\} = \frac{\sigma_1^2\,\sigma_2^2}{2} \tag{8}$$

where $E\{\cdot\}$ denotes the expected value operator and the σ_k^2 are as previously defined.

The relationship between the noise variance and threshold value is related by P_{FA} which in turn depends on the radar signal processing. As a result, there will be different thresholds computed for linear and quadratic detection schemes. The estimate $\overline{n}$ directly influences the detection thresholds, and hence captures the impact of RNSS interference on P_D and P_{FA}.

3.2.2 Antenna models

3.2.2.1 Air route surveillance radar

The parameters used for the primary radar antenna system are a composite of those found in currently fielded Federal Aviation Administration (FAA) air route surveillance radar (ARSR). In particular, the rotation period was assumed to be 12 seconds and the main beam was modelled as shown in Figs 1, 2 and 3 with a peak gain of 34 dBic. This simplified main beam pattern was used to speed the simulation. Generally radar patterns include side lobes that decrease in amplitude with angular separation from boresight. First lobes are usually at least 20 dB below peak gain. In order to further simplify the simulation, RNSS signals coming in outside eight degrees from boresight were afforded gain in discrete steps as shown in Table 1.

FIGURE 1

Radar main beam antenna gain azimuth profile at elevation angles 0 and 20 degrees

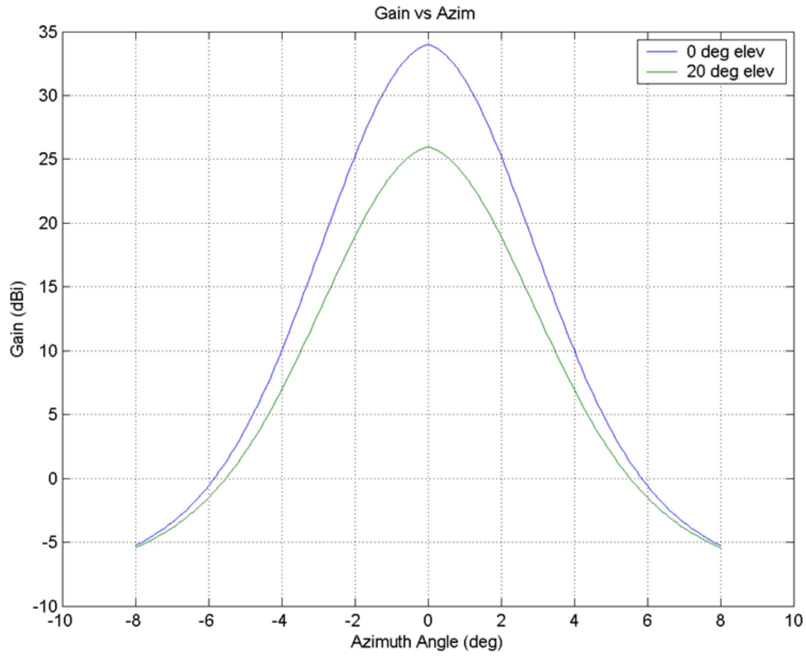

FIGURE 2

Radar main beam antenna gain elevation profile at 0 degrees azimuth angle

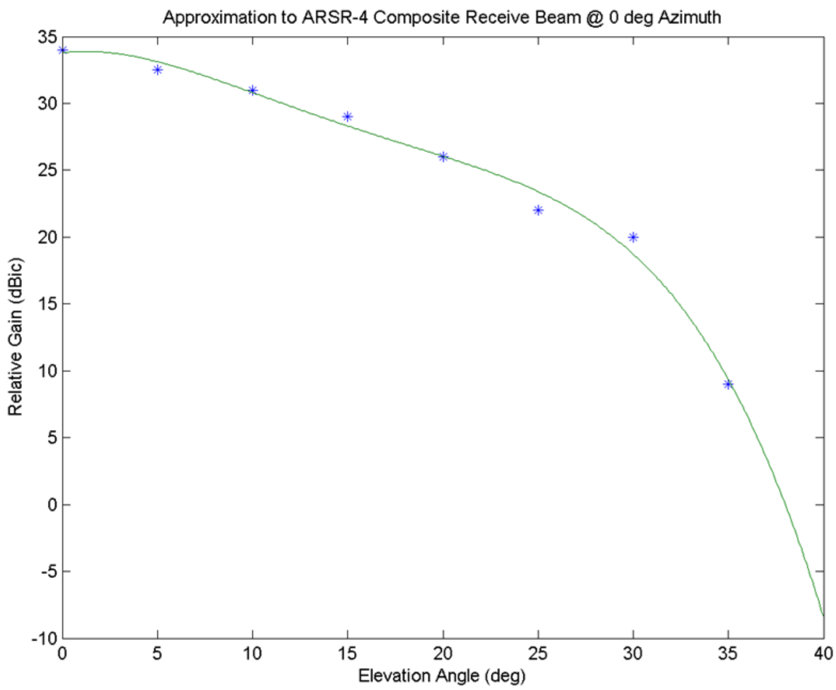

FIGURE 3

Modelled two-dimensional air route surveillance radar main beam gain pattern

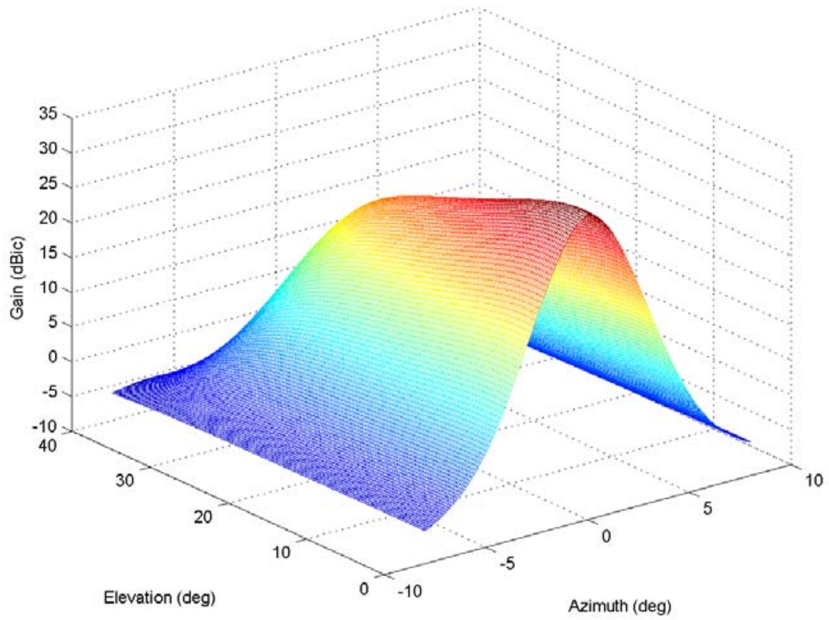

TABLE 1

Assumed radar antenna gain

Relative azimuth (θ) from bore sight (degrees)	Assumed radar antenna gain
$\theta \leq 8$	See Figs 1, 2 and 3
$8 < \theta < 30$	−6 dBic
$30 \leq \theta \leq 180$	−20 dBic

3.2.2.2 Air traffic control radar

A specific feature of aerodrome and en-route air traffic control (ATC) radars is a narrow antenna pattern in a horizontal plane. The pattern width is up to 2 degrees. Following expression of approximation of the ATC radar antenna pattern in the horizontal plane can be used:

$$G\begin{cases} G_{\max} - 2.5 \cdot 10^{-3}\left(\dfrac{D\theta}{\lambda}\right)^2, & 0 \leq \theta \leq 95\lambda/D \\ \max(G_{\max} - 25\log_{10}(\theta), -5), & \theta \geq 95\lambda/D \end{cases} \tag{9}$$

where:

- λ: operational wave length
- D: maximum antenna diameter
- $G_{\max}$: maximum antenna gain.

Figure 4 depicts an approximated radar antenna pattern in the horizontal plane. It is obvious that the pattern features a narrow main lobe of 2 degrees in width. The side-lobe levels are approximated as about −35 dB from the peak. The presented contribution estimates the radar antenna pattern in the horizontal plane using equation (9).

FIGURE 4

Air traffic control radar antenna pattern in the horizontal plane in the L2 frequency band

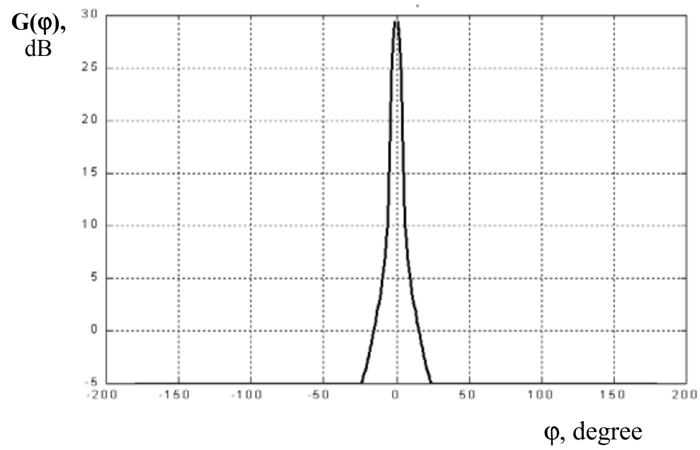

The ATC radar antenna pattern in the vertical plane is significantly wider as compared with that in the horizontal plane. Antennas with patterns approximated by $\mathrm{cosec}^2(\theta)$ are used most frequently. Also used are radar antenna patterns with narrow beams in the vertical planes. They are referred to as pencil-beam patterns. Combined antenna patterns are also used. Figure 5 depicts four types and shows the different antenna patterns.

FIGURE 5

Air traffic control radar antenna pattern in the vertical plane in the L2 frequency band

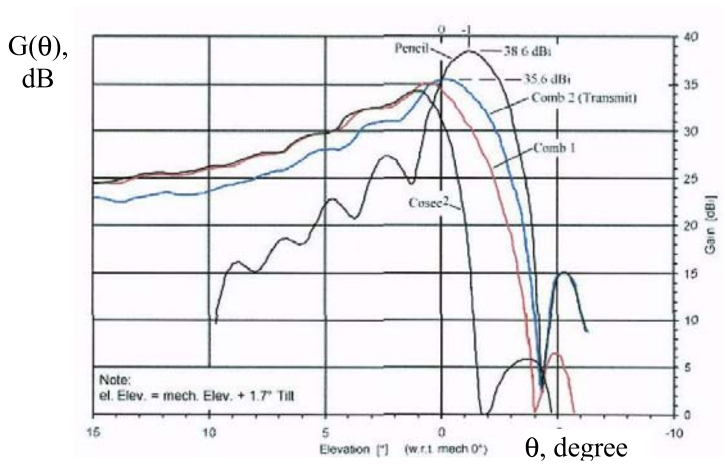

Analysis of the above plots shows that the antenna patterns are much wider in the vertical plane than in the horizontal one. For example the width of −3 dB pencil pattern is 6 degrees but for the other types of operational patterns it exceeds 10 degrees.

4 Protection criteria for radiodetermination radars

4.1 Protection criteria

Subject to Recommendations ITU-R M.1461 and ITU-R M.1463, in the case of continuous (non-pulsed) interference, an interference to noise (I/N) ratio of –6 dB should be used as the required protection level for the radiodetermination radars. In case multiple continuous sources of interference are present, this level represents the aggregate protection level.

This level of interference corresponds to increasing the ATC radar receiver noise temperature by 25%.

Alternative approaches to the above are presented in this Report. However, these approaches are applicable to case studies provided by administrations in their territories and should not be considered to supersede ITU-R Recommendations.

4.2 Relation between acceptable interference level and radar performance

Although not in ITU-R Recommendations, some administrations have indicated that another possible approach to use in their territories for RNSS interference is to use a carrier-to-(noise + interference) ($C/(N + I)$) protection criterion, coupled with a reduced service availability requirement, instead of the acceptable ratio of interference power I to noise power N. The proposed criterion takes carrier power level into account. It should be noted that rationale of the level permitted by the criterion has not been presented.

Under this approach, acceptable levels of $C/(N + I)$ ratio are discussed below. They were derived on the basis of reduced requirements for radar operation quality and current protection criteria. Primary indicators of radar operation quality are referenced to the assumed target detection (acquisition) probability P_D and P_{FA}. The above indicators are interrelated through such ratios as C/N, I/N or $C/(N + I)$. Particulars of such interrelations depend on different methods of signal reception and processing.

Two cases exist:

– operation of radars without optimal signal reception;

– operation of radars with optimal signal reception.

4.2.1 Radars without optimal reception of returned signal

For radars operating without optimal signal reception the correct detection probability P_D and P_{FA} are interrelated through the following expression:

$$P_D = P_{FA}^{\ 1/q} \tag{10}$$

where:

$$q = \frac{1 + C/N + (I/N)\rho^2}{1 + (I/N)\rho^2}$$

ρ: is interference and carrier correlation factor

C/N: is carrier-to-noise ratio

I/N: is interference-to-noise ratio.

Specified probabilities of detection P_D and P_{FA} provide for defining an acceptable value of $C/(N + I)$ using equation (10) and I/N = –6 dB, such as:

$$C/(N+I)=\frac{C/N}{1.25}$$

$$C/N=(\alpha-1)(1+0.25\rho^2)$$

where:

$$\alpha=\left(\log_{10}P_{fa}/\log_{10}P_D\right)$$

Table 2 shows acceptable values of $C/(N+I)$ for detection probability of $P_D = 0.9$ and false alarm probability of $P_{FA} = 10^{-6}$ with different values of interference/carrier correlation factor.

TABLE 2

Acceptable values of carrier-to-(noise + interference) for P_D = 0.9 and P_{FA} = 10−6 at different values of ρ

ρ	0	0.32	0.5	0.64	0.96	1.0
$C/(N+I)$, dB	20.17	20.28	20.44	20.59	21.07	21.14

Analysis of results presented in Table 2 shows that protection of radars operating without optimal signal reception as well as attaining the detection probability of $P_D = 0.9$ and false alarm probability of $P_{FA} = 10^{-6}$ require providing a sufficiently high level of $C/(N+I)$ ratio (from 20.17 dB to 21.14 dB subject to the interference and carrier correlation factors).

Moreover, variation of the correlation factor from 0 to 1 results in insignificant (by about 1 dB) increase in the acceptable $C/(N+I)$ ratio. Thus a conclusion may be drawn that selection of specific RNSS signal characteristics insignificantly affects a required $C/(N+I)$ ratio. The value of ρ = 0.32 is used hereafter.

4.2.2 Radars that use the burst of pulses

Studies were also conducted on the effect of a number of pulses in a burst at a threshold level of $C/(N+I)$ ratio which provides the specified probabilities of correct detection and false alarm. The studies were arranged for a case when a returned radar signal features no amplitude fluctuation. The threshold value of the $C/(N+I)$ ratio was defined using the following expression:

$$SNR=-5\log(M)+\left(6.2+4.52/\sqrt{M+0.44}\right)\log(A+0.12AB+1.7B) \tag{11}$$

where:

SNR: is a threshold level of carrier-to-(noise + interference) ratio

M: is a number of pulses in a burst,

$$A=\ln\left(0.62/P_{fa}\right),\ B=\ln\left(P_d/(1-P_d)\right)$$

The calculation results are presented in Fig. 6. Analysis of the results shows that increasing the number of pulses in a burst would result in reduction of $C/(N+I)$ ratio threshold level to 5.8 dB for $M = 8$ and it would be 13.6 dB for a case described by equation (10). It should be noted that most fielded radars in this band might not be capable of changing their operating parameters. Whether newer radars replacing them could be capable of making such adjustments requires further studies.

FIGURE 6

Carrier-to-(interference + noise) ratio as a function of a number of pulses in a burst

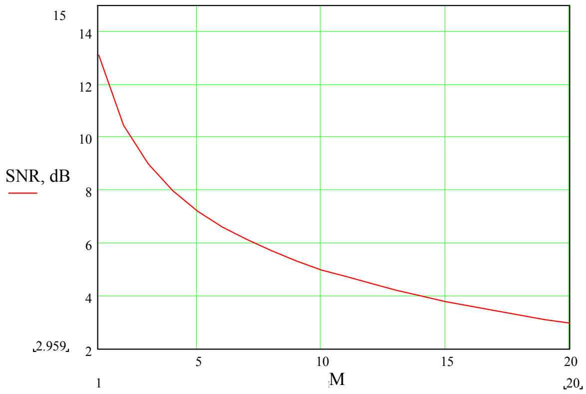

4.2.3 Radars with optimal reception of returned signals

Optimal reception is designed for improving the radar detection performances. It is based on employing correlators and matched filters.

The optimal reception is described with the following expression:

$$\left(\frac{C}{N_{tot}}\right)_{out} = \left(\frac{C}{N_{tot}}\right)_{inp} 2FT \tag{12}$$

where:

$$N_{tot} = I + N$$

F: is a frequency band occupied by a signal, Hz

T: is pulse duration in seconds.

Analysis of equation (12) shows that to improve $C/(N + I)$ ratio at a matched filter input it would be appropriate to use signals for which inequality of $FT >> 1$ is valid.

A matched filter and a correlator are known to operate with the same algorithm. However a matched filter is more preferable as compared with a correlator. It stems from the fact that voltage at a correlator output is defined by a signal autocorrelation function. The voltage is a function of delaying the reference signal triggering relative to the signal arrival moment δt. For certain value of the delay time the voltage at the correlator output would be zero in spite of a useful signal presence at the correlator input. In contrast, voltage is always present at a matched filter output when a useful signal is available at its input, though a certain delay $\delta t'$ exists.

When correlators or matched filters are used a threshold voltage level is defined by a specified false alarm probability as:

$$P_{fa} = \frac{1}{\sqrt{2\pi}\,\sigma} \int_{u_0}^{\infty} \exp\left(-\frac{u^2}{2\sigma^2}\right) du \tag{13}$$

where:

u: is voltage

u_0: is a threshold voltage

σ: is interference dispersion

P_{FA}: is false alarm probability.

Having defined a threshold voltage u_0 level using a specified P_{FA} from equation (13) a correct P_D could be derived as:

$$P_D = \frac{1}{\sqrt{2\pi}\,\sigma}\int_{u_0}^{\infty} \exp\left[-\frac{(u-s)^2}{2\sigma^2}\right]du \tag{14}$$

where:

s: received signal in voltage.

After simple transformation the following expression could be obtained:

$$P_D = \frac{1}{\sqrt{2\pi}}\int_{x_0}^{\infty} \exp\left[-\frac{(x-q)^2}{2}\right]dx \tag{15}$$

where:

q: is carrier-to-(interference + noise) ratio

x: u/σ.

Equations (13), (14) and (15) are derived assuming a "white noise"-like interference at the receiver input, i.e. the interference features a uniform spectral density at the receiver input to result in opportunity to derive the detection probability as a function of carrier-to-noise ratio at a fixed probability of false alarm.

An example is shown in Fig. 7 that delineates P_D as a function of carrier-to-(interference + noise) ratio for a false alarm probability of $P_{FA} = 10^{-6}$.

FIGURE 7

Probability of detection as a function of carrier-to-interference + noise ratio for a false alarm probability of $P_{FA} = 10^{-6}$

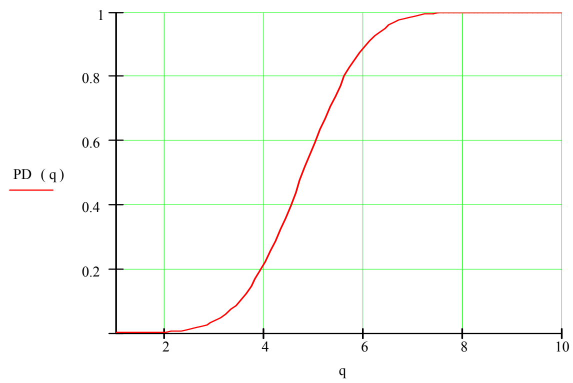

Values of q in Fig. 7 are non-dimensional. Analysis of the function shows that the value of carrier-to-(interference + noise) ratio should be of $q = 6.1$ (7.82 dB) to ensure a correct $P_D = 0.9$. Thus correlation processing or a match filter application would results in reducing a required value of carrier-to-(interference + noise) ratio by 12.4 dB.

The presented characteristic was derived for a single radar pulse. When a burst of M pulses is used a required carrier-to-(interference + noise) ratio could be additionally reduced in $\sqrt{M}$ times to result, however, in reduction of ATC radar resolution.

4.3 Consideration of statistical aspects of interference to radars from radio-navigation satellite systems

Assuming they could be met at the edge of coverage for minimum target cross-sections, the above protection criteria would provide for operation of the radiodetermination radars at specified P_{FA} and P_D values. Their employment would be appropriate for low mobile sources of long-term interference and for interference affecting a wide angle surveillance sector. At the same time each satellite of the RNSS systems causing harmful interference to the radiodetermination radars could be treated as a single-point interference sources moving in the sky. Therefore the radiodetermination antennas would be interfered with by any given satellite for a limited period of time at a particular azimuth. There are some instances when a RNSS satellite trajectory relative to the radar is along a near constant azimuth, in which case the interference could persist in the same azimuth up to one hour or more. Employment of the above radar protection criteria for 100% of a single radar's operation time would impose severe restrictions on the RNSS systems. Such severe requirements could be relaxed if it is assumed that it is allowed to avoid meeting the proposed protection criteria for a small time percentage, though this is not a usual approach for safety systems (see RR No. **4.10**).

In certain situations when the aircraft rate of change in range is less than change in cross-range, the effect from RNSS satellites on any particular radiodetermination radar azimuth would be short-term and can be predicted At any given instant, any RNSS satellite in view that is co-frequency/near-frequency to the radar will cause interference to that radar from the direction of the satellite. Even with numerous satellites per RNSS system, and numerous co-frequency RNSS systems, during the scan time a radar may experience interference from more than one direction, but not more than one satellite at any instant.

In a surveillance volume where the radar main beam, aircraft, and RNSS satellite signal sufficient to cause degradation in the probability of detection, the probability of detection of a particular aircraft under track will be reduced , but absent introduction of other interference sources (e.g. another satellite from another RNSS constellation) will recover after exiting the scenario to the pre-existing level. It is such a situation that features cases of peak interference and those of non-compliance with the protection criteria.

Taking the above into account and considering the discrepancy between the radar protection criteria of Recommendations and apparent successful long-term shared operation of existing RNSS systems and radars (though perhaps not co-frequency), it was proposed by some administrations to use an admitted percentage of time to exceed power criteria for interference in their territories.

Based on the estimates in § 4 for the current GLONASS system and for certain applications in some regions where 98% radar service availability meets operational requirements, the advanced radars employing chirped signals, matched filters, and correlators in the 1.2 GHz frequency band may tolerate the interference from GLONASS.

5 Simulation/estimation results

5.1 Time/amplitude characteristics of the global positioning system signals as viewed by a radar

5.1.1 Approach

The time/amplitude characteristics of global positioning system signals as viewed by a radar were used in a computer simulation that modelled (using Recommendation ITU-R M.1787) a representative RNSS constellation, and "flew it past" a modelled rotating primary radar antenna. Each "time step" in the simulation, power was summed for each satellite in view of the radar taking into account the respective radar antenna gain, satellite antenna gain, space loss, and interaction geometry.

In order to determine the *I*/*N* ratio, the following assumptions were made:

– Radar receiver bandwidth = 420 kHz. Since the interference was assumed to be on-tune to the radar, this results in about an 11 dB reduction in the received signal power.

– Radar receiver noise level = −143 dBW in a 420 kHz bandwidth. This value was based on System 1 as defined in Annex 1 of Recommendation ITU-R M.1463-2.

– Allowed losses in the antenna-to-receiver path are 4.1 dB. This value was based on System 1 as defined in Annex 1 of Recommendation ITU-R M.1463-2.

– The antenna assumptions provided in § 3.2 were used.

5.1.2 Sampling period

Due to the rapid rotation rate of the radar (5 rpm) relative to the slow movement of a satellite through the radar's swath, the time sample interval (i.e. simulation "time tics") must be chosen to be fairly small. For example, using an interval of 0.1 seconds means that the radar rotation will be sampled every 3 degrees, which is a little wider than the two-sided 3 dB beamwidth of the radar mainbeam. Unfortunately, increasing the sample period could result in under-estimating the maximum received power. Figures 8 and 9 show the results of running the simulation against the same RNSS/radar geometry using 0.20 seconds and 0.05 seconds time sample intervals, respectively. In each case, the simulation is run over a 15 minute period. A power measurement or 'blip' is received from the satellite at least every 12 seconds while the satellite is in the swath of the rotating beam. With a 0.05 seconds time step (1.5 degree angular step), several power measurements from a satellite can be received per scan; but for the coarser 0.20 seconds time step (6 degree angular step), no more than one strong measurement can be received per scan. Therefore a smaller sampling interval is needed to avoid underestimating RNSS impacts on the radar. As a compromise between simulation accuracy and simulation run-time, an interval of 0.10 seconds was chosen for the data analysis.

FIGURE 8

Received power, 0.20 second sampling interval

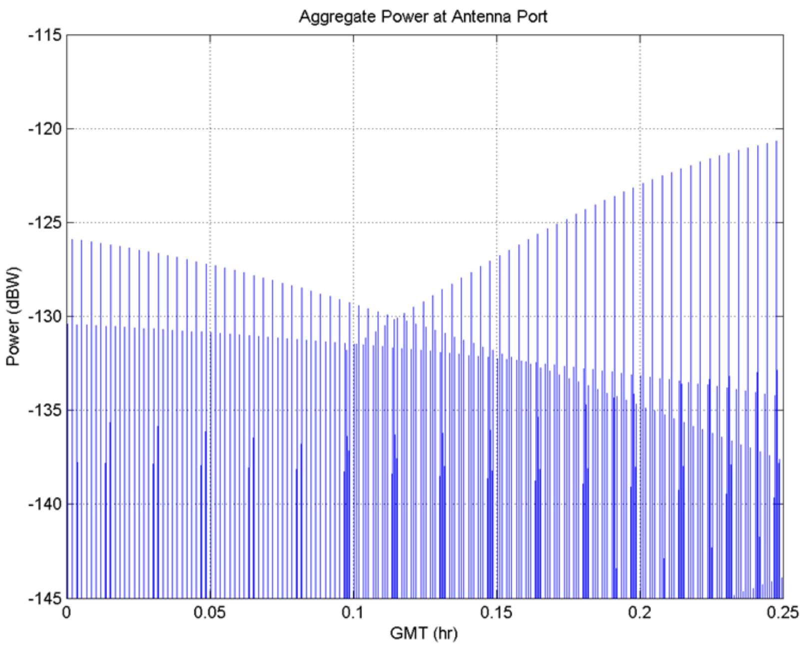

FIGURE 9

Received power, 0.05 second sampling interval

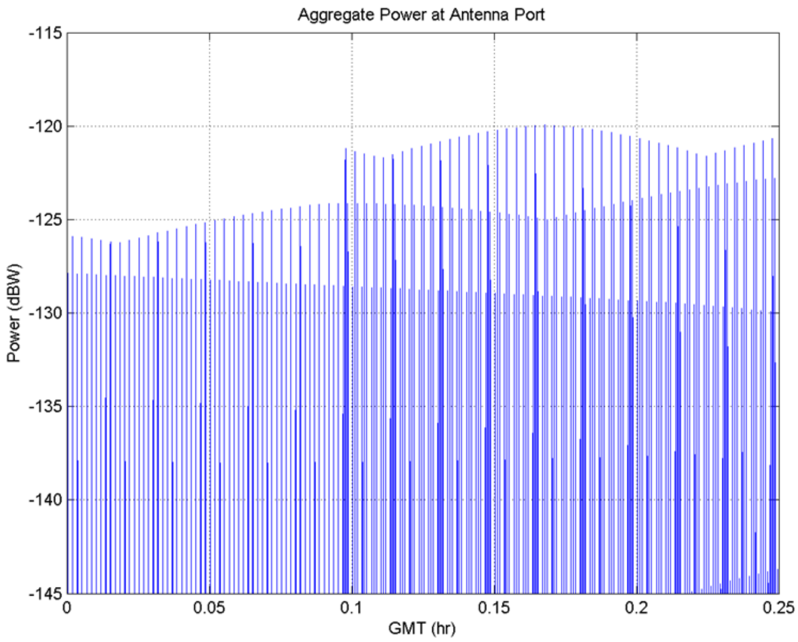

5.1.3 Results

Given the nature of the interaction – orbiting satellites being received by a rotating radar antenna – the perceived interference varied with time. In addition, time constraints precluded running the simulation over the full 3-day repeat cycle of the satellite orbits to determine worst-case conditions. Instead, for this initial analysis, four 1-hour periods were examined.

Figure 10 shows the aggregate received power for the first 60 min simulation period along each azimuth or radial. The power level shown is before the radar's 420 kHz bandwidth filter and before the antenna-to-receiver path loss, so as discussed above, a level of −128 dBW corresponds to an aggregate power level of 0 dB. There are 300 12-sec scans in the 60 min period, and as shown in the figure, only some of the radials are affected by the RNSS.

FIGURE 10

Aggregate power along radials for first 1-hr. period

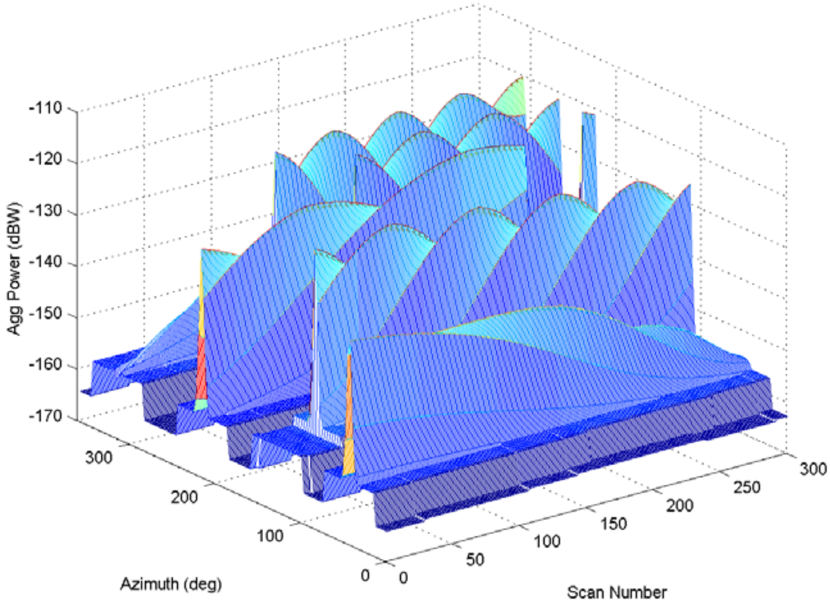

The simulation was also run over the next three hours in 1 hr. segments. The maximum aggregate power level of the full signal (i.e. before accounting for the reduced radar receiver bandwidth) observed in the total four hour time period was about −120 dBW. Additional observations:

5.1.3.1 Time vs. level for a single radial

Figure 12 shows the *I*/*N* ratio along one of the radials depicted in Fig. 11. The maximum *I*/*N* for this radial and 1 hr. time period is seen to be 8 dB, and the *I*/*N* level exceeds −6 dB – the current ITU-R radar protection criteria – for about 25 min of the 1 hr. period. This *time of occurrence* of the RNSS signal is fairly characteristic of the RNSS/radar interaction. Figure 11 shows a polar depiction of the percentage of time the RNSS level exceeds an *I*/*N* of −6 dB for that same 1 hour period. As one can see, the percentage ranges from zero for radials where no satellites were in view, to almost 60%. The maximum percentage of exceeding −6 dB *I*/*N* toward one radial over any one hour period, seen over the 4 hours simulated was just under 91%.

FIGURE 11

Percentage of time aggregate radio-navigation satellite service system exceeds −6 dB interference to noise ratio vs. radial angle

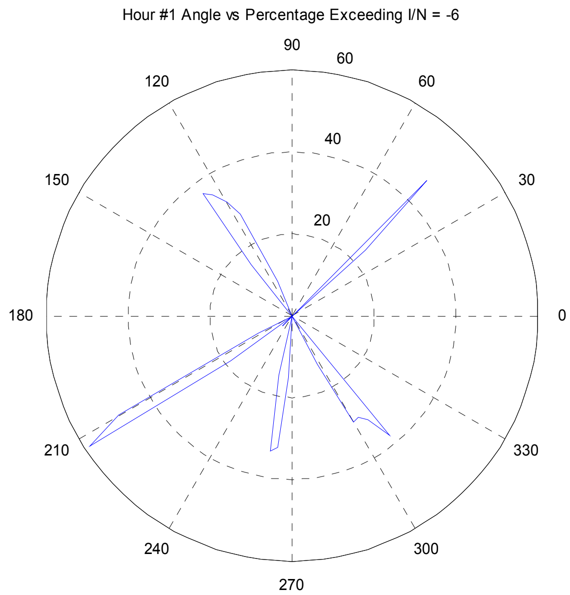

5.1.3.2 Time vs. interference to noise ratio for adjacent radials

As another example, Fig. 12 shows *I*/*N* along several adjacent radials in a different 1 hr window (the fourth hour). The radials are separated by 3 degrees. Again, *I*/*N* on each radial can be seen to exceed −6 dB during significant portions of the 1 hour period.

FIGURE 12

Interference to noise ratio along adjacent radials over a 1 hr period

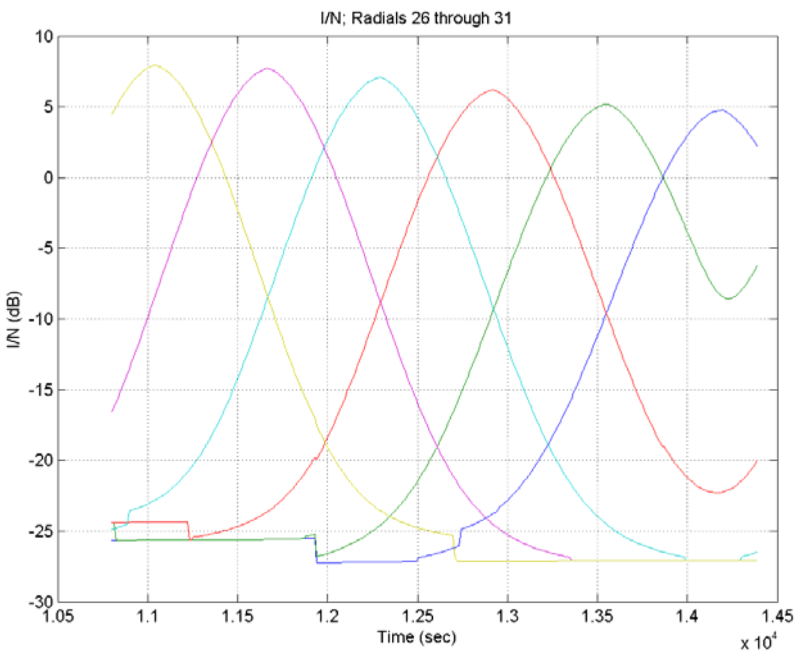

5.1.3.3 Multiple radials at a given time

On any given scan, there can be several radials affected by the global navigation satellite system, depending on which way the radar is pointed. For example, in Hour #3, scan #116, there is significant received power toward Radials 11, 30, 69, 83, 99, 15, 64, 75, 97 and 112 as shown in Fig. 13.

FIGURE 13

Interference to noise ratio for scan #116 of the third hour

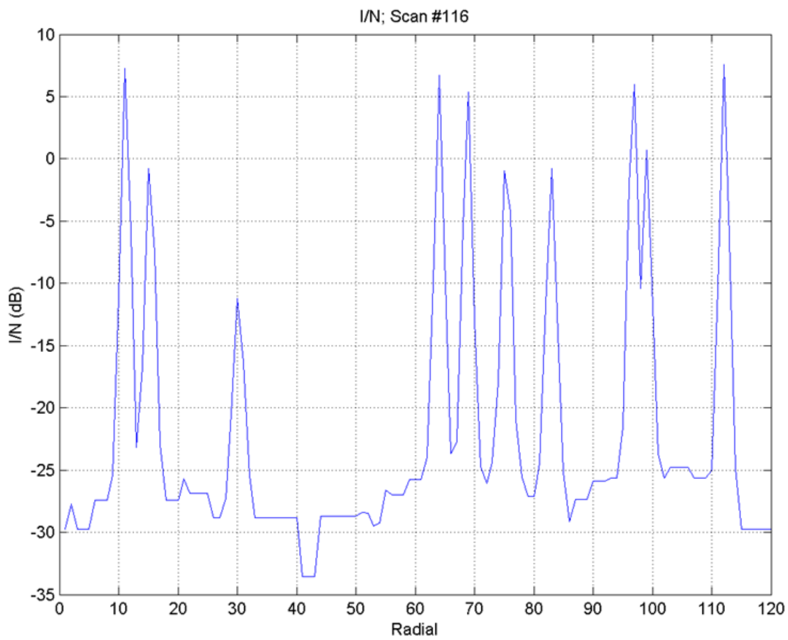

Figure 14 shows *I*/*N* vs. time for five of the affected radials in Fig. 13: Radials 11, 30, 69, 83, 99 between times 7 000 and 11 000 sec. Scan #116 occurs at time 8 580 sec, and is denoted with an arrow in Fig. 13. The *I*/*N* values at this time correspond to the *I*/*N* values for the corresponding radials shown in Fig. 13.

In combination, Figs 13 and 14 show that multiple radials in a scan can be impacted, and that each of those radials can be impacted for significant periods of time. The figures also show however that there are radials receiving very little RNSS interference during the simulation period. Figure 15 tries to provide perspective on the overall environment seen by the radar through the use of a cumulative distribution function relating the *I*/*N* seen by the radar to the percentage of time that *I*/*N* is exceeded. For hour #3 for example, an *I*/*N* of −6 dB is exceeded – toward some direction – about 9% of the time.

FIGURE 14

Interference to noise ratio vs. time for radials 11, 30, 69 83 and 99

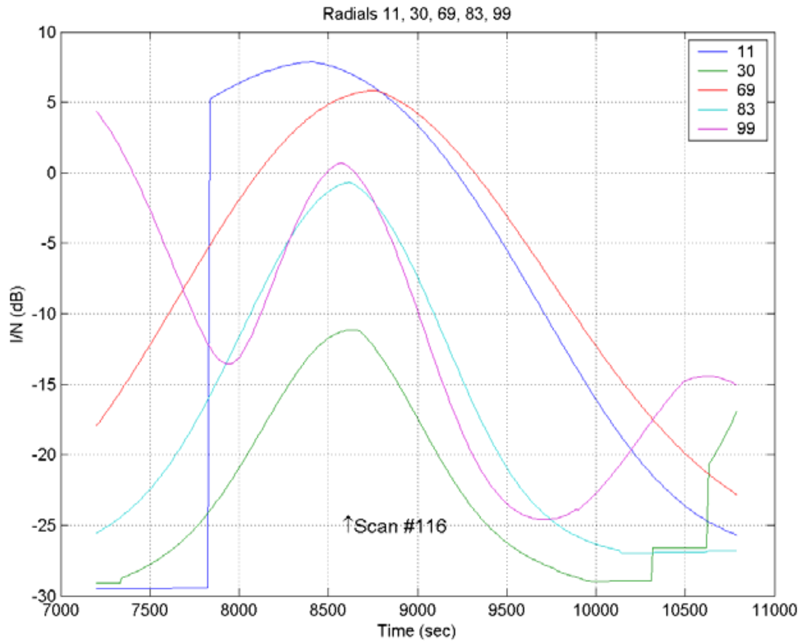

FIGURE 15

Cumulative distribution function of interference to noise ratio for hour #3

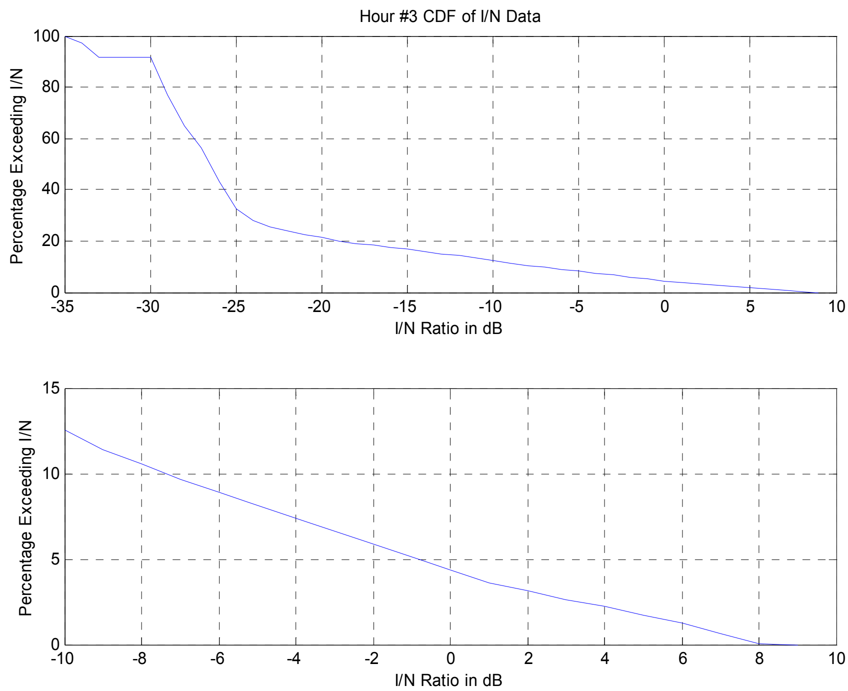

5.1.4 Conclusions using Recommendation ITU-R M.1463 radar protection criterion

This contribution provides results from simulations that take into account both the orbital motion of RNSS satellites and the rotation of a radar antenna using the indicated assumptions. The results for the assumed RNSS system have shown that interference exceeds the current ITU-R protection criteria in § 4.1 for significant periods of time. The operational impact of such interference needs to be determined on a case-by-case basis. This information should be taken into account in any studies of RNSS/radar compatibility, and utilized in characterizing undesired signals for any interference testing accomplished in support of that draft statistical studies work programme.

5.2 Estimation of effect from interference caused by the GLONASS System on the performance of radiodetermination radars operating in the frequency band 1 215-1 260 MHz using alternative radar protection criteria

An antenna model described in § 3.2.2.1 was used in the conducted simulation for which results have been analysed in the section under consideration. It should be noted that radar protection criteria beyond those in agreed ITU-R documentation are utilized for this section, and as such the results apply only in some administrations in their territories. In addition, for the purposes of this analysis, it is assumed that the only RNSS constellation is GLONASS.

5.2.1 Returned signal power level

The radar operation zone (detection distance) is defined by a minimal power of a returned signal (actual sensitivity) meeting the requirement of correct detection probability and false alarm probability.

Such a power may be estimated using equation (10) and I/N = –6 dB. Actual sensitivity of a receiver having a passband of 0.69 MHz would be −124.2 dBW for detection probability of $P_D = 0.9$, false alarm probability of $P_{FA} = 10^{-6}$ and correlation factor of $\rho = 0.32$. In the absence of interference the receiver sensitivity could be reduced to −127.7dBW and detection distance could be increased accordingly. Further increasing in receiver sensitivity while meeting the protection criteria (I/N = –6 dB) and maintaining a constant noise temperature would be inappropriate because a signal of power below −124.3 dBW would be received with probability below 0.9. It is obvious that extension of radar receiver operational bandwidth would result in deterioration of its sensitivity because equipment thermal noise power and that of acceptable interference would increase (Table 3). Enlargement of the passband from 0.69 MHz to 6.4 MHz would result in sensitivity degradation by 10 dB. The studies for radars with different passbands assumed appropriate values of minimum signal level as shown in Table 3.

TABLE 3

Radar receiver sensitivity as a function of operational bandwidth

Reception bandwidth, ΔF (MHz)	Interference I in the ΔF bandwidth (dBW)	Noise level in the ΔF bandwidth (dBW)	Signal level in the ΔF bandwidth (dBW)	Probability of detection
0.66	−151.6345572	−145.6345572	−124.4	0.900
0.69	−151.4415057	−145.4415057	−124.2	0.900
0.78	−150.8537257	−144.8537257	−123.65	0.900
1	−149.8299966	−143.8299966	−122.57	0.900
1.2	−149.0381841	−143.0381841	−121.8	0.900
2.5	−145.8505965	−139.8505965	−118.6	0.900
4.4	−143.3954698	−137.3954698	−116.15	0.900
6.4	−141.7681968	−135.7681968	−114.5	0.900

5.2.2 Interference situation simulation

Simulation of space stations assumed circular orbits and consideration of node precession in the equatorial plane due to irregular sphericity of the Earth. Such an orbital model presents satellite movement in the Earth-centred inertial reference.

Simulation of interference caused by the GLONASS system assumed a radar location in a point with assigned latitude. Estimations considered three probable points including those in the equator and at latitudes of 35° N and 70° N. The radar antenna rotates in the horizontal plane and could receive signals reflected from an aircraft in the angle sector of 0 to 360°. The antenna pattern of the simulated ATC radar features a narrow main lobe in the horizontal plane, the pattern being described by equation (9). The $\mathrm{cosec}^2(\theta)$-type antenna pattern is assumed for the vertical plane. Interference is caused by the constellation of satellites changing their location with time. That variation results in changing the power of aggregate interference received at the radar antenna from a fixed direction for different moments of time. Polarization isolation was not considered.

The studies simulated a scenario when an aircraft enters the ATC radar operation zone and moves towards the radar (aerodrome radar scenario). Scenario when an aircraft passes by the radar in its operation zone (en-route radar scenario) has not been considered because it would be knowingly better due to a narrower pattern of the radar antenna in the horizontal plane as compared with that in the vertical plane. The radar operation zone was assumed subject to actual sensitivity of the radar.

Detection probability estimates presented in the paper are associated with the worst case of carrier-to-noise ratio, i.e. for a moment when an aircraft is just entering the ATC radar operation zone. For other points in that zone the detection probability would be higher as compared with that presented in the given paper.

Effect estimation for interference caused by the GLONASS system to the ATC radar considered every probable route of aircraft flight. Simulation was performed for all azimuths with a step of 6 degrees.

Interference power at the radar receiver front end was estimated by summing up the power of interference caused at the radar receiver front end by each currently visible RNSS satellite, such as:

$$P_\Sigma = \sum_{i=1}^{N} P_i G_{Ri} G_i \lambda^2 \Big/ (4\pi R_i)^2$$

where:

- i: index of a specific satellite
- P_i: power transmitted from the i-th satellite
- N: a number of RNSS satellites visible from the ATC radar
- G_{Ri}: radar antenna gain in the direction of the i-th satellite
- G_i: the i-th satellite antenna gain in the direction of the radar
- R_i: a distance from the radar to the i-th satellite
- λ: operational wave length.

Interference power from separate satellites was summed up with consideration that different GLONASS satellites transmit navigation signals in different frequency bands. Note that this approach would not be appropriate for other RNSS constellations using CDMA waveforms. Power of signal produced by the i-th satellite in the passband of the radar receiver was defined as:

$$P_i = \int_{-B/2}^{B/2} S(f, f_i)\, df$$

where:

B: operational bandwidth of the radar receiver

S(*f,fi*): is transmitted signal spectral power density.

It is worth mentioning that the maximum aggregate interference caused by the GLONASS satellite constellation would be at 1 246 MHz. Therefore the estimations were conducted assuming that frequency.

The main stages of the studies are discussed below:

1) The first stage estimated compliance with the existing protection criteria of $I/N = -6$ dB considering the admitted interference time percentage of 2% as well as probability of detection at the boundary of the radar operation zone without optimal reception algorithms.

The C/(N+I) approach and interference protection based on 98% time availability are not supported by all administrations and some are of the view that it would not be appropriate for use in ITU-R studies concerned with sharing or compatibility with other services. For this purpose the distribution function for *I/N* was calculated for the assumed radar position and for each azimuth as well as the ratio levels corresponding to 2% of time ($_{2\%}$) were defined. Based on the obtained information, ratios of received interference power to receiver intrinsic thermal noise as a function of azimuth ($_{2\%}$)(φ) were plotted. Example of such relations is shown in Fig. 16 for different latitudes of deployed ATC radars with 0.69 MHz operation bandwidth. There, a red solid curve corresponds to a threshold $I/N = -6$ ratio and a blue dotted curve corresponds to ($_{2\%}$)(φ).

FIGURE 16

Examples of $_{2\%}$ ratios as a function of azimuth

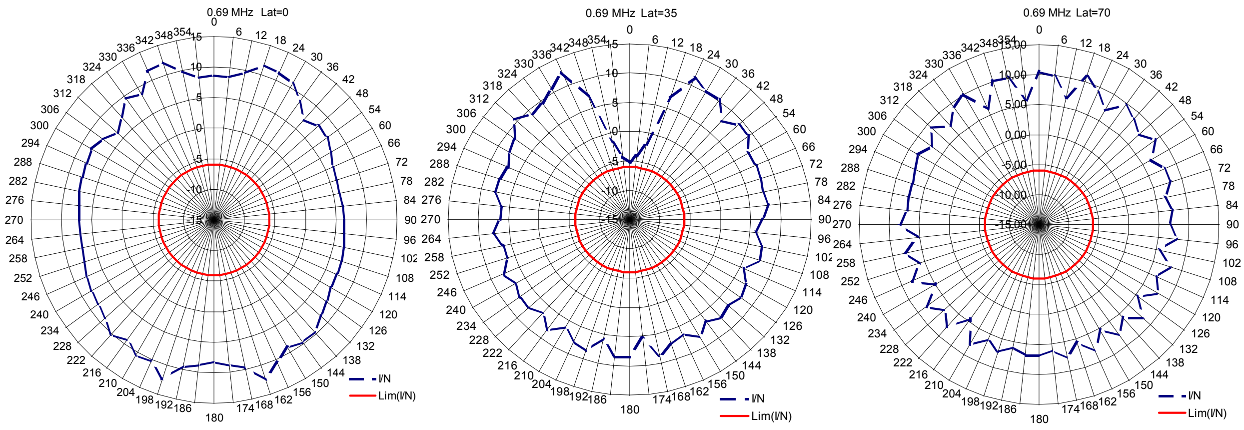

a) Latitude of 0 degrees b) Latitude of 35 degrees c) Latitude of 70 degrees

The top 2% of *I/N* levels are removed to produce Fig. 16. The blue line in the plot is the peak *I/N* that the radar will experience 98% of the time and for less than 2% of the time, *I/N* is greater than the blue line. These values are used as input to Fig. 17, which is the estimated probability of detection at the *I/N* levels of the blue line. The analysis shows that even when only using the resulting *I/N* that is not exceeded 98% of the time (i.e. omitting the top 2% of the interference), the radar cannot meet the required P_D of 90% in all radials.

Probability of detection at the boundary of the radar operation zone was defined for the obtained values of $I/N_{2\%}$. Estimations were conducted for radars without optimal signal reception based on equation (10) for false alarm probability of $P_{FA} = 10^{-6}$ and correlation factor of $\rho = 0.32$. Examples of estimates are shown in Fig. 17.

FIGURE 17

Examples of detection probabilities as a function of azimuth for radars without optimal reception

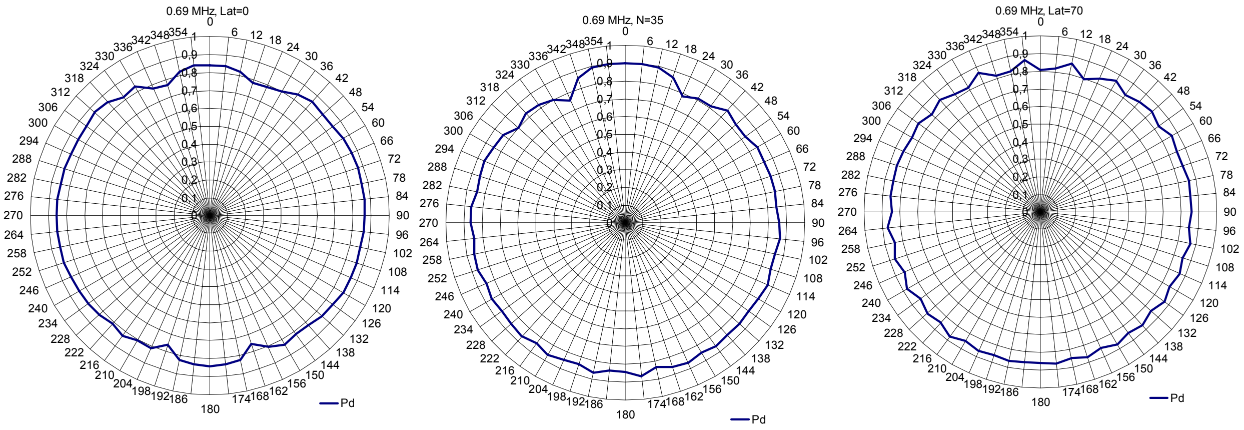

a) Latitude of 0 degrees b) Latitude of 35 degrees c) Latitude of 70 degrees

It may then be useful to investigate the impact past the IF-stage in the receiver of a radar system that utilizes chirped pulses with matched filters and correlators. This is the *(C/(N+I))* method that is used next in the analysis.

2) The second stage estimated the compliance with protective $C/(N + I)$ ratios proposed in § 4.1 in view of 2% admitted interference time percentage. Probability of detection at the boundary of the radar operation zone with optimal signal reception was also estimated.

For this purpose the distribution function for $C/(N + I)$was calculated for the assumed radar position and for each azimuth as well the ratio values corresponding to 2% of time ($C/(N + I)_{2\%}$) were defined. Based on the obtained information, ratios of ($C/(N + I)_{2\%}$)(φ) were plotted. Examples of such relations are shown in Fig. 18 for different latitudes of deployed ATC radars with a 0.69 MHz operation bandwidth.

Omitting the top 2% of *I/N* levels, Fig. 18 shows the results of *C/(N+I)* derived from the *I/N* of Fig. 16 and equations (10) and (12). Where the red curve is the required *C/(N+I)* of 20.28 dB without optimal signal processing techniques, the blue curve is the calculated $C/(N+I)_{2\%}$ (peak I after removing the top 2% of I), and the green curve is the required *C/(N+I)* of 7.82 dB with optimal signal processing techniques (matched filter and correlators). Since the calculated $C/(N+I)_{2\%}$ levels in all radials are greater than the required *C/(N+I)* of 7.82 dB with optimal signal processing techniques (radar processing gain here is particular to the GLONASS signals and the advanced radars), the detection probabilities approaches close to 100%, see Fig. 19, in all radials, meeting the required probability of detection of 90%.

FIGURE 18

Examples of $C/(N + I)_{2\%}$ ratios as a function of azimuth

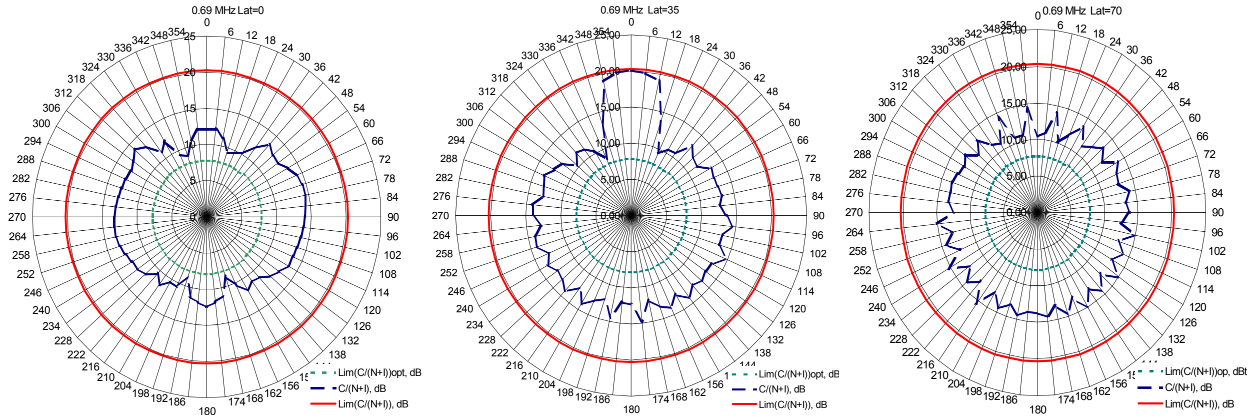

a) Latitude of 0 degrees b) Latitude of 35 degrees c) Latitude of 70 degrees

Estimations of detection probability at the boundary of the radar operation zone were conducted for radars with optimal signal reception based on equation (13) using the above obtained values of $C/(N + I)_{2\%}$ and for false alarm probability of $P_{FA} = 10^{-6}$. Examples of estimates are shown in Fig. 19.

FIGURE 19

Detection probabilities as a function of azimuth for radars with optimal reception

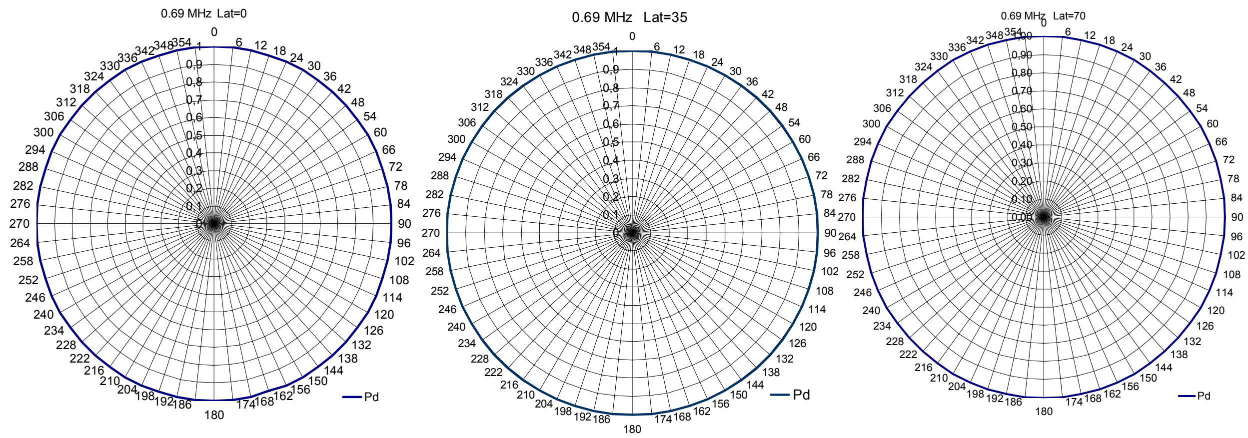

a) Latitude of 0 degrees b) Latitude of 35 degrees c) Latitude of 70 degrees

3) The third stage studied the effect of frequency tuning-off on detection probability.

4) The fourth and final stage dealt with the effect of optimal signal processing applications on variation in detection distance.

5.2.3 Analysis of simulation results

5.2.3.1 Analysis of estimates for *I*/*N* ratio and for correct detection probability

Analysis of the obtained results enables drawing a conclusion that the *I*/*N* ratio defined in an arbitrary (random) direction for a radar located on the equator would significantly exceed −6 dB for each considered frequency band of the ATC radar operation and for a selected radar antenna type. In line with that, probability of correct detection would be below 0.9, i.e. between 0.75 and 0.88. Extension of the operational frequency band would result in increasing the maximum correct detection probability. To that end, it would be of 0.85 for an operational radar bandwidth of 0.69 MHz and it would be of 0.88 for a radar with an operational bandwidth of 6.4 MHz. Figure 20 shows the correct detection probabilities as a function of azimuth angle of observation for three points of radar location and for all considered operational frequency bands. When an ATC radar location is moved to the north direction, the I/N ratio in the north sector features a reduction of interference caused by the GLONASS satellites, approaching the limits specified in Recommendations ITU-R M.1461 and ITU-R M.1463. That angle sector is adjacent to the north direction. Its size is a function of radar location latitude and the level of I/N ratio reduction is defined by radar operational bandwidth. Maximum reduction in I/N ratio occurs at radar location point which approaches the latitude of 35° N. In that sector the correct P_D approaches the required value of 0.9. With further shifting to the north the angle sector size decreases and the I/N ratio again exceeds the threshold level of −6 dB and the correct detection probability becomes below 0.9. When a radar is located in the point at latitude 70° N that sector disappears completely. Similar results could be obtained for shifting a radar location point to the south direction. Obviously, however, the radar location is driven by the function the radar is performing, and it cannot be arbitrarily sited and the analysis results could change for other RNSS constellations.

5.2.3.2 Results analysis for estimation of carrier-to-(noise + interference) ratio and correct detection probability with optimal reception of a returned signal

For some systems, the feasibility of improving the correct detection probability by using an optimal reception was also studied. Analysis of the obtained results shows that the $C/(N + I)$level exceeds the threshold level of 7.82 dB defined in § 4.2.3 for all considered plots. Probability of correct detection is within a range of 0.98-0.999 if a service availability of 98% meets the operational requirements of the radar. Thus application of optimal signal processing enables providing a specified correct detection probability for random points of radar location and azimuth of an appropriate signal. Figure 21 shows $C/(N + I)$ ratio as a function of azimuth observation angle for three points of radar location and for all considered operational frequency bands.

FIGURE 20

Correct detection probability of detection as a function of azimuth angle φ

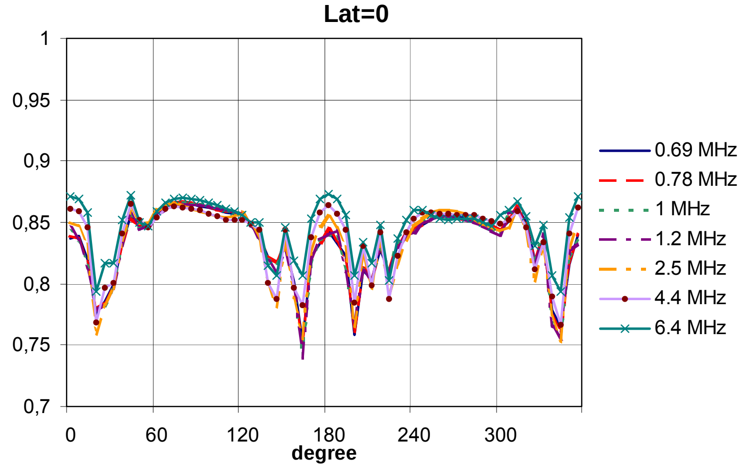

(a)

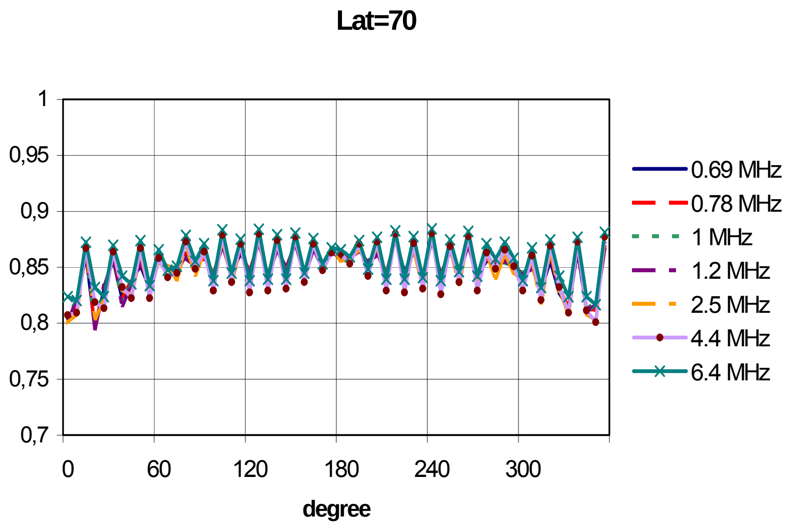

(b)

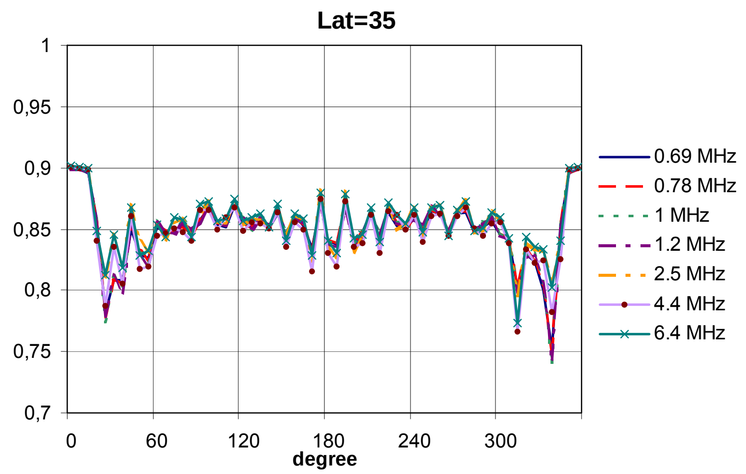

(c)

FIGURE 21

Carrier-to-(noise + interference) as a function of azimuth angle φ

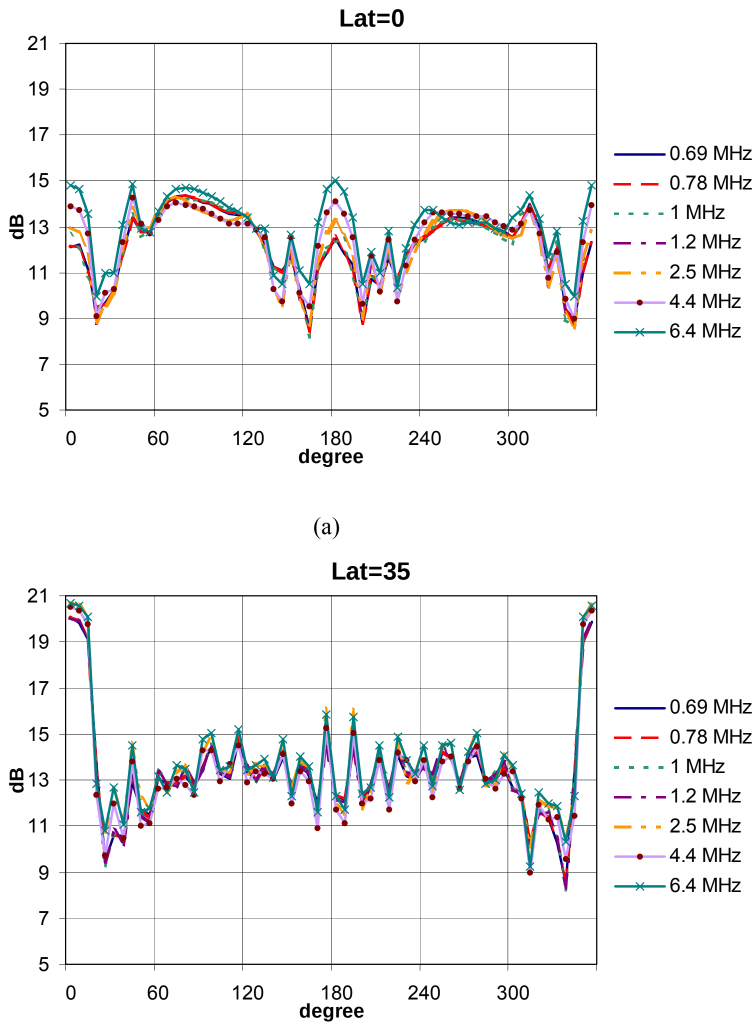

(a)

(b)

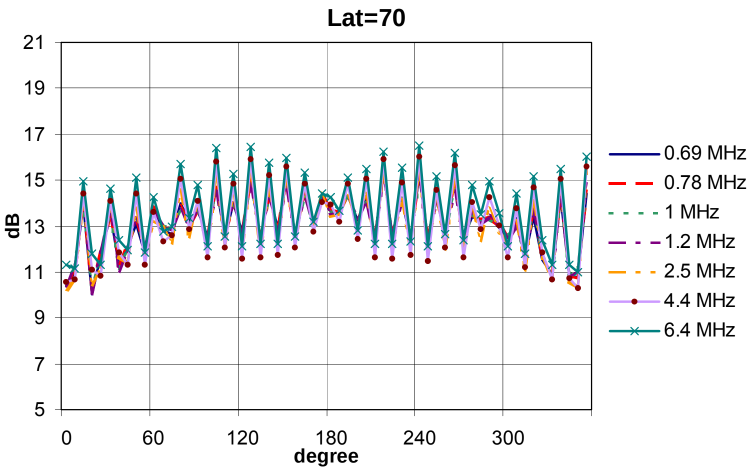

(c)

5.2.3.3 Effect of frequency tuning-out on correct detection probability

The effect of ATC radars tuning-out the worst 1 246 MHz frequency was also studied. For that purpose the interference effect on an equator located ATC radar operating at frequencies of 1 242.9375 MHz and 1 240 MHz in the bandwidth of 0.69 MHz was estimated.

It was determined that the *I*/*N* ratio values were much higher than the threshold level of −6 dB, as specified in Recommendations ITU-R M.1461 and ITU-R M.1463, for the 1 242.9375 MHz carrier. Accordingly, correct detection probability was below 0.9 when optimal processing was not used. Optimal processing ensures attaining the correct detection probability approaching to unity.

Operation at the 1 240 MHz frequency would result in significant reduction of interference power and *I*/*N* ratio. That ratio was found to be below the threshold level of −6 dB for a wide angle sector. It means that the correct detection probability would attain the level of 0.9 for all observation directions. Application of optimal processing enables increasing the correct detection probability up to unity.

It should be noted however that as the number of RNSS constellations increases, frequency-tuning may no longer be a viable approach.

5.2.3.4 Effect of optimal signal processing on detection distance

As it was mentioned above, detection (acquisition) distance is a function of radar pulse power, sensitivity and vehicle RCS. Detection distance was estimated for RCS of 5 m^2 (which is greater than the usual assumed 1 to 2 m^2 RCS), pulse signal power of 45 dBW, operational bandwidth of 0.69 MHz and correct detection probability of 0.9. It was shown that the maximum detection distance was 80 km without interference and without optimal signal processing. This is not acceptable for effective radar operation. It is obvious that the detection distance would decrease with increasing the power of interference.

Optimal processing of returned radiolocation signal would increase the distance of vehicle acquisition up to 170 km without interference.

Current aerodrome radar detection distance is usually specified at the level of at least 150 nm. It indirectly confirms the fact that such radars use optimal signal processing. Otherwise such radars would require a higher level of *I*/*N* ratio exceeding −6 dB to be in discrepancy with the current situation of successful sharing.

5.2.4 Conclusions

Analysis of the obtained results makes it possible to draw the following conclusions:

1) A radar operating in the frequency band used by the GLONASS system standard accuracy signals and employing no optimal signal processing could not ensure the correct detection probability of 0.9.

2) Optimal signal processing makes it possible to attain correct detection probability from 0.98 to 0.999 for random location of radars and observation azimuth, under GLONASS interference assuming a 98% radar service availability is acceptable and the particular advanced radars employing chirp signals, matched filters, and correlators.

3) The following criterion, not based on ITU-R Recommendations, was used for protecting the radars with optimal signal reception:
   – $C/(N + I)$ ratio at radar receiver front end may be below the threshold level of 7.8 dB for no more than 2% of time.

4) Signal waveform affects insignificantly (within 1 dB) the threshold levels of carrier-to-(interference + noise) ratio.

5) Tuning-out the worst-case frequency (operational radar frequency should not coincide with the frequency band used for transmitting the GLONASS system standard accuracy navigation signals) makes it feasible to attain the correct detection probability of 0.9 without optimal processing of returned signals.

6) Practically required radar detection distances (at least 150 km) for $I/N = -6$ dB and meeting the requirements on detection probability and false alarm probability could not be ensured without optimal signal processing or without usage of probing signals in the form of bursts of pulses. It indirectly confirms preferable operation of radars with optimal signal processing (employing chirp signals, matched filters, and correlators, resulting in high radar processing gain) and 98% service availability in order to tolerate the GLONASS interference.

7) Usage of M-pulse bursts. The method could improve carrier-to-noise ratio at the radar receiver front end although it would result in resolution deterioration.

8) Employment of received returned signal optimal processing.

9) Operation of double-frequency band ATC radars with one of the frequency bands beyond the frequency band 1 215-1 300 MHz.

6 Radar/radio-navigation satellite service compatibility measurements

6.1 System 2 – Generic radio-navigation satellite service system test

This test gathered data using a radar system similar to that documented as system 2 in Recommendation ITU-R 1463. The tests used targets and RNSS signals injected into the front end of the radar. It also includes an experiment where the effect of RNSS signals on live targets is evaluated. The detailed description of this test is in Annex 2 of this Report. The summary of test results is described below:

– The P_D of simulated radar targets (of the minimal acceptable RCS) for single channel operation was degraded by 0.15 (from 0.90 to 0.75) at $I/N = -6$ dB (current ITU criteria).

– The P_D of simulated radar targets (of the minimal acceptable RCS) for dual channel operation with interference on both channels was degraded by 0.10 (from 0.90 to 0.80) at $I/N = -6$ dB.

– This degradation appears to be statistically independent of the RNSS modulation type. Note however that all modulations tested were wider than the radar IF bandwidth. However, it is expected that the bandwidth of most RNSS signals will exceed the bandwidth of the radar receiver.

– The live sky tests showed that with an *I/N* of + 20 dB and a 10 Mbps interfering signal, the radar lost track of three identified targets near the edge of its coverage range. The radar also lost other targets within the wedge (closer to the radar), but they could not be identified before they exited the ATC Regional Centre's control.

– Live sky tests demonstrated the loss of targets by an L-band radar in the presence of RNSS interference, but do not provide quantitative data on target loss percentages. The hardline coupled procedures described in this section do provide such data.

Figure 22 below is an example of RNSS and a fixed channel radar (system 2) search strobes as a function of azimuth and UTC time, recorded from 12-14 March 2012. The thin lines of different colours represent the paths of respective RNSS satellites indicated in the legend of the plot. The thick lines outside the thin lines are the strobes experienced by radar system 2, where the search strobes can sometimes last up to 3 hours as in this example.

FIGURE 22

Radar system 2 search strobe as a function of azimuth angles and time

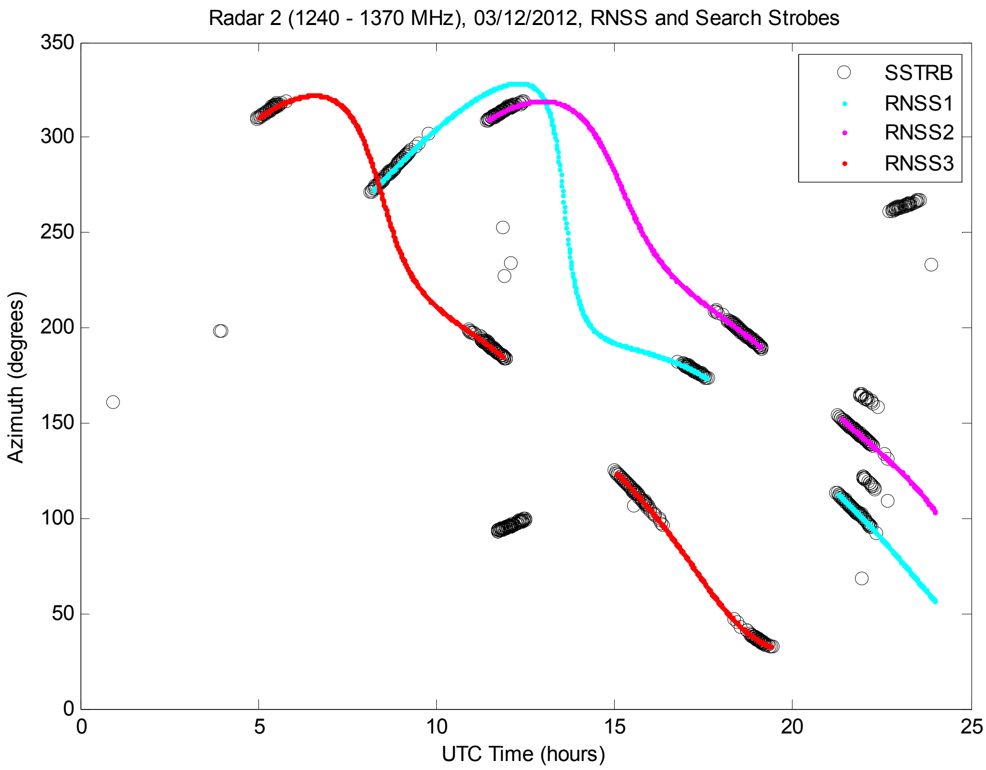

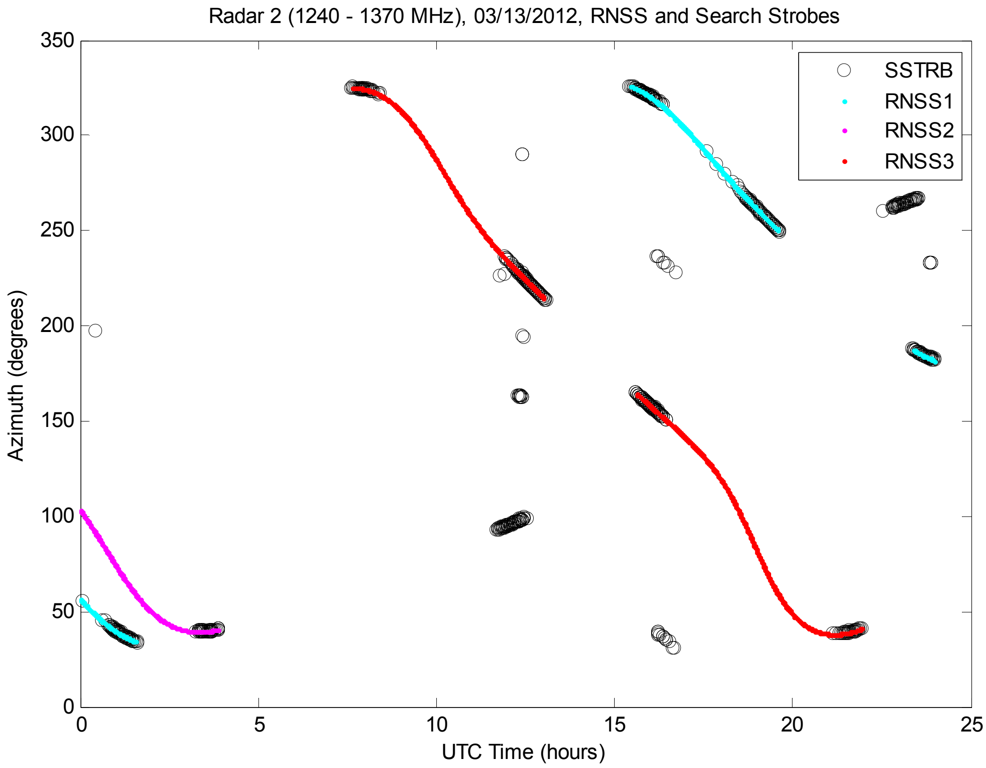

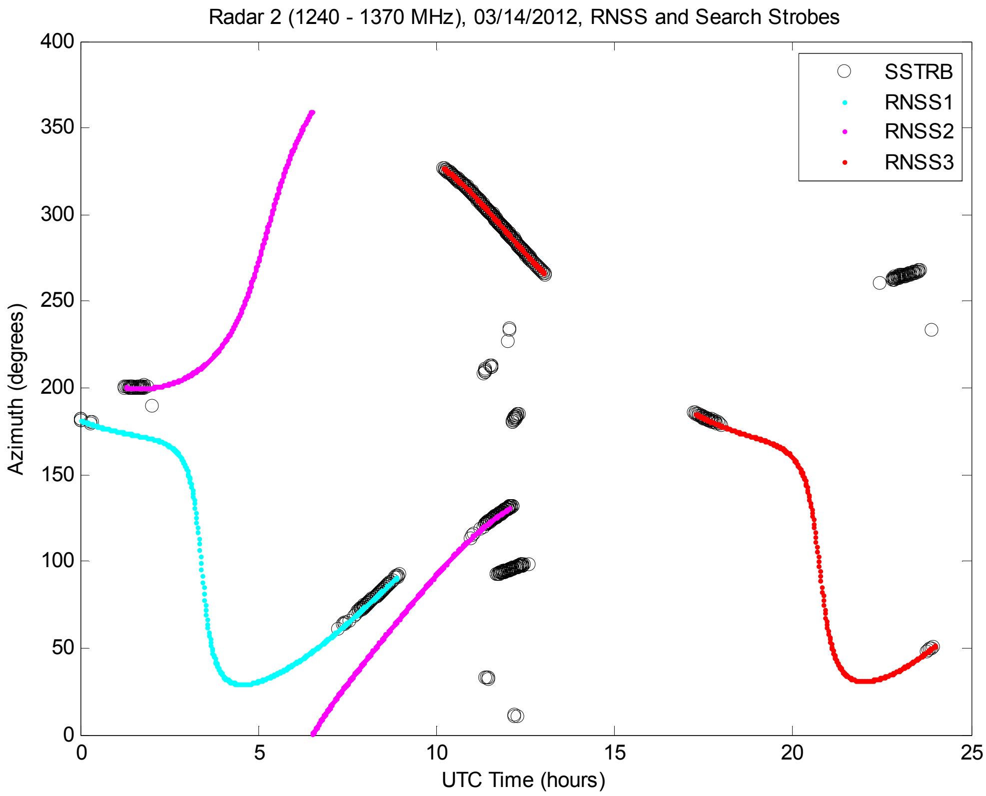

The observed strobes are caused by satellites from two different RNSS systems. It should be noted, however, that there are other radars in this category which will only observe strobes due to one RNSS network. Not all radars in this frequency band generate strobes, but lack of strobes does not necessarily indicate an interference-free environment, nor do they indicate an outage or full loss of detection in the affected radar beams. It is worth noting that, in some cases, the coverage areas of radars overlap to various degrees, reducing the radio frequency interference (RFI) impact as seen by any single radar in those cases.

6.2 System 5 – GALILEO/Compass test

A real-world radar/RNSS interference test was conducted utilizing radiated RF signals in May 2007. The radar used for this test is similar to those documented in Recommendation ITU-R M.1463 and is representative of a class of radars in general use for air traffic control at more than 160 locations worldwide. The objective of this test was to measure the interference effects introduced by the RNSS signals on radars operating in the 1 260 to 1 300 MHz frequency band. In particular, the test was aimed at quantifying the operational impact when an active radar target and RNSS signal source are both present in the radar's main beam, and the radar is utilizing a frequency near that of an RNSS satellite. The detailed description of this test is provided in Annex 6 of the Report. The summary of the test is as follows:

– The test-bed radar is equipped with a high gain antenna. Antenna 3 dB beamwidths are on the order of 2 degrees. This antenna produces a pencil beam that is steered in azimuth and elevation to cover an area 360 degrees in azimuth by approximately 20 degrees vertically. The radar's operational requirement specifies that it detect a reference target at 160 nmi with 0.8 probability.

– The results contains data gathered using a radar system similar to that documented in ITU-R 1463 system 5. It consists of a test completed using radiated targets and RNSS signals. It evaluates the relationship between I/N and P_D.

– Noise and interference testing indicate that Galileo E6 and Compass B3 signals are prominently visible in the radar receiver's intermediate frequency band and function to raise the radar noise floor. It is evident that the RNSS signal bandwidth is much greater than the radar's receiver bandwidth. It was also evident that at nominal RNSS signal levels the recommended −6 dB I/N ratio of Recommendation ITU-R M.1463 are exceeded. The measured data agrees with predicted results generated by an analytical model.

– The test further studied the relationship between I/N, P_D and P_{FA}. The result of these measurements is a complete data set that ties radar P_D to I/N as specified in the measurement methodology outlined in Recommendation ITU-R M.1461. Again, analytical modelling was used to verify the measured results, with measured and modelled data in agreement. The test showed impacts on P_D at higher I/N ratios, with an impact to P_{FA} under certain limited conditions. Further testing is recommended to fully understand these effects and quantify operational impacts.

6.3 System 5 – GALILEO/Primary Surveillance Radar Test

This section provides information about the performance and results of a representative compatibility measurement campaign between a signal transmitted by the European GALILEO system in the RNSS and the receiver of a Primary Surveillance Radar (PSR) operating in the radiodetermination service. The detailed description of this test can be found in Annex 7.

Main objective of the campaign was to determine in a most realistic configuration the sharing conditions of PSRs operating co-frequency with the E6-signals of the GALILEO system in the frequency band 1 260-1 300 MHz.

The measurement scenario was defined in line with the definition used as performance criteria in desktop studies for PSRs and radar expert considerations in ITU-R.

A further objective was to contribute to the determination of appropriate protection criteria for radar systems as some Administrations believe the present definition given by Recommendation

ITU-R M.1461 that the I/N must not exceed −6 dB may be too rigid and does not take modern radar processing capabilities and operational aspects into account. The campaign actually was based on an innovative approach to investigate the actual statistics of the radar under various grades of applied interference in a worst-case coupling geometry.

This section reflects data gathered using a radar system similar to that documented in ITU-R 1463 system 5. It consists of a test completed using radiated targets and RNSS signals. It evaluates the relationship between interference-to-noise ratios and probability of detection (P_D).

The used system, a RRP-117 (Remote Radar Post), manufactured by Lockheed-Martin Corp., is a NATO certified system operated in more than 120 sites in all six continents. The used radar is of Category 5 as defined in Recommendation ITU-R M.1463. It is also important to note that the IF-bandwidth of the radar receiver is less than about 3.5 MHz, which corresponds to a significant filter effect for the 40 MHz-wide GALILEO E6-signal.

The result of the compatibility measurements performed with the campaign is showed that Galileo E6 signal can degrade P_D from 100% to 75% at E6 power level of –122 dBm.

However, for a better comprehension of the results the conditions under which this behaviour may occur are repeated as follows:

The shown impact on radar performance can only occur under worst-case conditions, i.e. when:

1) the target is at the maximum instrumented distance of the radar;
2) the target has a radar cross section of 1 m^2 (e.g. size of a Cessna);
3) the target is in direct line of view with the GALILEO "satellite";
4) interference from other sources (transmissions from other radars, other services) is not present;
5) one satellite is in view. (*Note: Due to the constellation geometry only one GALILEO satellite at any time can be in view of the instantaneous radar beam. See § 2.2.*)

The statistical analyses show that the probability of occurrence of the worst case is predictable as to occur for less than 0.2% per 24 h-days or in absolute terms 173 sec/24 h.

7 Technical and operational methods for reduction of interference to radars

This section describes methods which can be used by radars operating in the frequency band 1 215-1 300 MHz to reduce the effects of interference from RNSS signals. They are techniques which have been or are being used to reduce interference from other sources.

7.1 Reduction of interference by techniques used by primary radar

Primary radar operation depends on receiving radar return signals of sufficient power to be detectable above the radar receiver's noise floor. One effect of noisy RFI, such as a phase shift keying (PSK) RNSS signal, is to raise this noise level. This can cause the target return to be less detectable and possibly lost.

Frequency management techniques and radar characteristics used to reduce or accommodate interference fall into five categories:

– frequency separation between radar and RNSS signals;
– frequency hopping and agility;
– high-gain receiving antennas and polarization;
– raising the power of radar transmissions; and
– data processing.

The characteristics of radars used to discriminate targets can also have the effect of reducing the impact of interference from RNSS signals.

7.1.1 Frequency separation and agility

By operating outside of the frequency band of a RNSS signal, it is possible for the radar to avoid interference. A variation of this is for a radar to simultaneously operate on multiple frequencies (frequency diversity), and that some of these frequencies operate outside of the RNSS. In either case, the radar may receive target returns, at some frequency, without RNSS RFI which may allow the radar to meet its performance objectives. Unfortunately, this frequency diversity technique will not work if the automatic gain control and adaptive threshold setting techniques for each channel are not independent of each other, or if the radar performance objectives require reception of all transmitted channels. With the expansion of RNSS, frequency separation may not be a viable interference mitigation technique if sufficient spectrum is not available for the operation of radars.

Some radars are capable of randomly hopping on discrete frequencies across the entire frequency band. However, radars that use frequency hopping as part of their operating characteristics face additional challenges in trying to avoid RNSS interference. Other radars employ a frequency-agility technique, which samples the spectrum to identify frequencies available for transmitting, based on undesired signals not exceeding the radar's noise threshold, and then transmits on those frequencies. Note that the use of this technology would require implementation of some form of coordination between adjacent radars to ensure they are not selecting the same frequencies. For the most part, such coordination does not currently exist between radar systems.

7.1.2 High-gain receiving antenna and polarization

The purpose of a highly directional antenna is to locate and position the target in space. The use of such antennas on ATC radars, however, can contribute to the reduction of the duration or occurrence of interference effects of RNSS signals towards any specific radar look angle. However, it increases the level of that interference when it is present.

High-gain antennas have a narrow main beam. An antenna's beamwidth is inversely proportional to its gain. Hence, at any single moment, the chance that both target and interferer are within the main beam of the radar is reduced as the antenna gain increases. However, RNSS RFI is increased by the antenna's gain, and can interfere with radar returns.

But away from the main beam, the RNSS RFI comes through antenna side lobes that act like weaker side beams to the antenna's main beam. So while the RNSS signal is now received much weaker than when in the main beam, target signals in the main beam are relatively stronger and detection is unaffected. However, when the RNSS signal and desired targets are in the main beam, or if signals received in the side lobes are of sufficient strength (e.g. due to the combination of factors such as strong RNSS signals, high radar side lobes, and/or simply the number of RNSS satellites "in view" to the side lobes), potential performance degradation may occur. However, it should be noted that use of high-gain antennas can be costly.

Another factor that might help in discriminating against some RFI is polarization. This technique is used to reduce the effect of clutter generated by weather however, is it usually not a normal operating technique and, for the majority of radars, can readily induce up to a 3 dB loss in received signal power. While some radars are capable of changing from a linear polarization to a circular polarization, most radars in this frequency band only do so for rain. If the radar transmits a RHCP signal, then it will receive a left-hand circular polarization signal. Current RNSS systems in the frequency band 1 215-1 300 MHz transmit RHCP signals. For side lobe reception and low elevation angles, RNSS RHCP signals can become depolarized into a more linearly polarized signal.

7.1.3 Target data processing algorithms

Use of target data processing capabilities is a function available for controllers to use on some radars. It is the controllers' decision as to whether or not to use such data processing information. Such information lets the controller know that the radar did not detect the target, but may suggest a possible target position. Such a technique is not presently used in conjunction with the radars mentioned earlier. If data processing algorithms were implemented, it may help radar operators when RNSS interference is present. It does so by indicating where missed targets were expected to be found and relieving operators of the burden of estimating the position of lost targets. However, target date processing algorithms in general are unique to each type of radar and are not based on the characteristics of undesired signals.

Target data processing algorithms are post-detection signal processing techniques that extrapolate target data to estimate future target detections, increase sensitivity for expected targets, and cause targets that have dropped detections to persist for a few more antenna scans. It is important to note that this technique does not mitigate the effects of the interference on target detection, and depending on the operational requirements of the radar it may not mitigate that interference or improve compatibility.

Modern radars use Doppler processing and a variety of techniques to determine the velocity as well as the range of a moving target.

It is necessary to conduct further studies to identify the data algorithms used in the radio-navigation radars and compare the number of scans that the track is maintained to the number of scans the RNSS satellites are in the radar main beam.

7.1.4 Additional radar transmitted power

Increasing radar-transmitted power directly increases the power of return signals. This, in turn, increases the signal-to-noise ratio at the radar detector and increases the probability of detection of any target. While this can be used to overcome the effect of RNSS RFI, this approach is not necessarily available to all radars either due to technical limitations or spectrum assignment constraints. However, since some radars operate at power levels below the sustainable maximum power, it can be used to mitigate RNSS RFI. Unfortunately, increasing power will usually have a small effect at best since most radars cannot increase their transmit power by more than a couple decibels if at all.

Even if it is possible to increase transmitted power, the increased cost may be prohibitive. Besides the additional increase in cost of the supplied power, there is also the additional cost of hardware. In particular, running at higher power usually entails either more components; e.g. additional power amplifiers, or running existing transmitter components at higher power. In the former case, there will be the cost of additional components. In the former case, running components at higher power usually shortens their life expectancy that, in turn, means higher maintenance costs.

7.2 Operational techniques using multiple systems

The following are operational factors that can assist an ATC system in monitoring aircraft in the event a primary radar can no longer track aircraft in some part of its service volume.

7.2.1 Use of beacons

Secondary surveillance radars are used extensively to monitor the progress of aircraft through the airspace. They also provide aircraft identification information. The beacons operate outside of the RNSS frequency bands and therefore are not susceptible to interference from RNSS signals. However, primary radar coverage must be maintained since beacons are cooperative systems that can be disabled accidentally or intentionally. While use of beacons can assist in identifying cooperative targets, they do not meet the needs of government requirements that must detect and track non-cooperative targets.

7.2.2 Overlapping coverage

Some radars have overlapping coverage. To avoid interference between radar systems within interference range of each other, the radars use different frequencies. Consequently, depending on the RNSS system design, two radars looking at one target may not both have interference from the same RNSS systems at the same time. Hence, one of the radars may be able to detect the target without RNSS RFI from the same satellite.

Again, this is not done for the purpose of mitigating RNSS RFI, but rather to minimize the impact during a radar outage and provide smooth operational performance. However, it could have the positive consequence of reducing the impact of interference from RNSS signals, depending on who is responsible for controlling that aircraft.

It should be noted that this technique works best at higher altitudes where radar line of sight coverage is the greatest. At lower altitudes, overlapping coverage is less likely, but target visibility is limited by the Earth's curvature and ground obstructions. Hence radar range for lower elevations is necessarily shorter, and, since received signal power increases inversely to the fourth power of the target range, may impact target detection more than RNSS RFI.

7.3 Characteristics of radio-navigation satellite service systems to improve compatibility with radar

The effectiveness of many of the approaches described below depends on the characteristics of the radars operating in the frequency band, so an RNSS system design should include an understanding of the affected radar systems.

7.3.1 Radio-navigation satellite service systems signal power

RNSS signals do not generally very much in the total signal power, from a single satellite, since many RNSS receivers have omnidirectional antennas and some need as much as 34 dB·Hz of carrier-to-noise ratio in order to acquire any one RNSS signal. Once a signal is acquired, the needed level also varies with the bit rate of a signal's data. However, an RNSS signal's power spectral density (PSD) can and does vary in an inverse relation to the signal's bandwidth. RNSS signal power should be limited to augment compatibility with radar services. It should be noted that higher data rates in RNSS signals might necessarily require an increase in RNSS signal power.

7.3.2 Radio-navigation satellite service systems signal bandwidth

RNSS signals vary in their bandwidths according to their intended use. A signal intended purely for signal acquisition may not carry data and require little or no data bandwidth. However, many RNSS signals broadcast navigation data and employ some kind of code-division multiplexing which requires coding bandwidth on the order of 2 to 20 MHz. (The bandwidth is double the bit rate of the code, and such signals have co interference proportional to the inverse of the code's length.)

The advantage to increasing bandwidth is because power spectral density (PSD) can be lowered. However, widening bandwidths opens RNSS receivers to more noise as well, and a wider signal shares more with non-RNSS systems too. The advantage of narrowing a signal's bandwidth is that it shares less of its frequency band with other systems. However, the PSD of a signal increases as the bandwidth decreases, the peak PSD is higher, and sharing with co-frequency systems becomes more difficult.

7.3.3 Pulsed radio-navigation satellite service systems signals

Radar systems generally have an innate ability to reject some interference from pulses dissimilar to their own. Pulsing RNSS signals is feasible, but likely to be impractical. The major difficulty is that some RNSS users track carrier phase, and, due to the difficulty of building RNSS transmitters that maintain phase-coherence from pulse to pulse, this would be technically difficult. In addition, differential-RNSS methods could not be used with pulses short enough to avoid interfering with radar systems. Current RNSS systems will also have major power problems with providing pulsed power. Indeed, some RNSS satellites are designed with power amplifiers intended to provide a constant power output. These amplifiers are much more efficient and reliable than the linear amplifiers needed for pulse.

7.4 Consideration of statistical aspects of interference to radars from radio-navigation satellite service systems

RNSS systems which have the potential to cause harmful interference to radiodetermination radars could be treated as single-point interference sources moving in the sky. Under this assumption the radiodetermination antennas would be interfered with for a limited period of time at each azimuth of their pattern. Some studies have shown that the effects from RNSS systems on radiodetermination radars would be of a short-term and predictable nature due to the high selectivity of radar antenna in azimuth, the continuous changing in position of radar antenna main lobe direction and that of a craft under tracking, and variation of positions of interfering RNSS satellites.

Annex 1

References

1. Recommendation ITU-R M.1787-1 – Description of systems and networks in the radio-navigation-satellite service (space-to-Earth and space-to-space) and technical characteristics of transmitting space stations operating in the bands 1 164-1 215 MHz, 1 215-1 300 MHz and 1 559-1 610 MHz.

2. Recommendation ITU-R M.1463-1 – Characteristics of and protection criteria for radars operating in the radiodetermination service in the frequency band 1 215-1 400 MHz.

3. Document 8B/28 – Use of statistical and operational aspects in the radar’s protection criteria. France contribution, November 2003.

4. Document 8B/57 – Methods to enhance compatibility between radars and RNSS signals in the 1 215-1 300 MHz band, U.S.A, August 2004.

5. Document 8B/59 – Time/amplitude characteristics of RNSS signals as viewed by a radar, USA contribution, August 2004.

6. Document 8B/60 – Results of interference susceptibility tests of a 1 250-1 300 MHz band aeronautical primary radar system radar with RNSS signals, USA contribution, August 2004.

7. Document 8B/71 – Work programme on radar protection criteria, France contribution, August 2004.

8. Document 8B/72 – Proposed new preliminary draft new Report on RCS fluctuation impact, France contribution, August 2004.

9. Document 8B/81 – Estimation of effect from interference caused by the GLONASS system on performance of radiodetermination service radars operating in the 1 215-1 260 MHz frequency band, Russia contribution, August 2004.

10. Document 8B/228 – Revision of WD 8B/57, USA contribution, September 2005.
11. Document 8B/232 – Working document on studies to evaluate the compatibility between RNSS and radars in the band 1 215-1 300 MHz, USA contribution, September 2005.
12. Document 8B/292 – Preliminary elements regarding the Resolution 608 which deal with RNSS in the band 1 215-1 300 MHz, France contribution, September 2005.
13. Document 8B/370 – Proposed revisions to the working document towards a preliminary draft new Report on studies regarding the impact of the radio-navigation satellite service into radiodetermination services systems receiver, March 2006.
14. Document 8B/481 – Proposal for a preliminary draft new Report ITU-R, Russia contribution, August 2006.
15. Document 8B/489 – Potential technical issues with aviation use of RNSS service links in the 5 GHz band, USA contribution, August 2006.
16. Document 8B/588 – Proposal for a preliminary draft new Report ITU-R, Russia contribution, May 2007.
17. Document 8B/600 – Data requirements, techniques, and factors which contribute to the satisfactory operation of radars and RNSS in the band 1 215-1 300 MHz, USA contribution, June 2007.
18. Document 8B/602 – RNSS interference into radars, UK contribution, June 2007.
19. Document 8B/621 – Results of measurements related to the impact of the GALILEO RNSS into radars operating in the radiolocation service in the 1 260-1 300 MHz band, Germany contribution, June 2007.
20. Document 5B/12 – Working document toward development of a methodology for assessing radar performance in the presence of radio-navigation satellite service (RNSS) signal in the 1 215-1 300 MHz band, USA contribution, January 2008.
21. Document 5B/13 – Working document towards a preliminary draft new ITU-R Report M.[RNSS-RDS] – Compatibility of the radio-navigation-satellite service with radiodetermination service system receivers in the 1 215-1 300 MHz band, USA contribution, January 2008.
22. Document 5B/14 – Elements for a preliminary draft new Report ITU-R M.[RNSS_RDS], USA contribution, January 2008.
23. Document 5B/15 – Working document towards a preliminary draft new ITU-R Report "measurements on the performance of radars operating in the presence of radio navigation satellite service (RNSS) signals", USA contribution, January 2008.
24. Document 5B/16 – Elements for a preliminary draft new Report ITU-R M.[RNSS_RDS], USA contribution, January 2008.
25. Document 5B/810 Annex 8 – WD PDNR ITU-R M.[RNSS-RDS], Annex to WP 5B Chairman's Report, November 2011.
26. J.I. Marcum – A statistical theory of target detection by pulsed radar, IRE Trans. Information Theory, vol. IT-6, pp. 59-145, April 1960.
27. P. Swerling – Probability of detection of fluctuating targets, IRE Trans. Information Theory, vol. IT-6, pp. 269-308, April 1960.
28. D.P. Meyer and H.A. Mayer – Radar target Detection, San Diego, CA, Academic Press Inc., 1073.

Annex 2

System 2 – Generic radio-navigation satellite service system test

Introduction

One of the principal radars operating in the frequency band 1 215-1 300 MHz is Test Radar 2. In June 2004, tests were conducted on an operational unit of this radar to investigate its susceptibility to RNSS signal interference. This section reports the results of that testing.

1 Description of long-range l-band radar

1.1 General description of the radar

The radar that was tested is an L-band, long-range radar that detects weather and aircraft within a radius of about 200 nautical miles (370 kilometres). It provides data concerning the location and strength of weather as well as range, azimuth, beacon code, altitude, and emergency status of aircraft. The radar has two channels denoted as F1 and F2, requiring at least 25 MHz of frequency separation between those two channels. Each channel consists of a synchronizer, a frequency generator, a transmitter, weather and target receivers, a receiver processor, and a digital target extractor (DTE). The radar uses frequency separation and orthogonal polarization for two channels so that they can transmit and receive via the same antenna for the diplex mode of operation. The radar transmits RF energy on a low beam, and receives reflected RF energy on both the low beam and a high beam. The high beam is used to detect aircraft at short ranges and the low beam is used to detect aircraft at longer ranges and to detect weather.

1.2 Receiver processing

Each channel in the radar receiver has both normal and moving target indictor (MTI) video available. The normal and MTI video both have identical CFAR processing. Both channels contain independent CFAR circuitry. The CFAR samples the input signal at 1/8 mile intervals from 5/8 miles before the target to 5/8 miles after the target to determine the mean nose level from the appropriately delayed main target signal.

The radar also contains integrator-adder circuitry that functions on the normal and MTI video. The integrator-adder contains a digital video integrator with a 7/8 feedback factor to provide video integration. The integrator digitally sums, into a single output, all of the target-hit video occurring within the radar antenna's 1.1-degree (3 dB points) azimuth beamwidth. Within that beamwidth, there can be approximately 12 consecutive target hits or echo returns at the same range and azimuth. Also, since the integrator operates synchronously with the radar's transmitter, asynchronous pulses (from other nearby radars) are automatically eliminated from the video output.

Both receiver processors in Channels A and B are electrically identical. Each receiver processor contains a target processor function. After detection the target information is digitally processed into suitable form for identification by the DTE. When operating in diplex mode, processed target videos in each radar channel are digitally summed with the adjacent channel target videos before distribution to the DTE. The cross-channel target videos summation feature enhances target detection. Cross-channel video summation during duplex operation improves the probability of target detection since a fluctuating target fade in one channel should not be experienced in the opposite channel due to frequency-polarization diversity between the two channels.

1.3 Antenna characteristics

The radar uses a dual horn-fed parabolic reflector enclosed in a radome and mounted on a dual drive pedestal. The antenna forms two cosecant-squared beams shaped for additional high elevation gain. The two beams are almost identical. The azimuth beamwidth of both beams is 1.1 degrees at the 3 dB points. The upper beam has coverage from 3.6 to 44 degrees in elevation while the lower beam covers 2 to 42 degrees in elevation. The antenna rotates at 5 revolutions per minute (rpm).

A complete list of the relevant radar technical parameters is contained in Annex 4.

2 Test set-up

The radar's performance was monitored by both observing targets on the radar's plan position indicator (PPI) and through the use of built-in target counting software. Desired signal targets were generated using RF signal generators and additional testing was accomplished using live traffic. In addition to the desired signals, signal generators were used to inject simulated RNSS emissions into the radar receive path. Radar P_D performance was evaluated as a function of the calibrated interference-to-noise ratio at the intermediate frequency (IF) output of the radar receiver.

2.1 Desired signals

2.1.1 Injected targets

In order to speed testing, a total of 40 injected test targets, 10 targets per radial generated along four separate radials, were separated in range to allow for easy determination of missed targets and monitored for 5 consecutive antenna rotations (a total of 200 targets for any one data point). Each target, regardless of range, was set to the same power at the receiver input, making each target "equivalent" in terms of receiver P_D. The target power was then adjusted to a level that provided an average "target P_D" in the absence of interference of about 90 per cent. Note that the target P_D was not counted on a per-pulse basis. Any one target or "blip" on the radar screen also has in itself an intrinsic P_D for each individual pulse within the group of pulses that defines that target. The target generator produced about 12-13 pulses per target. As long as the radar integrated enough of the 12-13 pulses to define a target and produce a "blip" on the display, it was counted as a good target. As a result, the actual P_D per pulse in the group of pulses that defines the target may be lower than 90 per cent. The P_D per pulse was monitored by the internal data collection software. However, it was not used as an overall performance parameter of interest. The simulated targets on the PPI were manually counted for each radar scan by a test participant.

In order to determine the equivalent RCS represented by the injected test target, a measurement was made at the end of the test cable connecting the signal generator and the waveguide. Accounting for the waveguide coupler and other losses between the injection point and the receiver, the target signal into the receiver IF was −107.2 dBm.

The radar requirement is for detection at main beam gain of a 2 m^2 target out to at least 195 nmi. One form of the basic radar equation is:

$$R = 0.282 \sqrt[4]{\left[\left(P_t G_r A_o A_e\right)/ P_r\right]}$$

where:

- P_t: peak transmit power in watts
- G_r: transmitter low beam gain
- A_o: test target RCS in square metres

A_e: effective antenna aperture, m^2

P_r: received target signal level

R: target range in metres.

In addition, the radar's specification allows for a total of 4.1 dB loss in the receiver-to-antenna path. This same loss is also present on the transmitter-to-antenna signal path. For the tested configuration then:

P_t: 5 MW – 4.1 dB loss = 1.945×10^6 W

G_r: a log(34.5 dB/10) = 2 818.38

A_e: $G_r\lambda^2/4\pi = 12.07$

P_r: −107.2 dBm + 4.1 dB = −103.1 dBm = 4.898×10^{-14} W

R: 195 NM = 361 235 metres.

Rearranging the equation to solve for the test target RCS for a received power of −107.2 dBm, the equation becomes:

A_o: $(R/0.282)^4/(\underline{P_tG_rA_e}/P_r)$

: $(361\,235/0.282)^4/[(1.945 \times 10^6)(2\,818.38)(12.07)/(4.898 \times 10^{-14})]$

: 1.99 m^2

2.1.2 Live targets

A limited amount of data was also collected using live "targets of opportunity". For that testing, the radar was set into its normal operational mode and the PPI screen was monitored for detected aircraft in the radar coverage area. Though the level of these targets was uncontrolled – being dependent on the interaction geometry between the radar and the aircraft itself – where possible the local FAA air traffic control centre was contacted to determine the aircraft type for specific targets of interest.

2.2 Undesired signals

2.2.1 General

RF signal generators and arbitrary waveform generators (AWG) were used to simulate CW and the following RNSS signals:

1) BPSK at 0.511 Mbits/s;

2) BPSK at 1.023 Mbits/s;

3) BPSK at 5.11 Mbits/s;

4) BPSK at 10.23 Mbits/s.

Actual RNSS signals contain data bits that are encoded into symbols that a spreading pseudorandom code further breaks into chips. However, the radar receiver does not discriminate the difference between phase changes representing either a chip or a bit for this type of interfering waveform. The radar receiver processes the BPSK signals as band-limited constant amplitude noise sources, which fall into all of the range cells. Since the noise-like BPSK signal falls into all of the range bins, the CFAR processing cannot eliminate it and the CFAR raises the target detection threshold.

The emission spectrum for each RNSS signal was measured and recorded, and tuned to the frequency of the radar channel(s) under test. The RNSS signal simulator had the capability to generate I/N ratios of −12 to + 30 dB at the receiver RF input, however testing was usually accomplished only over the subset of that range where meaningful P_D data could be collected. For each signal type, calibrations were performed to allow for conversion between signal generator settings and the resultant *I*/*N* level using the process described in Annex 3.

2.2.2 Duration of RNSS signals with injected targets

For the injected desired signal tests, the undesired signals were also injected into the radar at the RF input path to the receiver with durations equal to the main beam dwell time and overlaying them on the desired targets at the same azimuth. As shown below, the dwell time for the main beam of the radar's antenna is 0.04 seconds through a stationary object. This dwell time was used as the duration of the RNSS interference source for the simulated targets tests. For any live target, this time may be different due to the motion of the aircraft.

$$DwellTime = \frac{Antenna\_3dB\_beamwidth}{5rpm} = 0.04 \text{ seconds}$$

2.3 Live target tests

For the live target tests, like the injected target tests, the undesired signals were injected into the radar at the RF input path to the receiver. Because of the mobile characteristics of the live targets however, the injection occurred for a longer time. In particular, the injection was controlled so as to cover approximately a 40-degree sector of the radar scan. In addition, for a given set of live targets, only a single level of *I*/*N* could be tested. These tests did not attempt to simulate a RNSS satellite vehicle's exact behaviour as it moved or passed through the radar's antenna beam at any particular azimuth. The actual dwell time of such an event and its periodicity can be found in USWP8B04-01. The methodology for these tests is contained in § 3.3.2 of this Report.

2.3.1 Test procedures

2.3.1.1 Injected target tests

– For the injected target tests, the desired signal targets were overlaid with one of the RNSS interference signals at a given *I*/*N* and observed for 5 complete scans. This resulted in a total of 200 possible targets (5 scans × 10 targets/radial × 4 radials/scan), and probability of detection was calculated as the number of observed targets divided by 200. The test was then repeated at a different *I*/*N* level. For these tests the transmitter was turned off and though the antenna was still rotating and receiving external signals, a spectrum analyser measurement showed that none were present. When testing was completed for a given RNSS type, a different RNSS interference was used and the testing repeated. Testing was performed with:

– Interference and targets on one channel and the other channel disabled.

– Interference and targets on both channels.

Baseline "no interference" measurements were made before and after each "interference on" data set. For each baseline test 200 targets were generated.

2.3.1.2 Live target tests

For these tests, since the target amplitude was largely uncontrolled, the procedure followed was to operate the radar without injected interference for 15 scans, then turn on the injected RNSS interference at a fixed *I*/*N* for 15 scans, and finally turn off the injected interference for 15 scans. This allowed for examination of targets within the RNSS-interfered sector to determine whether there was any discernible impact to the target due to the RNSS interference. The targets were recorded from the PPI display to a data file for all 45 scans. Upon replay of the data file to a laptop computer, it was observed that the effect of the RNSS interference generally manifested itself as a reduction of a "reinforced target" (i.e. a target that had secondary surveillance radar (SSR) beacon reply, and a correlated primary radar return) to a "beacon-only target". Since the SSR operates in the 960-1 215 MHz frequency band, the injected RNSS interference did not impact its operation. For targets of interest where a skin-track was lost but the beacon reply was still present, an attempt was made to determine the type of aircraft that was being tracked by contacting the local FAA air traffic control centre (ATCC) in Kansas City and providing them associated beacon code. The ATCC was then able to use the beacon code and provide the flight number and type of aircraft to the test personnel.

3 Test results

3.1 Simulated targets with single channel operation

A plot of the target P_D versus the I/N ratio for the radar operating in single channel mode with simulated targets and simulated RNSS interference is shown below in Fig. 23. The figure shows that as the I/N ratio increases, the target P_D drops. At an I/N level of −6 dB, the target P_D has dropped below the baseline value of 0.9. Detection of simulated radar targets (of the minimal acceptable RCS) for single channel operation was degraded by about 0.15 (from 0.90 to 0.75) at the I/N level of −6 dB (current ITU criteria).

FIGURE 23

Radar single channel operation with interference

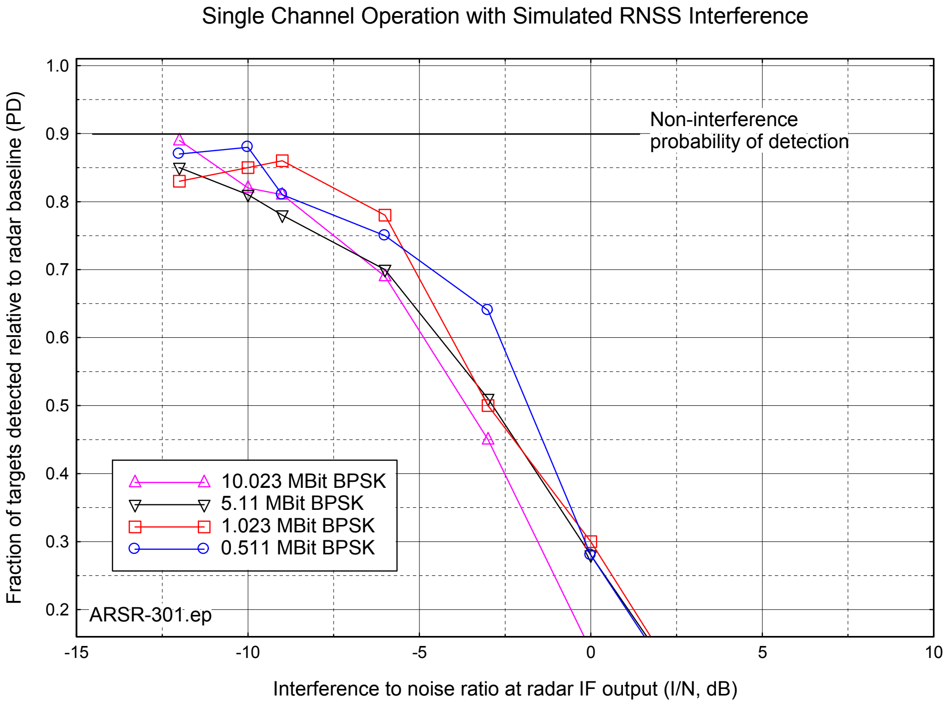

3.2 Simulated targets with dual channel operation

A plot of the target P_D versus the I/N ratio for the radar operating in dual channel mode with simulated targets and simulated RNSS interference on both channels is shown below in Fig. 24. The figure shows that as the I/N ratio increases, the target P_D drops. The figure shows that although the baseline target Pd per channel was set to the 90 per cent value, the overall baseline target P_D is reinforced (improved) with dual channel operation. Note however that dual channel operation only makes the radar perform better to a point, at I/N ratio of −6 dB, the target P_D has still dropped below the baseline value. Detection of simulated radar targets (of the minimal acceptable RCS) for dual channel operation was degraded by about 0.10 (from 0.9 to 0.80) from the improved dual-channel baseline) at $I/N = -6$ dB.

Although the channels have independent receiver hardware, they did not behave in a statistically independent manner. Indeed, the −6 dB single-channel values are centred around 0.74, and, assuming the channels have nearly the same performance, one would expect statistically independent channels to show a centre value of about $1 – (1 – 0.74)^2 = 0.9324$ instead of 0.8.

FIGURE 24

Radar dual channel operation with interference on both channels

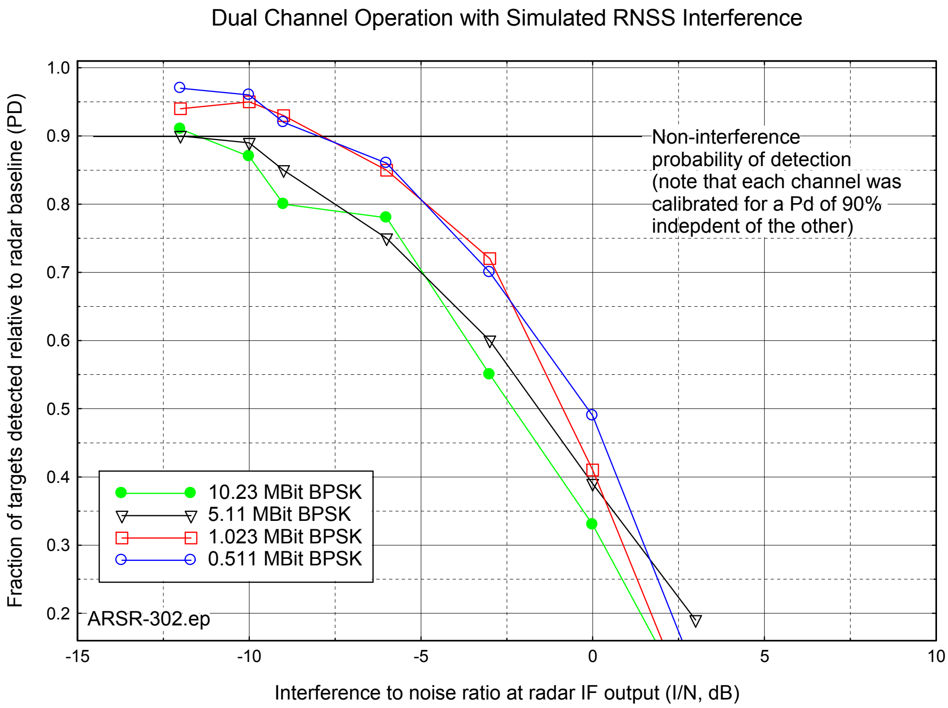

3.3 Results of live sky tests

The 10 Mbs RNSS waveform was injected into the radar's RF circuitry between the antenna and the receiver. The I/N ratio was set to +20 dB for a 40 degree wide azimuth wedge between 160-200 degrees. Figure 25 shows a recording of the aircraft traffic for a full 360 degree view of the PPI for 45 antenna rotations (scans). Interference was present for scans 16-30. The figure shows aircraft that were tracked with the radar and beacon. Tracks that are dark represent targets that have both radar track and beacon data. Tracks that are light represent targets with only beacon data.

FIGURE 25

Overall PPI display for 45 scans

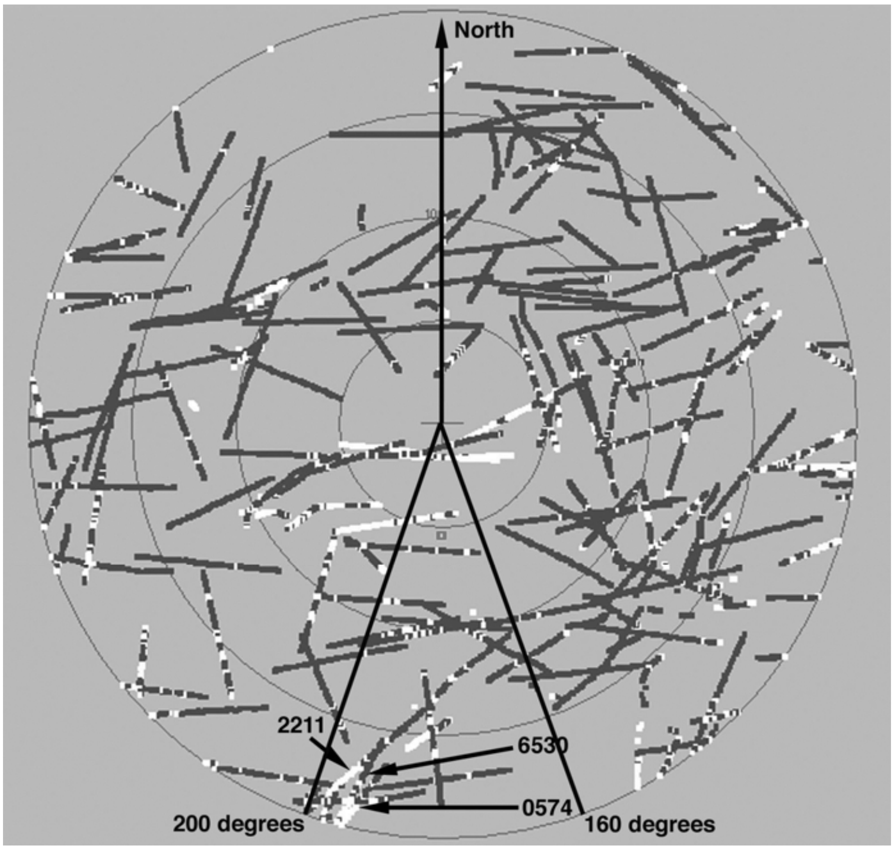

Figure 25 shows one aircraft (identified via the beacon flight number) within the 160-200 degree wedge of interest that had radar and beacon data for the initial 15 scans (no interference), then only beacon data for the next 15 scans (10 Mbs RNSS interference), and finally radar and beacon data for the final 15 scans (no interference). The maximum range on the PPI is 200 nautical miles. The figure shows that the simulated RNSS interference caused the radar to lose track of this target. The radar also dropped other targets within this wedge, but the aircraft flew outside of the ATCC's control area before the aircraft type could be identified. Figure 25 also shows that other parts of the PPI (without injected interference), display some aircraft that have intermittent radar data along with their beacon tracks. These are aircraft that may not be fully in the radar's antenna beamwidth due to their altitude and range. These aircraft were not analysed.

Figure 26 shows the details for the three aircraft of interest. Flight 2211 was an MD-80 observed before, during, and after the interference was injected. The aircraft's initial track is dark, then it goes light, then it goes dark again. Flight 6530 (DC-8 Type 7) and 0574 (TLF-04) entered the wedge when the interference was already on. Their tracks start light and then go dark when the interference was removed.

FIGURE 26

Details of PPI

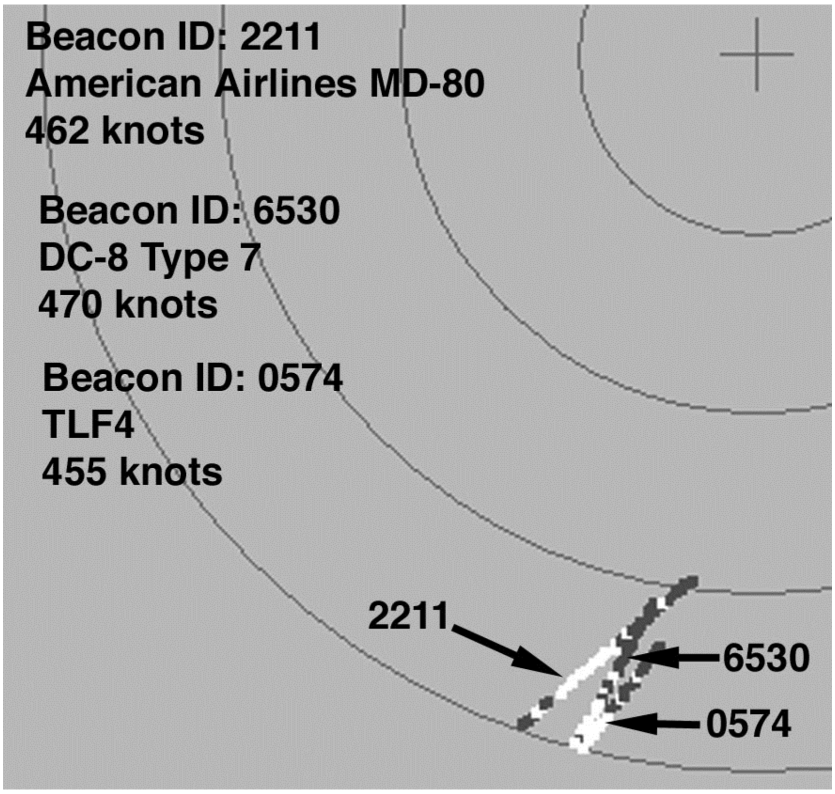

4 Conclusions

From the test data, the following general conclusions can be drawn:

– The P_D of simulated radar targets (of the minimal acceptable RCS) for single channel operation was degraded by 0.15 (from 0.90 to 0.75) at $I/N = -6$ dB (current ITU criteria).

– The P_D of simulated radar targets (of the minimal acceptable RCS) for dual channel operation with interference on both channels was degraded by 0.10 (from 0.90 to 0.80) at $I/N = -6$ dB.

– This degradation appears to be statistically independent of the RNSS modulation type. Note however that all modulations tested were wider than the radar IF bandwidth. However, it is expected that the bandwidth of most RNSS signals will exceed the bandwidth of the radar receiver.

– Radar dual frequency operation with interference on both channels did not significantly improve its performance in the presence of RNSS interference.

– The live sky tests showed that with an I/N of + 20 dB and a 10 Mbs interfering signal, the radar lost track of three identified targets near the edge of its coverage range. The radar also lost other targets within the wedge (closer to the radar), but they could not be identified before they exited the ATC Regional Centre's control.

– Live sky tests are useful as a demonstration of the loss of targets by an L-band radar in the presence of RNSS interference, but do not provide quantitative data on target loss percentages. The hardline coupled procedures described in this section do provide such data.

Annex 3

Undesired signal calibration and IF selectivity

CW or RNSS signal calibration was performed as follows. The Agilent E4440A spectrum analyser, set in zero span mode and with the RMS detector selected, was connected to the radar channel 1 IF output. A CW signal tuned to the radar operating frequency was then injected into the radar RF port and a level was found that produced an [($I + N$)/N)] of 3 dB; equivalent to an I/N ratio of 0 dB. The undesired signal level was recorded, and identified to be equivalent to an I/N ratio of 0 dB. The process was repeated for channel 2, and for each type of RNSS signal. Using the calibrated I/N ratio of 0 dB, the other I/N values were determined.

In addition, a CW signal was swept in frequency and the response of the IF circuitry of the radar receiver was measured for each channel and recorded with the spectrum analyser. The 3-dB IF bandwidth of the radar receiver was determined to be 420 kHz. The measurements of the IF bandwidths are shown below in Figs 27 and 28. The frequencies of the IF outputs are 32 MHz. However, to show the frequency response in the X-axis, Figs 27 and 28 have been changed to reflect the swept frequency.

FIGURE 27

Channel 1 IF response

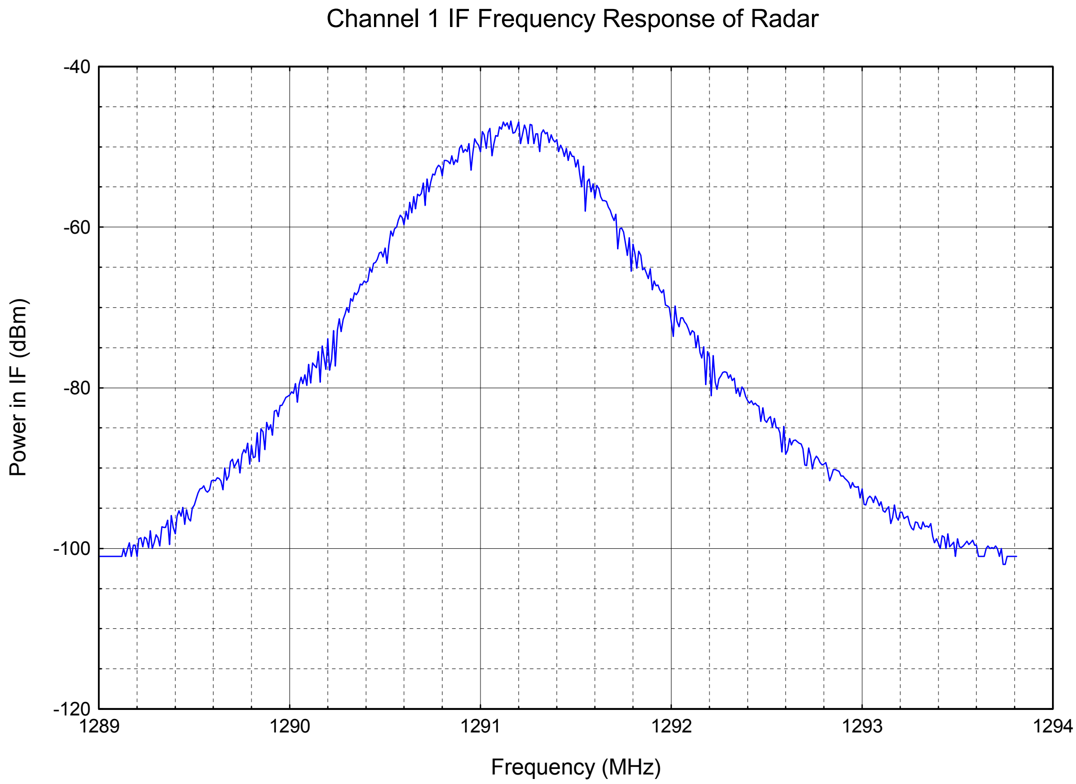

FIGURE 28

Channel 2 IF response

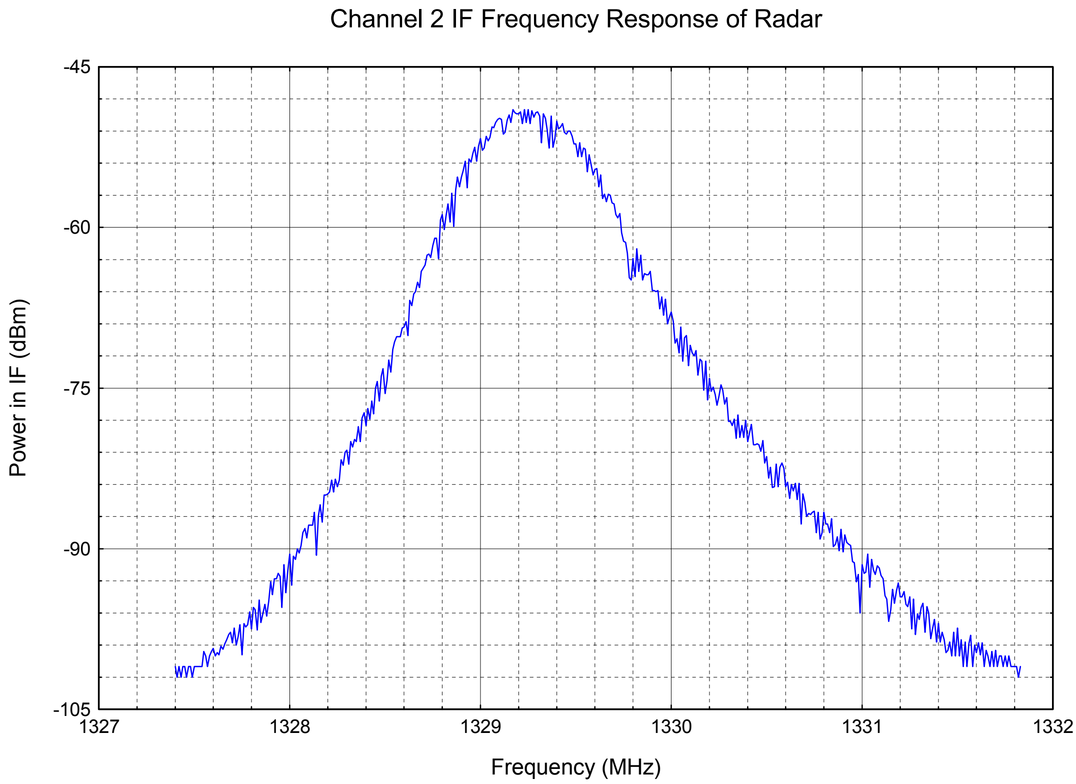

Annex 4

Radar technical characteristics

Parameter	Units	Value
Frequency range	MHz	1 250-1 350
Range	nmi	200
Altitude coverage	m	18 300
Distance resolution	nmi	0.25
Azimuth resolution	degrees	2
Receiver IF bandwidth	MHz	0.42
Pulse width	µs	2
Noise figure	dB	2
Pulse repetition frequency		310-364 (8 discrete 'prf's)
Receiver noise level	dBm	−113
Sensitivity normal	dBm	−115
Sensitivity MTI	dBm	−112

Parameter	Units	Value
False alarm rate		10^{-4} for 2 m^2 RCS
Antenna type		Dual horn reflector
Antenna main beam gain	dBi	Low beam 34.5 High beam 33.5
Antenna elevation beamwidth	degrees	CSC^2 3.6° to 44°
Antenna azimuth beamwidth	degrees	1.1
Antenna scan rate	rpm	5 (12 sec/rev)
Antenna polarization		Linear, circular

Annex 5

Radio-navigation satellite service system emission signal plots

FIGURE 29

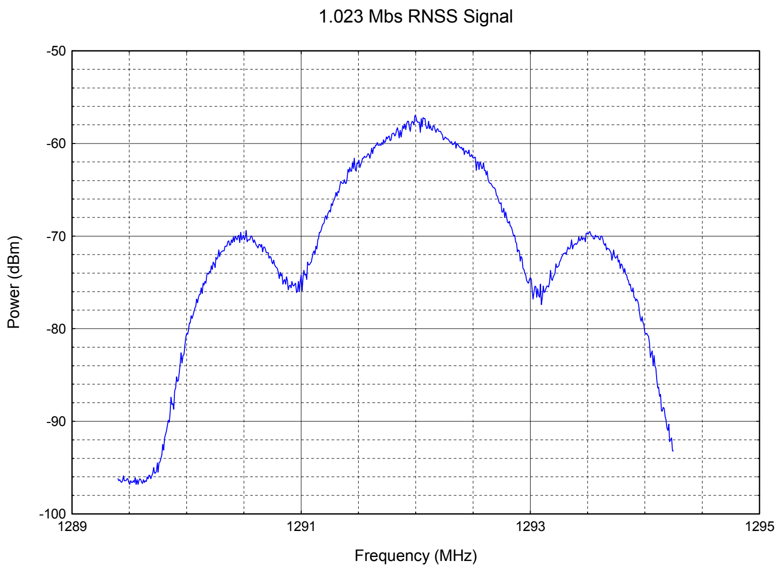

FIGURE 30

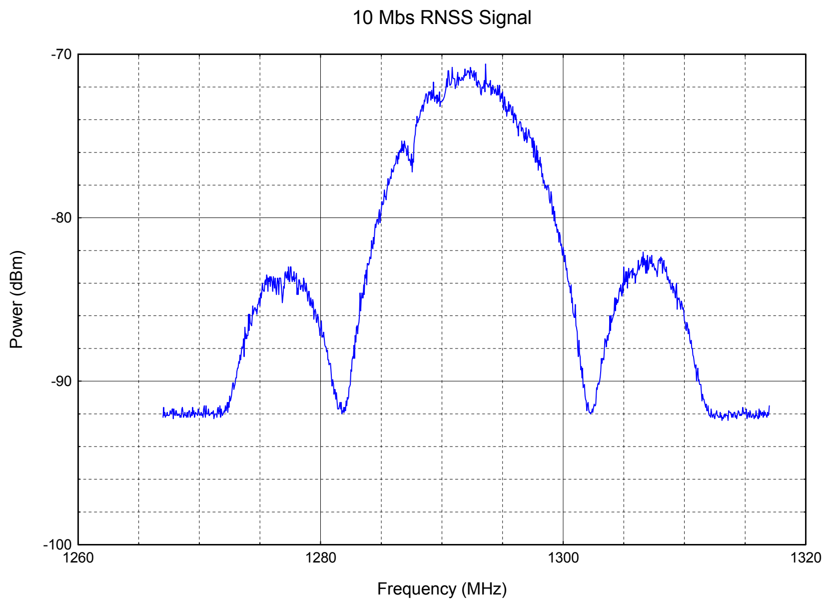

FIGURE 31

5 Mega bit Radio-navigation satellite service system signal

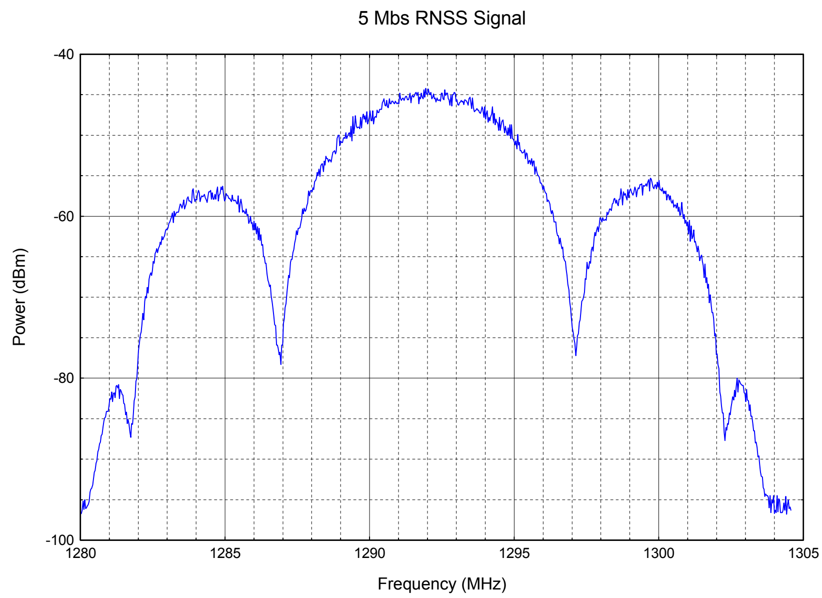

FIGURE 32

0.5 Mega bit Radio-navigation satellite service system signal

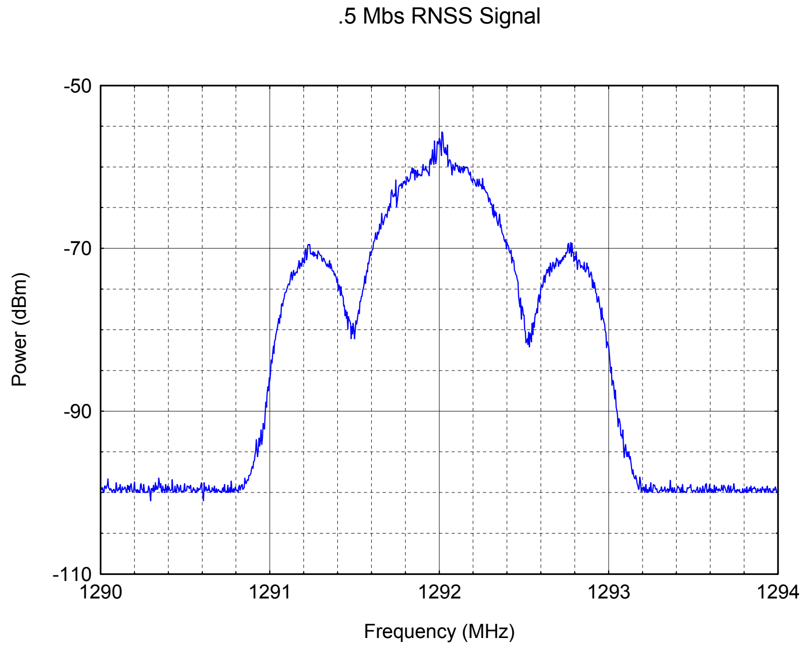

Annex 6

System 5 – GALILEO/Compass test

1.1 Description of radar/radio-navigation satellite service system interference test

A real-world radar/RNSS system interference test was conducted utilizing radiated RF signals in May 2007. The radar used for this test is similar to those documented in Recommendation ITU-R M.1463 and is representative of a class of radars in general use for air traffic control at more than 160 locations worldwide. The objective of this test was to measure the interference effects introduced by signals from RNSS systems on radars operating in the 1 260 to 1 300 MHz frequency band. In particular, the test was aimed at quantifying the operational impact when an active radar target and a signal from an RNSS system source are both present in the radar's main beam, and the radar is utilizing a frequency near that of an RNSS satellite.

1.2 Test set-up

The test set-up included a test-bed radar, RNSS signal generator, and target generator. As described, the test-bed radar used is representative of long range L-band surveillance systems currently used in the radio determination service. Calibrated RNSS and target signals were generated and transmitted via a horn antenna mounted on a tower, located approximately 400 metres from the test-bed radar. Reference measurements were made documenting all gains and losses in the test set-up assuring that the signal levels presented to the radar accurately represented a real world scenario. Metal fences between the test-bed radar and the reference target generator ensured that potential multipath was eliminated.

1.2.1 Test-bed radar

The test-bed radar is equipped with a high gain antenna. Antenna 3 dB beamwidths are on the order of 2 degrees. This antenna produces a pencil beam that is steered in azimuth and elevation to cover an area 360 degrees in azimuth by approximately 20 degrees vertically. The radar's operational requirement specifies that it detect a reference target at 160 nautical miles with a 0.8 probability.

The test-bed radar features multiple RF channels, many of which are near to the frequencies utilized by RNSS. For a fixed RF channel, the radar transmits and receives two independent contiguous sub-pulses. The received signals in each sub-pulse are independently processed and the baseband signals are then non-coherently summed.

1.2.2 Signals from systems in the radio-navigation satellite service

For the purposes of the test, two RNSS signals were considered: Galileo E6 and Compass B3. Since the specifications describing these signals are still in flux, the most updated information available at the time of the testing was used, and bracketed the data collected by testing at the published signal levels (nominal), and at signal levels both above and below the expected levels (multiple 3 dB steps).

Galileo E6 is a RHCP waveform with a carrier frequency of 1 278.75 MHz. Its specified maximum received power level on the ground is −152 dBW (−122 dBm). The spreading code is a combination of a Binary Phase Shift Keying (BPSK) CS data signal and a Binary Offset Carrier (BOC) PRS signal. The power spectral density of the Galileo E6 signal is given by following mathematical expression.

$$S_{E6}(f) = T_c \operatorname{sinc}^2\left(\pi(f-f_o)T_c\right) + 4T_c \operatorname{sinc}^2\left(\pi(f-f_o)T_c\right)\left[\frac{\sin^2\left(\dfrac{\pi(f-f_o)}{4f_s}\right)}{\cos\left(\dfrac{\pi(f-f_o)}{2f_s}\right)}\right]^2$$

where:

$$\operatorname{sinc}(x) \equiv \sin(x)/x$$

$T_c = 1/f_c$.

with

$f_c = 5.115$ MHz and

$f_s = 10.23$ MHz.

Compass B3 is circularly polarized (CP) waveform with a carrier frequency of 1 268.52 MHz. Its spreading code is BPSK(10) with a specified maximum received power level on the Earth's surface of −150.5 dBW (−123.5 dBm). The power spectral density of the Compass B3 signal is given by:

$$S_{B6}(f) = T_c \operatorname{sinc}^2\left(\pi(f-f_o)T_c\right)$$

where $T_c = 1/f_c$ and $f_c = 10.23$ MHz. The RNSS signals used in the test were generated by a programmable Agilent Vector Signal Generator (VSG), with the levels and bandwidth structures verified against published specifications for both systems. The comparison of measured vs. predicted power spectral densities of these two RNSS signals are shown in Fig. 33.

During the test no 40 MHz transmit mask was used, because the test was centred at the RNSS frequencies and therefore the 40 MHz characteristic did not affect the rest result.

FIGURE 33

Measured vs. predicted power spectral densities of a) Galileo E6 and b) Compass B3 signals

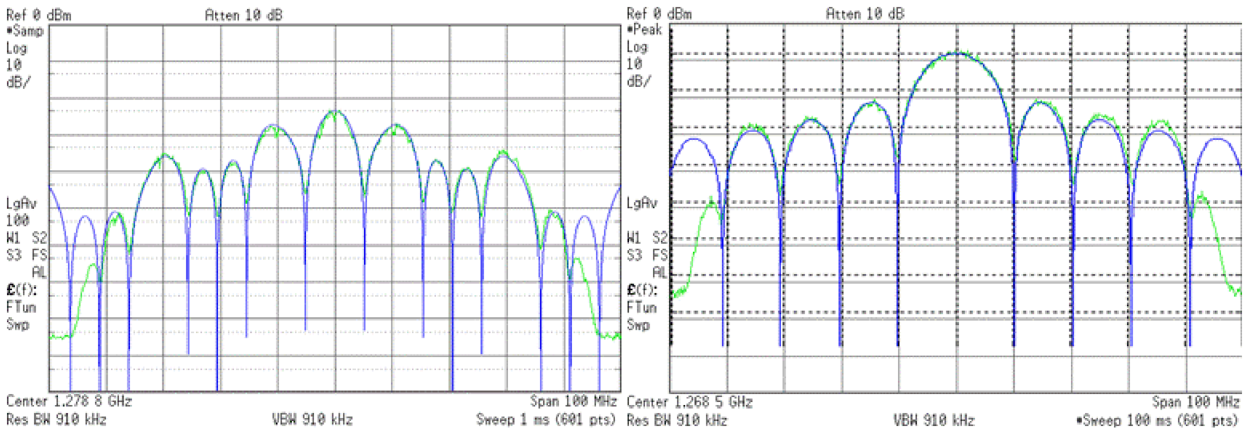

1.2.3 Radionavigation satellite service and target signal generator

The reference radar target was generated using a radar target generator (RTG) that receives the transmitted radar pulse, delays it in time, appropriately adjusts amplitude, and retransmits it to simulate a test target located at a programmable distance from the radar. The RTG and RNSS satellite waveforms generator (VSG) were located in a small building and fed a calibrated-gain horn antenna mounted on a tower located approximately 400 m from the radar.

The RTG can produce radar return pulses that simulate targets of varying distance and RCS. It receives and stores the radar pulse using DRFM technology, and then generates a time-delayed, amplitude-adjusted signal to simulate a returned pulse from a given target RCS and range.

Both the Galileo E6 and the Compass B3 waveforms were generated using the Agilent VSG. Prior to the test, a link budget calculation analysed the gains and losses present in the test set-up and determined the required power settings on the VSG. For Galileo E6, with a specified maximum power density of −152 dBW, the vector signal generator was set to present a power level at the radar of −154 dBW, to include appropriate cross polarization loss (RHCP to HP). For the Compass B3 signal, with a specified maximum power density of −150.5 dBW, the VSG was set to produce a power level of −152.5 dBW. RNSS signal levels presented at the radar were confirmed using an independent reference system consisting of a calibrated antenna and an Agilent spectrum analyser. Figure 34 shows the equipment set-up for the target and RNSS simulation suite.

FIGURE 34

Radar target generator (RTG) and radio-navigation satellite service source equipment configuration

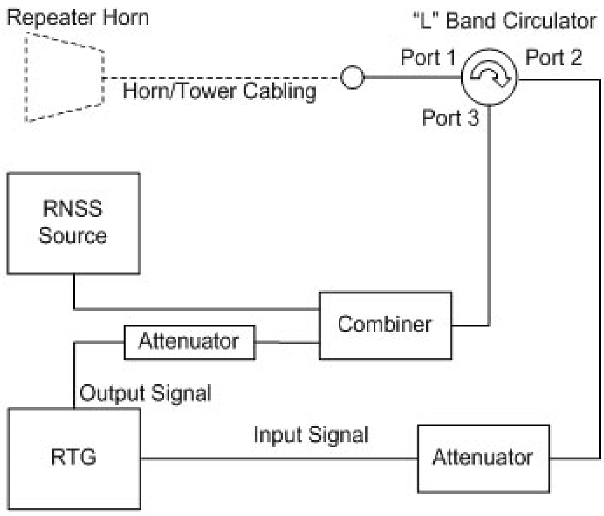

1.3 Test data

Four types of data were collected during the test: calibration measurements, noise and interference measurements, probability of detection data, and probability of false alarm data.

1.3.1 Calibration data

Calibration data was collected each day at the beginning and end of each test interval to determine and verify the system noise floor, and to verify the consistency of the test set-up. The measurements were made with the radar's antenna stationary and pointing in the direction of the repeater tower. A continuous wave (CW) signal was generated using the VSG and transmitted via the horn antenna to the test-bed radar. This signal was observed using calibrated spectrum analysis equipment and sampled in the radar receiver's intermediate frequency (IF) band. The output of the VSG was increased until a 3 dB increase in the radar's noise floor was observed. This condition corresponds to the situation where the interference power is equal to the radar's system noise floor as observed in the radar's receiver, allowing the radar receiver's self-noise level to be verified. This condition occurred with a VSG setting of −69 dBm. An example of a CW measurement is shown in Fig. 35. It is worth noting that although the testing occurred over a several-day period, the radar noise floor and system variables measured using this method remained constant throughout all testing.

FIGURE 35

Example radar noise floor measurement

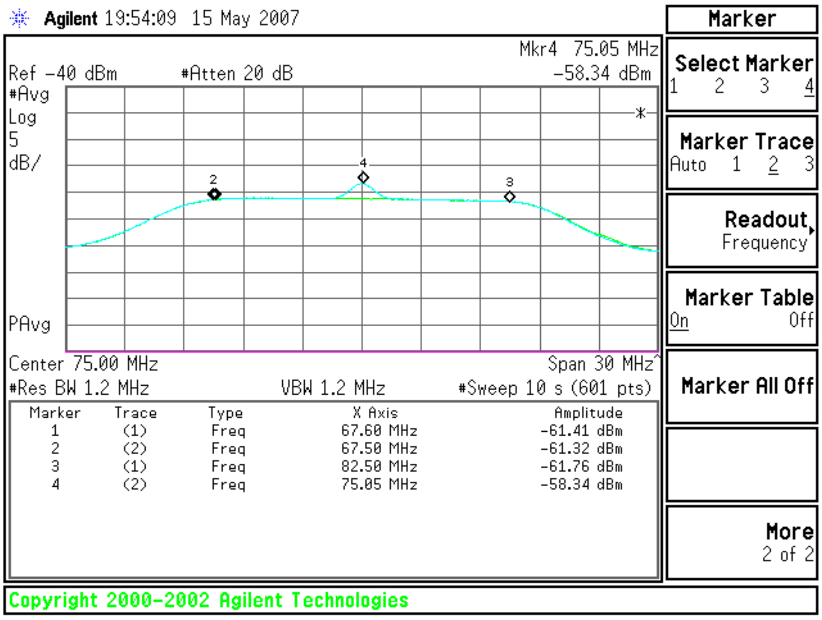

1.3.2 Noise and interference data

Similar to the calibration data set-up, the noise and interference data was collected using a calibrated spectrum analyser and with the radar's antenna stationary and pointing at the horn tower. This measurement resulted in a data set showing the observed strength of each sample RNSS signal as received and processed by the radar's receiver. The test-bed radar's IF bandwidth is 20 MHz bandwidth.

Examples of system self-noise and RNSS interference measurements are shown in Fig. 36 (Galileo) and Fig. 37 (Compass). In these figures, the frequency distribution of the RNSS signals (magenta) and system noise (blue) are shown for numerous radar channels near the RNSS carrier frequency. As previously mentioned the radar transmits and receives two independent contiguous subpulses. These two sub-pulses are located at ±7.5 MHz with respect to the centre of the IF and indicated by 0 Hz on these plots. The received signals in each subpulse are independently processed and the baseband signals are then non-coherently summed.

It is evident from these figures that the RNSS signal bandwidth is much greater than the radar's receiver bandwidth. It is also evident that at nominal RNSS signal levels the recommended −6 dB *I*/*N* ratios of Recommendation ITU-R M.1463 are greatly exceeded. Because of the difference in frequency between the radar and the RNSS signal the RNSS spectrum is non-uniformly spread across the radar's IF frequency band. Consequently, the RNSS signal has the effect of unevenly increasing the noise floor of the two subpulses. As will be shown later in the analysis section, this leads to interesting results.

FIGURE 36

Galileo E6 signal observed in the radar receiver's IF frequency band (magenta) for several frequencies near the Galileo RNSS signal. Also shown is the system noise spectrum (blue), with no RNSS signal present. The two sub-pulses are located at ±7.5 MHz with respect to the centre of IF. The bandwidth of each sub-pulse is about 1 MHz

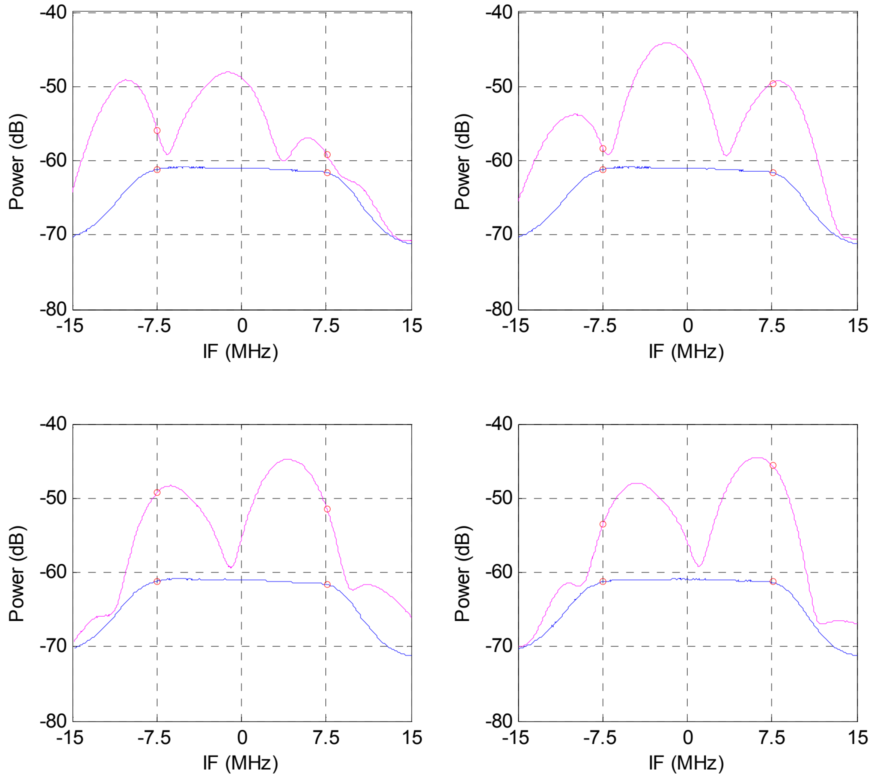

FIGURE 37

Compass B3 signal observed in the radar receiver's IF frequency band (magenta) for several frequencies near the Compass RNSS signal. Also shown is the system noise spectrum (blue) with no RNSS signal present. The two sub-pulses are located at ±7.5 MHz with respect to the centre of IF. The width of each sub-pulse is about 1 MHz

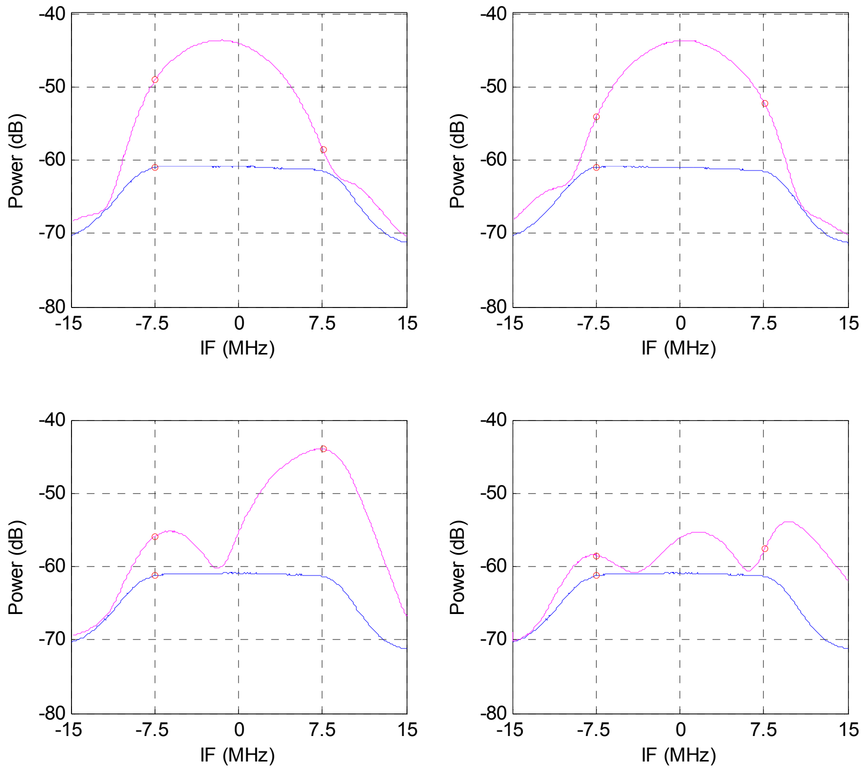

1.3.3 Probability of detection data

To collect P_D data the radar was allowed to resume normal operation rotating at 5 RPM. To collect a statistically significant data set, 200 samples were integrated for each P_D measurement (each test taking approximately 40 minutes). For each test the target signal generator was used to generate a reference target and the vector signal generator was used to generate an appropriate RNSS signal.

Each P_D test interval started with a baseline measurement with no RNSS signal present. This baseline measurement was used to confirm the target signal generator created an appropriate reference target with a P_D of 0.8 in accordance with the specified level of performance for this radar. By setting the target signal level in this way, averaging over hundreds of scans, real-world target variations as modelled by Swerling are accommodated.

With the target generator set to this power level, additional P_D measurements were conducted with the RNSS signal under test enabled. The VSG power level was set to numerous values to allow for variations in RNSS signal power as measured at the face of the radar's antenna to be studied. The result of these measurements is a complete data set that ties radar P_D to I/N as specified in the measurement methodology outlined in Recommendation ITU-R M.1461.

The summary of the P_D data plotted as a function of I/N is shown in Fig. 38. The plot shows the results for E6 at channel F1 and F2, and B3 at channel F3.

These RF channels were chosen because they were near the RNSS carrier frequencies where the greatest impact on the radar performance was expected. In this plot, the measured P_D data is plotted as a function of estimated I_{avg}/N at the radar receiver's IF, where Iavg is the average of the RNSS interference power in the two subpulses. As expected, a reduction in P_D is observed as I_{avg}/N increases.

FIGURE 38

Probability of detection as a function of interference-to-noise ratio

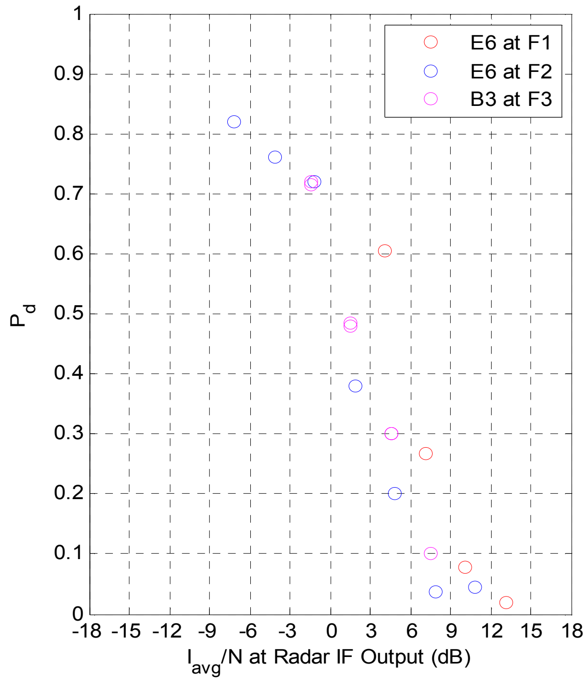

1.3.4 Probability of false alarm data

A similar test set-up was used to investigate the effect of RNSS signals on the radar's P_{FA}. The same test configuration was used for these tests except the use of the target signal generator was not required for this measurement. Initially, the number of false detections was documented for the noise only case. Then, RNSS signals were added for each set of P_{FA} measurements. The summary of the P_{FA} data is shown in Table 4. While no conclusion may be reached on the impact of the presence of the RNSS signal on the total number of false detections, an increase in the number of false detections was observed along the radial direction of the horn tower for the Galileo E6 waveform. No such increase was observed for the Compass B3 waveform for the power levels tested.

TABLE 4

Summary of probability of false alarm detection tests

Waveform	Power level	Scans	Total No. of FA	No. of FA from RNSS
Galileo (F1)	Nominal + 3 dB	207	35	15
Galileo (F1)	Nominal	207	45	9
Galileo (F1)	Nominal – 6 dB	207	30	1
Galileo (F1)	Nominal – 9 dB	206	32	2
Baseline (F1)	No RNSS	208	25	0
Compass (F3)	Nominal + 3 dB	207	31	0
Compass (F3)	Nominal	207	45	1
Compass (F3)	Nominal – 6 dB	207	32	2
Compass (F3)	Nominal – 9 dB	207	41	1

1.3.5 Validation of measured data

1.3.5.1 System noise calculation

The system noise floor of a radar system is computed from:

$$N = kT_sB$$

where:

k: Boltzmann's constant

T_s: system noise temperature

B: receiver bandwidth.

For the test-bed radar $k = -228.6$ dB, $T_s \sim 700$ K and $B \sim 1$ MHz. Therefore, the specified system noise floor is approximately −110.5 dBm.

In the May 2007 test the CW measurement showed that the interference power was equal to the system noise floor when the VSG is set to −69 dBm. The radar's self-noise level can be verified from this VSG output power. The link budget for this calculation is shown in Table 5. Based on this calculation, the estimated noise floor from the measurement is −111.8 dBm. Therefore, the measured noise floor is about 1.3 dB lower than the calculated value based on the specified system noise temperature as listed in the radar's specification.

TABLE 5

Link budget table for system noise calculation

			Unit	Value
f			MHz	1 267.00
λ			m	0.24
VSG power level	dBm	−69	dBW	−99.00
Hardware loss			dB	6.05
G_t			dB	13.15
P_tG_t			dBW	−91.90
λ^2			dB	−12.51
$(4\pi)^2$			dB	21.98
R^2	m	372	dB	51.41
G_r			dB	36.00
$I = N$ level			dBW	−141.81

1.3.5.2 Interference and noise measurements at intermediate frequency

Examples of RNSS signal levels as measured in the radar receiver's IF were shown in Figs 36 and 37. To verify the accuracy of these measurements, a RNSS spectral prediction model was developed. Assuming maximum incident power P_{inc}, the RNSS spectrum in radar receiver's IF band is given by:

$$S_{IF}(f) = H_{IF}(f)P_{inc}G_rL_rL_pS_{RNSS}(f - f_C + f_{IF})$$

where $H_{IF}(f)$ is the radar's IF filter response, G_r = radar antenna gain, L_r = receiver loss, L_p = polarization mismatch loss, and $S_{RNSS}(f)$ = power spectral density of the RNSS signals.

In Fig. 39(a), the measured RNSS spectra at the IF frequency band for E6 at F1 and F2, and B3 at F3 are shown. The predicted RNSS spectra are shown in Fig. 39(b). The predicted spectral shape closely replicates the measured data. The predicted interference-to-noise ratio is in agreement with the measured value by about 2 dB.

FIGURE 39

Measured and predicted radio-navigation satellite service system spectra for Galileo E6 at F1 and F2 and Compass B3 at F3

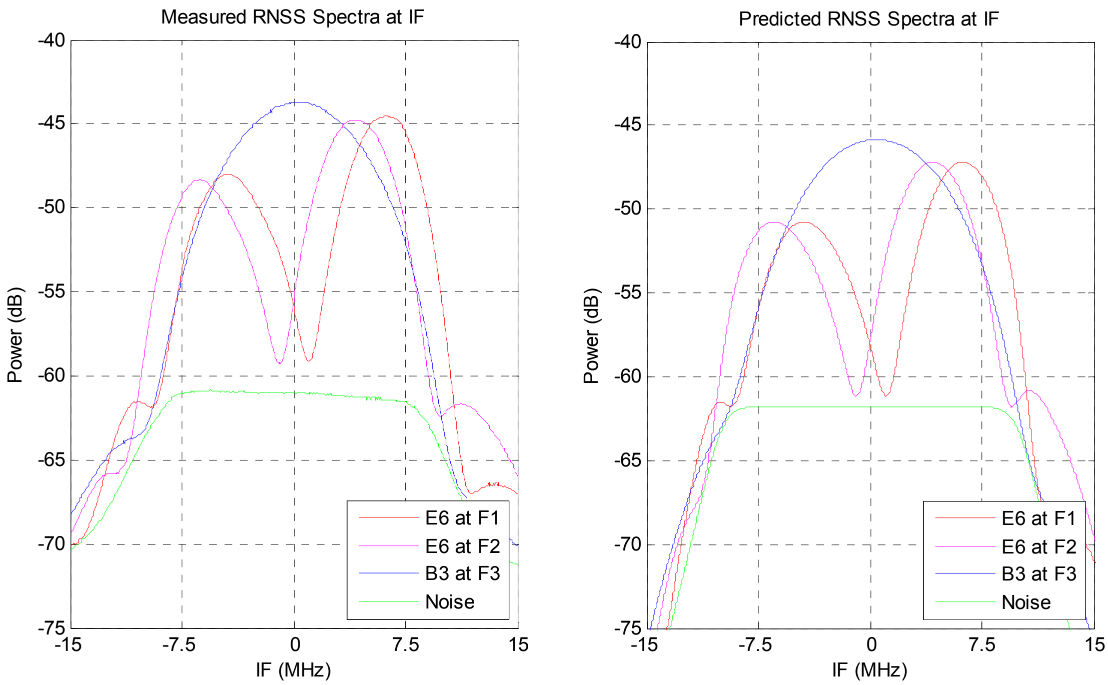

(a) (b)

1.3.5.3 Analysis of probability of detection and probability of false alarm measurements

In this section an analytical model was used to predict P_D and P_{FA} and compare these predictions to the measured data set collected during the May 2007 test. For a fixed RF channel, the radar transmits and receives two independent contiguous sub-pulses. Each pulse is processed independently and the power sum of the two channels is used for the detection process. The analysis is based on a receiver processing model as outlined in Annex 2.

It is assumed that the radar receiver sees the RNSS interference as white noise. Since the sum of two Gaussian random variables is also Gaussian, it is assumed that the $(I + N)$ in the two subpulses are Gaussian random variables, each with variance σ_1^2 and σ_2^2. First these two parameters are estimated from the noise measurements. These variances are then used to compute the detection thresholds and, consequently, P_D and P_{FA}.

1.3.5.3.1 Detection logic model

The radar detector declares a radar return a target if the signal is above a threshold y_{th}. This threshold is set so that real targets are reliably detected, and so that the P_{FA} does not exceed the desired CFAR. The radar's detection logic consists of a number of CFAR thresholds, a requirement driven by different operating environments. Both constant value thresholds as well as cell-averaging CFAR thresholds are used in an attempt to keep P_{FA} as constant as possible.

The analysis, considers only the detection logic which tests a signal against noise. In this case, the threshold is determined from an estimate of the background noise power made from a measurement gathered when the radar is not transmitting. In the case of dual diversity channel radars, the noise variance is estimated by averaging over a number of range cells and the two sub-pulse channels. The detection threshold is then given by the product of this noise estimate and a predetermined bias. The relationship between this bias and P_{FA} is well known and is given by:

$$P_{fa} = 1 - I\left[\frac{Y_b}{\sqrt{N}}, N-1\right]$$

where Y_b is the bias normalized to twice the noise power, N is the number of non-coherent pulses integrated, and I is the incomplete gamma function in Pearson's formula given by:

$$I(u,P) = \int_0^{u(P+1)^{1/2}} \frac{e^{-t}t^P}{P!}dt$$

In this radar's case, $N = 2$, and setting $P_{FA} = 10^{-6}$ and solving for Y_b, results in $Y_b = 16.7$. Therefore, the CFAR threshold is given by:

$$y_{th} = 2Y_b\overline{n} = 33.4\overline{n}$$

1.3.5.3.2 Predicted probability of detection

The detailed calculation of probability of detection is provided in Annex 6. It is given by:

$$P_D = \begin{cases} \dfrac{1}{(\sigma_2^2 - \sigma_1^2)}[(\sigma_2^2 + a^2)e^{-y_{th}/2(\sigma_2^2+a^2)} - (\sigma_1^2 + a^2)e^{-y_{th}/2(\sigma_1^2+a^2)}] & (\sigma_1^2 \neq \sigma_2^2) \\ e^{-y_{th}/2(\sigma^2+a^2)}\left[\dfrac{y_{th}}{2(\sigma^2 + a^2)} + 1\right] & (\sigma_1^2 = \sigma_2^2 = \sigma^2) \end{cases}$$

Using estimates of σ_1^2 and σ_2^2 derived from noise and interference measurements, it can be predicted based on this equation. Initially, σ_1^2 and σ_2^2 was set to *kTB* and vary the signal power a^2 to achieve a P_D of about 0.85. With this signal power, P_D was determined for the (noise + interference) case. Figure 40 shows how the measured data compares to the P_D vs. interference-to-noise ratio as predicted by the analytical model. The model (with its assumption of a Swerling II target) matches the measured data for Galileo E6 and Compass E3 RNSS signal interference very well. This model can now be used to predict the impact on P_D as a function of I/N ratio.

FIGURE 40

Predicted and measured probability of detection as a function of I_{avg}/N. The predicted probability of detection is shown in solid lines

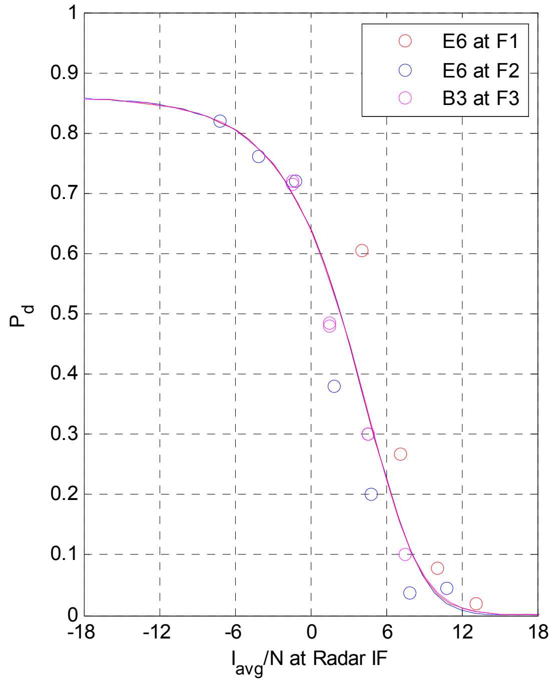

1.3.5.3.3 Predicted probability of false alarm

The results from the P_{FA} test are summarized in Table 3. Although the sample size was limited, the test revealed that an increase in number of false detections was observed along the radial direction of the horn tower for the Galileo E6 waveform. However, no such increase was observed for the Compass B3 waveform for the power levels tested.

The analytical expression for the probability of false alarm is derived in Annex 7 and is given by:

$$P_{FA} = \begin{cases} \dfrac{1}{(\sigma_2^2 - \sigma_1^2)}\left[\sigma_2^2 e^{-y_{th}/2\sigma_2^2} - \sigma_1^2 e^{-y_{th}/2\sigma_1^2}\right] & (\sigma_1^2 \neq \sigma_2^2) \\ e^{-y_{th}/2\sigma^2}\left[\dfrac{y_{th}}{2\sigma^2} + 1\right] & (\sigma_1^2 = \sigma_2^2 = \sigma^2) \end{cases}$$

Figure 41 shows P_{FA} as a function of I/N. Also shown in this plot is the case when $\sigma_1^2 = \sigma_2^2 = \sigma^2$ (balanced channel case). For the balanced channel case, the P_{FA} is constant at 10^{-6} and is independent of I/N. This is expected because the radar's constant false alarm rate function is based on measured noise power in the two sub-pulses and assumes the noise is Gaussian (balanced channel case). The P_{FA} curves for similar RNSS interference signals, however, show that P_{FA} varies as a function of I/N. Moreover, Galileo E6 appears to cause a greater increase in P_{FA} at F1 (red) than at F2 (blue). This result follows from the fact that while the CFAR threshold is based on the convolution of two chi-squared density functions with 2 degrees of freedom and the same variance, the actual P_{FA} is computed from the convolution of two chi-squared density functions with 2 degrees of freedom, but with different variances.

It can be shown that P_{FA} increases as the ratio of the two subpulse variances increases. The values of σ_1^2/σ_2^2 for Galileo E6 at F1 and F2 and Compass B3 at F3 are tabulated in Table 6. The P_{FA} curves in Fig. 41 show that P_{FA} is worst for the E6 F1 case where the ratio of σ_1^2/σ_2^2 is 7.19, followed by B3 F3 (1.93) and E6 F2 (1.52). Given fixed average noise power, the P_{FA} impact will be greater for the cases when the ratio σ_1^2/σ_2^2 is increased.

On closer inspection of the graph, it appears that in some cases P_{FA} can increase from 10^{-6} to 10^{-4}, a rate 100 times greater than desired. Interpretation of these results requires caution. Remember that this result applies only to the case when the RNSS source is in the radar's main beam and the radar is tuned to the RNSS frequency band. A statistical analysis which incorporates the likelihood of this scenario must be considered before any conclusion can be drawn about operational impacts.

TABLE 6

Ratio of (interference + noise) power between the two sub-pulses

	Ratio σ12/σ22
Balanced	1
B3 at F3	1.93
E6 at F2	1.52
E6 at F1	7.19

FIGURE 41

Predicted probability of false alarm

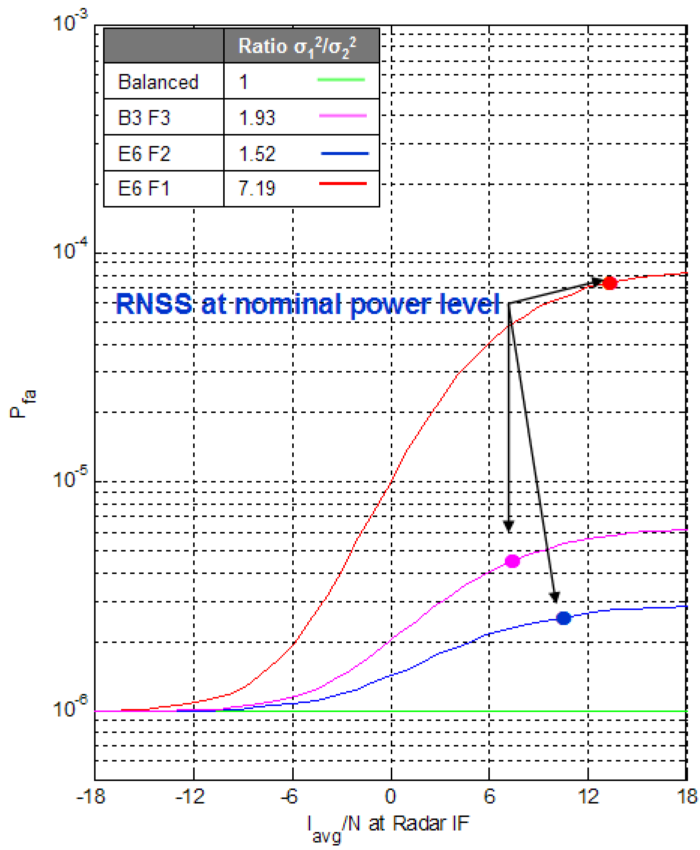

1.4 Conclusions

A real-world radar/RNSS interference test was conducted utilizing radiated RF signals in May 2007. The objective of this test was to measure the interference effects introduced by the RNSS signals on radars operating in the 1 260 to 1 300 MHz frequency band. In particular, the test was aimed at quantifying the operational impact when an active radar target and RNSS signal are both present in the radar's main beam, and the radar is utilizing a frequency near that of an RNSS satellite.

Noise and interference testing indicate that Galileo E6 and Compass B3 signals are prominently visible in the radar receiver's intermediate frequency band and function to raise the radar noise floor. It was also evident that at nominal RNSS signal levels the recommended −6 dB *I*/*N* ratios of Recommendation ITU-R M.1463 are exceeded. The measured data agrees well with predicted results generated by an analytical model.

The test further studied the relationship between *I*/*N*, P_D, and P_{FA}. The result of these measurements is a complete data set that ties radar P_D to *I*/*N* as specified in the measurement methodology outlined in Recommendation ITU-R M.1461. Again, analytical modelling was used to verify the measured results, with measured and modelled data in close agreement. The test showed significant impacts on P_D at higher *I*/*N* ratios, with an impact to P_{FA} under certain limited conditions. Further testing is recommended to fully understand these effects and quantify operational impacts.

Annex 7

Calculation of probability of detection and probability of false alarm

In this class of radars, a quadratic detector is used at the output of each sub-pulse channel where the output is the squared magnitude of the signal. Therefore, radars in this class use a non-coherent summing detection process.

The power at the output of each sub-pulse channel results in following signal:

$$V = I^2 + Q^2$$

where *I* and *Q* are the in-phase and the quadrature component of the signal.

If the input signal is noise only, then *I* and *Q* are zero-mean Gaussians random variables with variance σ^2 and *V* is a chi-squared distributed random process with two degrees of freedom, whose PDF is given by:

$$f_V(V) = \frac{1}{2\sigma^2}\exp\left(\frac{-V}{2\sigma^2}\right)$$

On the other hand, if the input signal is (noise + a Swerling II target), then *V* is a non-central chi-squared distributed random process with two degrees of freedom:

$$f_V(V) = \frac{1}{2(\sigma^2 + a^2)}\exp\left(\frac{-V}{2(\sigma^2 + a^2)}\right)$$

Since the radar signal of interest is the non-coherent sum of the two sub-pulses represented by:

$$W = V_1 + V_2 = I_1{}^2 + Q_1{}^2 + I_2{}^2 + Q_2{}^2$$

If it is assumed that V_1 and V_2 are independent, then the PDF of W is given by the convolution integral:

$$f_W(W) = \int_0^W f_{V_1}(W-S) f_{V_2}(S) dS$$

The closed form solution to the above integral is possible. The noise-only PDF $f_{W,0}(W)$ is given by:

$$f_{W,0}(W) = \int_0^W \frac{1}{2\sigma_1^2} \exp\left(\frac{-(W-S)}{2\sigma_1^2}\right) \frac{1}{2\sigma_2^2} \exp\left(\frac{-S}{2\sigma_2^2}\right) dS$$

Solving this integral results in:

$$f_{W,0}(W) = \begin{cases} \dfrac{1}{2(\sigma_2^2 - \sigma_1^2)}\left[e^{-W/2\sigma_1^2} - e^{-W/2\sigma_2^2}\right] & (W > 0, \sigma_1^2 \neq \sigma_2^2) \\ \dfrac{We^{-W/2\sigma^2}}{4\sigma^2} & (W > 0, \sigma_1^2 = \sigma_2^2 = \sigma^2) \end{cases}$$

where σ_1^2 and σ_2^2 denote the noise power in subpulse 1 and 2, respectively.

For the (noise + Swerling II target) case with the signal amplitude a, the PDF $f_{W,1}(W)$ is given by:

$$f_{W,1}(W) = \int_0^W \frac{1}{2(\sigma_1^2 + a^2)} \exp\left(\frac{-(W-S)}{2(\sigma_1^2 + a^2)}\right) \frac{1}{2(\sigma_2^2 + a^2)} \exp\left(\frac{-S}{2(\sigma_2^2 + a^2)}\right) dS$$

Solving this integral results in the following expression for (noise + target) PDF:

$$f_{W,1}(W) = \begin{cases} \dfrac{1}{2(\sigma_2^2 - \sigma_1^2)}\left[e^{-W/2(\sigma_1^2 + a^2)} - e^{-W/2(\sigma_2^2 + a^2)}\right] & (W > 0, \sigma_1^2 \neq \sigma_2^2) \\ \dfrac{We^{-W/2(\sigma^2 + a^2)}}{2(\sigma^2 + a^2)^2} & (W > 0, \sigma_1^2 = \sigma_2^2 = \sigma^2) \end{cases}$$

By definition P_D is given by:

$$P_D = \int_{y_{th}}^{\infty} f_{W,1}(W) dW$$

which yields the following expression for P_D:

$$P_D = \begin{cases} \dfrac{1}{(\sigma_2^2 - \sigma_1^2)}[(\sigma_2^2 + a^2)e^{-y_{th}/2(\sigma_2^2 + a^2)} - (\sigma_1^2 + a^2)e^{-y_{th}/2(\sigma_1^2 + a^2)}] & (\sigma_1^2 \neq \sigma_2^2) \\ e^{-y_{th}/2(\sigma^2 + a^2)}\left[\dfrac{y_{th}}{2(\sigma^2 + a^2)} + 1\right] & (\sigma_1^2 = \sigma_2^2 = \sigma^2) \end{cases}$$

Similarly, P_{FA} is given by:

$$P_{FA} = \int_{y_{th}}^{\infty} f_{w,0}(W) dW$$

Once again, this integral can be solved and results in the following expression for P_{FA}:

$$P_{FA} = \begin{cases} \dfrac{1}{(\sigma_2^2 - \sigma_1^2)}\left[\sigma_2^2 e^{-y_{th}/2\sigma_2^2} - \sigma_1^2 e^{-y_{th}/2\sigma_1^2}\right] & (\sigma_1^2 \neq \sigma_2^2) \\ e^{-y_{th}/2\sigma^2}\left[\dfrac{y_{th}}{2\sigma^2} + 1\right] & (\sigma_1^2 = \sigma_2^2 = \sigma^2) \end{cases}$$

Annex 8

System 5 – GALILEO/Radar Test

1 System 5 – GALILEO/Radar Test

1.1 Description

This Annex provides information about the performance and results of a representative compatibility measurement campaign between a signal transmitted by the European GALILEO system in the RNSS and the receiver of a Primary Surveillance Radar (PSR) operating in the RDS.

1.1.1 General approach

An operational military air surveillance radar, representative for more than 120 similar radar installations worldwide was temporarily taken out of service and used for this campaign. For the definition of the interference conditions the measurement scenario was implemented as a worst-case configuration by “fixing” a radar target with a RCS of 1 m^2 at the maximum instrumented distance of the radar beam. A representative GALILEO signal was transmitted towards the radar antenna in direct bore sight line of sight from “behind” the target by providing the typical received power level as specified by the GALILEO Signal In Space – Interface Control Document (SIS-ICD).The main criterion for the radar performance under interference conditions was the impact of spread spectrum signals on the radar operational P_D.

1.1.2 Objective

Main objective of the campaign was to determine in a most realistic configuration the sharing conditions of PSRs operating co-frequency with the E6-signals of the GALILEO system in the frequency band 1 260-1 300 MHz.

The measurement scenario was defined in line with the definition used as performance criteria in desktop studies for PSRs and radar expert considerations in ITU-R Working Party 8B.

A further objective is to contribute to the determination of appropriate protection criteria for radar systems as the present definition given by Recommendation ITU-R M.1461 that the I/N must not exceed −6 dB is apparently too rigid and does not take modern radar processing capabilities and operational aspects into account. The campaign actually was based on an innovative approach to investigate the actual statistics of the radar under various grades of applied interference in a worst-case coupling geometry.

2 Test set-up

2.1 Overview

To perform the measurements as described before, the test architecture comprised:

– RRP-117 primary surveillance radar in a radome located about 30 m above the top of the mountain Döbraberg at an altitude of 825 m;

– radar target generator (RTG) which was located at a height of about 35 m of a 75 m high tower on top of a mountain (Schneeberg) at 1 050 m, 29 km away from the Döbraberg position (Figs 42 and 43);

– GALILEO signal generator (GSG) with RF-power amplifier and a RHCP helical antenna precision attenuator;

– frequency monitoring car of the German Regulatory Authority (BNetzA) to check the actual frequency occupation conditions in the frequency band 1 260-1 300 MHz.

The monitoring car was initially located on the Schneeberg to avoid overload by the direct radar transmissions. However, experience showed that the car had to be relocated later to Döbraberg to observe exactly the same frequency band conditions as the radar receiver (Fig. 42). The set-up had to be modified so that the monitoring receive antenna had eventually to be on the same height as the radar antenna (protected by attenuator) because signals seen by the radar could not be seen from a lower position.

FIGURE 42

Overall geometry provided by the test set-up

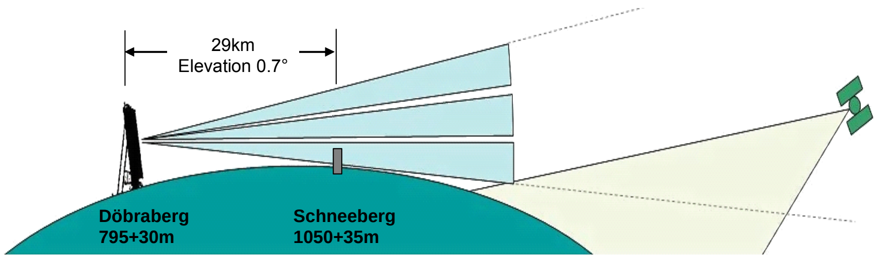

2.1.1 Geometry of the sites used

The measurement set-up comprised two sites, which offered a very good mutual optical and RF direct-line-of-sight visibility, respectively. At one site the radar system, mounted on top of a concrete tower of 30 m located on a mountain at 800 m altitude. The second site is located at a direct line-of-sight distance of about 29 km on a platform of a 75 m concrete tower, formerly used for US and NATO Electronic Countermeasures activities, on top of the mountain Schneeberg in an altitude of 1 050 m. The Schneeberg is located at an azimuth of 148° from Döbraberg. The geometry resulted in an elevation angle of 0.7° for the radar spot beam due to the distance between and the altitude of both sites (Fig. 43).

The radar site, operating as one of the German operational radars for long-range airspace surveillance, was taken out of the network for the period of measurements but remained otherwise operative.

FIGURE 43

Terrain profile of test sites to determine mutual visibility

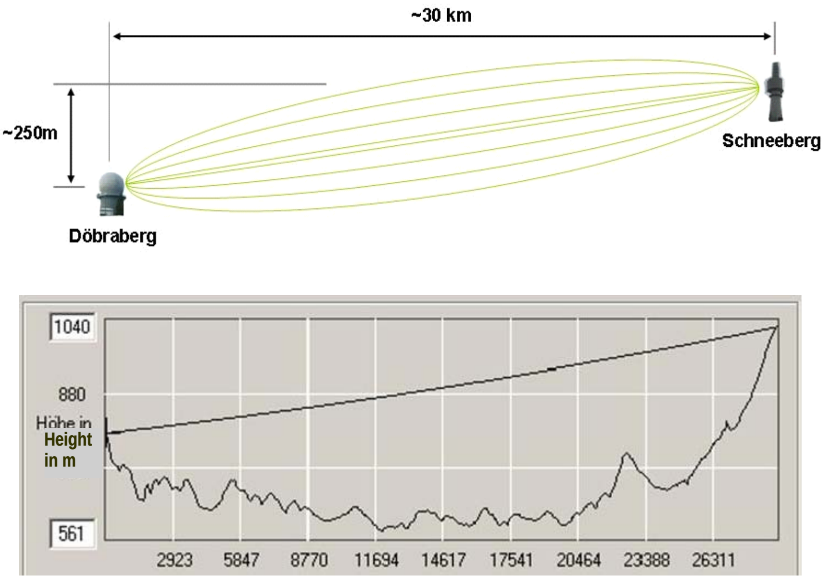

The Schneeberg site comprised a NATO certified Radar Target Simulator operated from a height of 35 m above ground by an expert operator from NAMSA. The GALILEO E6-signal generator was operated in close vicinity to the radar target simulator to ensure that both signal power, GALILEO and the radar returns, origin from the same direction, thus located in the same cell. It was shown in independent check-up that no deteriorating RF interaction between the two equipments occurred.

2.2 Characteristics of the used test equipment

2.2.1 RRP-117 – Radar

The used system, a RRP-117 (Remote Radar Post), manufactured by Lockheed-Martin Corp., is a NATO certified system operated in more than 120 sites in all six continents. Operation in this frequency band combined with the FPS families advanced pencil beam architecture including the monopulse beam control (MBC) allows for detection and tracking as well as adaptability to changing environmental conditions. The long-range radar has the capability to provide data to both air surveillance and en-route air traffic control (ATC). It comprises an air surveillance radar (ASR) and a secondary surveillance radar (SSR) as well as subsystems for simulation. It delivers complete 3D-target information in real time, correlated with SSR-data.

The combination of L-band operating frequencies with MTI/MTD processing, side-lobe nulling, and advanced CFAR processing allows the radar to detect targets in the presence of ground and weather clutter. The radar automatically adapts to and rejects land, sea, or weather clutter for maximum system performance. Velocity discrimination is also used to reject low velocity targets, such as birds.

The radar families pencil beam capability allows complete flexibility in customizing the beam patterns to optimize performance in challenging terrain and clutter applications. The pencil beam architecture offers the flexibility to “look down” from elevated sites to detect aircraft in valleys.

The used radar is of Category 5 as defined in Recommendation ITU-R M.1463 (Table 7). Note that for reasons of security, the figures provide an indication of characteristics but are not necessarily identical to the radar used. There are 100 possible operating frequencies (bandwidth 15 MHz each), which are restricted used by eight radar sites within Germany.

The radar delivers 3D-target information in realtime, correlated with data from the integrated Secondary Radar System with an antenna mounted on top of the primary radar as shown in Fig. H-3. The surveillance volume is divided into two sub ranges: a short range (SR) of 5 to 80 nautical miles and a long range (LR) of 80 to 250 nautical miles and a height range of 0 to 100 000 feet. The coverage zone is achieved by rotation at a speed of six revolutions per minute. A phased array creates pencil beams that can be electrically controlled to generate a variety of scan patterns also called templates, but only one of those was used during this campaign.

The radar operation starts for each cell with the receiver determination of the actual background noise before the transmission is activated. This provides a reference for the instantaneous noise floor in that particular direction. After processing the returns, the next cell of the template is treated the same way. Each azimuth section is scanned non-sequenced. Without restriction, it can be concluded that the resulting range measurements derived at one position have no cross-impact on the measurements in the next cell. This also means that the radar adapts to a variety of noise conditions present at the time of range measurements. It is also important to note that the IF-bandwidth of the radar receiver is less than about 3.5 MHz, which corresponds to a significant filter effect for the 40 MHz-wide GALILEO E6-signal.

TABLE 7

Typical radar performance characteristics (System 5 – i.a.w. Rec. ITU-R M.1463)

Parameter	System 5	Units
Peak power into antenna	73.9	dBm
Frequency range	1 215-1 400	MHz
Pulse duration	2 ea 51.2 or 2 ea 409.6	μs
Pulse repetition rate	240-748	pps
Chirp bandwidth for frequency modulated (chirped) pulses	1.25	MHz
Phase-coded sub-pulse width	Not applicable	μs
Compression ratio	64:1 and 256:1	
RF emission bandwidth (3 dB)	0.625 or 1.25	MHz
Output device	Transistor	
Antenna type	Planar array with elev. beam steering	
Antenna polarization	Horizontal	
Antenna maximum gain	38.5	dBi
Antenna elevation beamwidth	2	degrees
Antenna azimuthal beamwidth	2.2	degrees
Antenna horizontal scan characteristics	5	rpm
Antenna vertical scan characteristics	−6 to +20	Degrees
Receiver IF bandwidth	1.25 and 0.625	MHz
Receiver noise figure	2.6	dB
Platform type	Fixed terrestrial	
Percentage of time system operates	100	%

2.2.1.1 Determination of the optimum bore sight pointing of the radar antenna

To determine the configuration where the antenna points directly towards the radiated GALILEO signal and the test target the radar was turned into receive mode and the antenna manually precisely pointed towards the GALILEO transmit antenna on the Schneeberg determining an azimuth of 148°. By means of the high-power sine-carrier option of the signal generator, it was possible to achieve a radar strobe on the screen. With normal power condition this never occurred unintentionally.

The maximum signal power was determined at a test point of the receiver input after the LNAs. Figure 44 shows the access point for the installation of a spectrum analyser into the receiver section (PE Cab) of the radar. Couplers had to be implemented in all channels to overcome phase distortion, which was immediately detected by the radar processor.

By means of software setting and fixing of the actual beam position, also the maximum receiver power level could be determined at an elevation angle of 0.7 degrees.

FIGURE 44

RRP-117 radar antenna with secondary surveillance radar-antenna on top

FIGURE 45

Accessing the receiver input in radar's PE cabinet

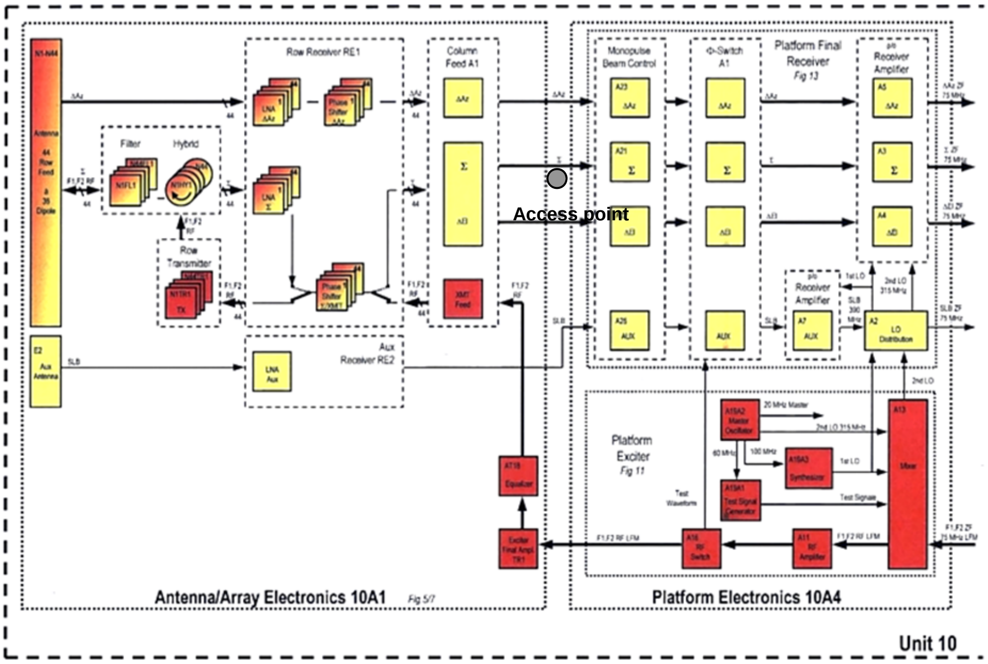

The radar provides all information on the actual measurements on displays and as data streams, which are recorded as raw data for off-line evaluation. Figure 46 shows a depiction of the radar console display with different targets types visible. Target returns from primary and secondary radars are both on screen, each marked to show their different origins.

During the measurement the simulated test target was centred to the display so that counting of detections after each scan period could easily be noticed and recorded.

The red line shown in Fig. 46, so-called jam-strobe, indicates in normal operation an RF source that is not interpreted as a target. At a given input power level, RF signals are not recognized as targets but either as unintentional interferer or as jammer in case of intentional interference. This feature allowed identifying the GALILEO signal azimuth in the figure when the generator was set to a signal more than 33 dB above nominal. GALILEO creates no jam strobe under nominal operation conditions.

FIGURE 46

Radar moving target indicator display showing range and altitude of targets with jam strobe

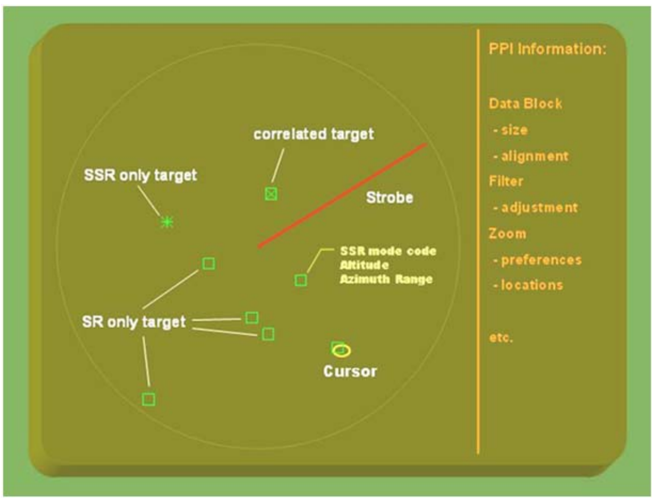

2.2.2 Characteristics of the radar target generator

The used radar target simulator is NATO certified equipment that can create virtual targets at any point between a few and more than 250 nautical miles. It is a new device, manufactured by Intersoft Electronics (IE) in The Netherlands.

The principal diagram on the options for equipment and set-up configuration is shown Fig. 47. The equipment receives radar signals with accurate interpretation and responds with a delayed and modified transmit signal in accordance with returns expected by the radar processor. In other words, for the radar under test, the artificial target appears as a real target.

Hence, the power conditions are representative and calculated as follows:

$$\boxed{\mathrm{delay}_{RTG} = \left(R_{Target} - R_{RTG}\right)\cdot\frac{2}{c}} : \text{c=299.792km/s - velocity of light}$$

$$\boxed{\mathrm{pathloss} = \frac{P_{RX}}{P_{TX}} = \frac{G^2\cdot\sigma\cdot\lambda^2}{(4\pi)^3\cdot R^4}} : \begin{array}{l}\sigma \text{ - radar cross section}\\ \text{G - gain of the radar}\end{array}$$

$$\boxed{\mathrm{pathloss}_{RTG} = \frac{P_{RX}}{P_{TX}} = \frac{G\cdot g\cdot\sigma\cdot\lambda^2}{(4\pi)^2\cdot R^2}} : \text{g - gain ot the RTG antenna}$$

The setting at the RTG conformed to these calculations and displayed the settings as shown in Fig. 47.

FIGURE 47

Simulation parameters to define the radar target

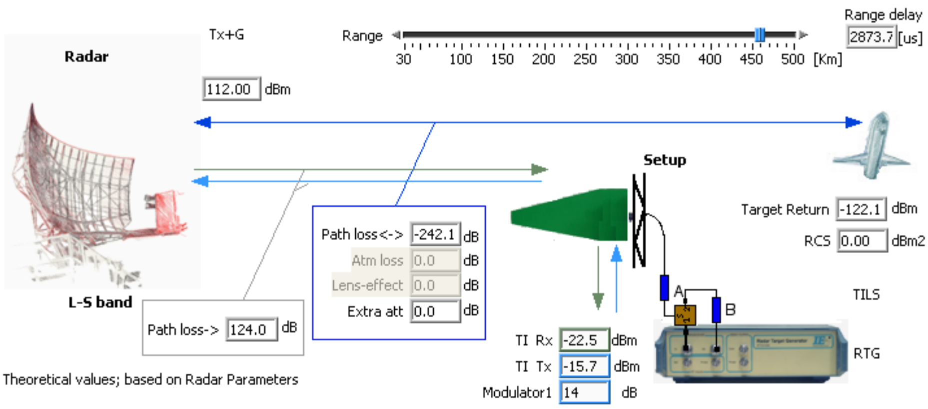

2.2.3 Characteristics of the GALILEO E6-signal generator

The dedicated signal generator unit created a representative GALILEO E6-signal with a spectral behaviour in accordance with the GALILEO SIS-ICD. The connected laptop created a pseudo-random bit stream to simulate navigation data message to ensure a most representative (noise-like) shape of the GALILEO signal.

The mathematical definition of the GALILEO E6-RNSS signal is as follows:

$$s_{E6}(t) = \frac{1}{3}\left\{\left[\sqrt{2}\cdot e_{E6-B}(t) - \sqrt{2}\cdot e_{E6-C}(t)\right] + j\cdot\left[2\cdot e_{E6-A}(t) + e_{E6-A}(t)\cdot e_{E6-B}(t)\cdot e_{E6-C}(t)\right]\right\}$$

forming a complex multiplex signal comprising three components as shown in Fig. 49 and a vector state diagram as shown in Fig. 48. The implementation of the signal is shown in Fig. 49 and the spectral shape in Fig. 50.

FIGURE 48

Phase state vector diagram of the E6-signal

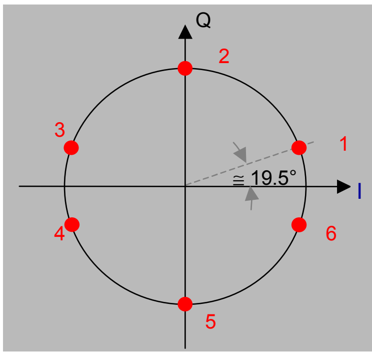

Phase-State	Exact I-Q-Values
1	$\left(2\cdot\sqrt{2} + j\right)/3$
2	j
3	$\left(-2\cdot\sqrt{2} + j\right)/3$
4	$\left(-2\cdot\sqrt{2} - j\right)/3$
5	–j
6	$\left(2\cdot\sqrt{2} - j\right)/3$

FIGURE 49

Synthesis of the simulated E6-signal

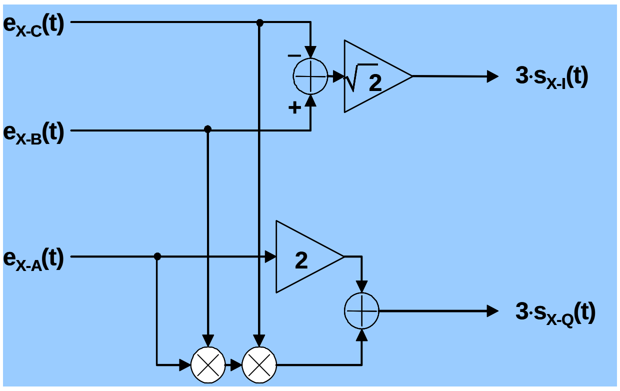

TABLE 8

Characteristics of the GALILEO E6-signal (SIS-ICD, European Commission)

Gal-E6 signal parameter	**Value**		
Carrier frequency	1 278.75 MHz		
Bandwidth	40 MHz		
Polarization	RHCP		
Pulse shape	Rectangular		
Multiplex scheme	Interplex		
Signal component	**E6-A**	**E6-B**	**E6-C**
Positioning service name (GALILEO)	PRS (G/Nav)	CS (C/Nav)	Pilot
Modulation	$BOC_{cos}(10,5)$	BPSK(5)	BPSK(5)
Chip rate (Mc/s)	5.115	5.115	5.115
Code length (chips)	Very long, non-periodic DS	5 115	511 500
Power share of signal component	4/9	2/9	2/9
Data content	PRS data	CS data	No data
Encryption	Yes	Yes	–
Data rate (symbol/s)	xx	1 000	–

FIGURE 50

Generated E6-signal with and without the external linear amplifier

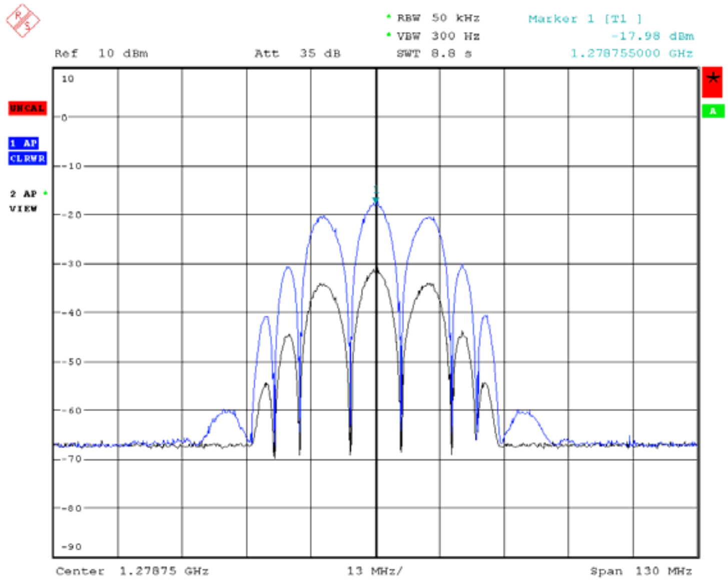

The signal generator provides a GALILEO E6-signal in accordance with the latest updates of the SIS-Interface Control Document published by the European Commission.

Further features were added to comply with two alternatives initially defined for the test architecture. The option of direct signal injection into the radar receiver was suspended in favour of the "over-the-air"-option. The composition of the E6-signal as such is not affected, but the way the signal is applied to the test set-up. For the case of over-the-air transmission from Schneeberg, a driver amplifier was added to provide sufficient power gain for an external linear power amplifier (14 dB). This was necessary to provide the required dynamic range of power variation. Gain and linearity of the external SSPA can be seen in the upper (blue) curve in Fig. 50.

FIGURE 51

Block diagram of the modified signal generator unit (Astrium Type: SGU)

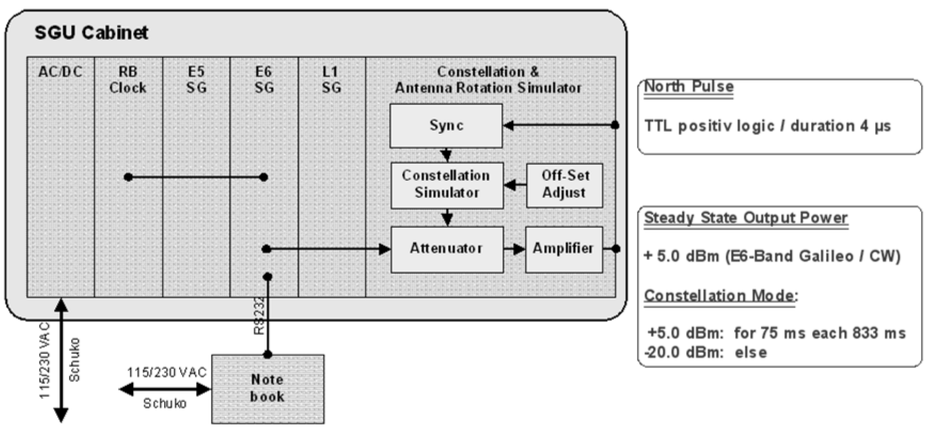

TABLE 9

Characteristics of the actually simulated E6-signal

Component	Modulation	Code	Period	Data	Shared pwr
E6A	BOCc(10,5)	Random code	100 ms	none	4/9
E6B	BPSK(5)	Truncated Gold code with 5 115 chips length	1 ms	Random data	2/9
E6C	BPSK(5)	Tiered code 10 230 × 50	100 ms	none	2/9
Product sig	–	–	–	none	1/9

To cope with the option of direct signal injection into the radar receiver, a special constellation simulator is added. Thus, the signal generator can operate in two modes:

– normal operation providing a permanent output signal at a set output power level;

– intermittent operation reacting to an external synchronization (not used in this campaign).

2.2.3.1 Normal operation of signal generator

The mode provides a constant E6-signal in line with the SIS-ICD. The output level can precisely be set to any levels of RF-power. With the added precision attenuator, stepping in minimum 1 dB steps over ±30 dB of RF-power range can be set.

2.2.4 Frequency monitoring car

The monitoring car for the surveillance of actual frequency occupation of the BNetzA is normally used for observations and measuring of transmit stations licence conditions and, in cases of interference objections, mitigation. It is therefore fully equipped with calibrated antennas in all frequency bands and the associated monitoring and processing equipment.

The integrated 10 m tower provides all means for observation, although the first location on top of the Schneeberg was assumed sufficient to detect any activity on the frequency band considering the very high mountain top and its free view in all directions. It also intended to protect the spectrum analyser from high-power radar signals.

2.2.5 Calibration of the GALILEO-E6 nominal receive power level

The GALILEO E6-signal is defined to provide a nominal power of −122 dBm at the output of a 0 dBi RHCP antenna located on the surface of the Earth at an elevation angle of greater than 10° (see Fig. H-9). The GALILEO satellites transmit the RNSS signals as shown in through an antenna with iso-flux characteristics radiating an e.i.r.p. as:

$$\delta EIRP_{nom}(\theta) = \begin{cases} 20\log_{10}\left(1.2701\cdot\cos(\theta) - \sqrt{0.0729 - 1.6131\cdot\sin^2(\theta)}\right) & [\mathrm{dB}] \quad \text{for} \quad 0° \le \theta \le 12° \\ 1.55 - 0.5326\cdot(\theta[°] - 12°) & [\mathrm{dB}] \quad \text{for} \quad 12° < \theta \le 15° \end{cases}$$

$$EIRP_{nom,E6}(\theta)\,[dB] = 30\,dBW \quad + \quad \delta EIRP_{nom}(\theta)\,[dB]$$

Thus, a 0 dBi-RHCP-receive antenna located at any point on the surface of the Earth within the coverage area of one satellite will experience this power level. A set-up as shown in Fig. 52 was implemented to expose the radar antenna with exactly this power level. A calibrated 0 dBi-linear vertically polarized antenna with a calibrated length of coax cable was installed in front of the radome on a catwalk. The fine orientation of the antenna was performed by heading towards the high power signal (34 dB above nominal) generated by the signal generator on the Schneeberg.

FIGURE 52

Minimum receiver power including typical atmospheric losses

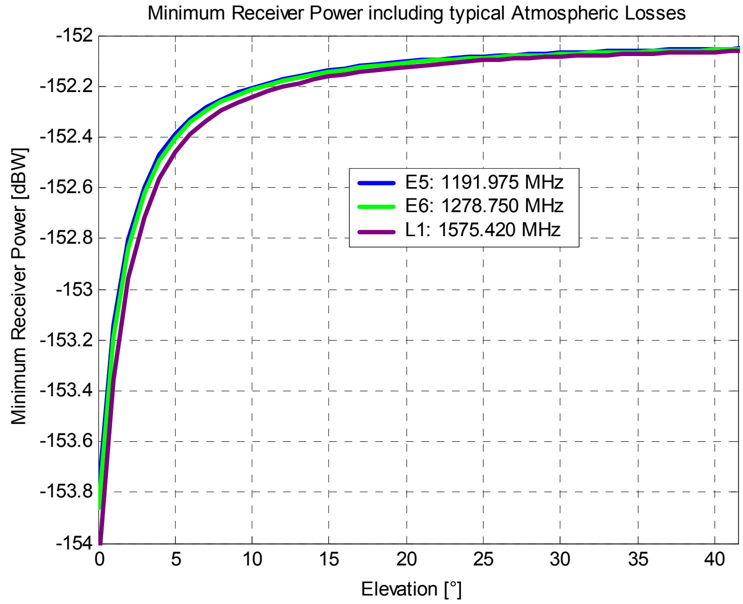

FIGURE 53

Determination of the nominal signal reference level for the GALILEO signal

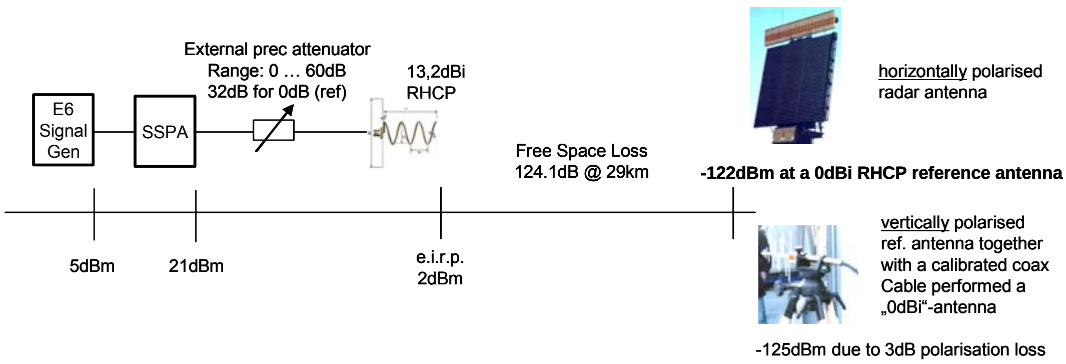

The link conditions are shown in Fig. 54.The calibration process was repeatedly performed over the campaign to verify the stability of the values. It was found to be within ±1 dB due to weather conditions, set-up, and measurement tolerances. Further measurements from inside the radome proved the transparency of the radome material at the given frequency. The measurements also included to determine already the equivalent injection level for the GALILEO signal into the radar receiver.

FIGURE 54

Receive CW-carrier signal at a 0 dBi antenna at 34 dB above nominal

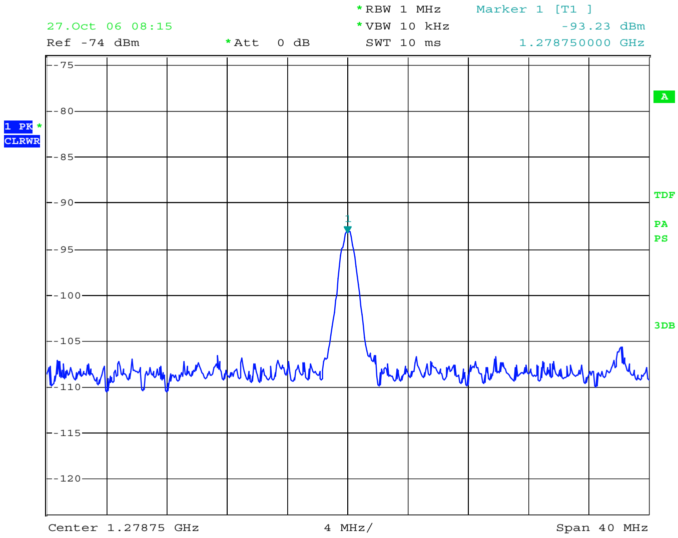

In a first step to determine the link conditions the signal generator was set to produce an unmodulated carrier at high output power enabling to optimize the pointing accuracy of transmitter and receiver antennas at both sites. The value of absolute received power was determined with a spectrum analyser.

In a second step the transmit power was reduced by means of a precision attenuator until the −122 dBm condition in front of the radar antenna was achieved. By switching the attenuator, the signal power could precisely be set in steps of 1 dB over a wide range of ±30 dB. After calibration and verification of the link conditions, the generator was switched to modulate the carrier with the E6-components producing the same RF-power but then over a total bandwidth of 40 MHz.

The verification of all equipments and facilities that was repeated frequently comprised:

– verification of nominal radar conditions (to avoid trends and adaptive noise compensation processes in the radar);
– verification of signal generator;
– verification of target simulator;
– verification of monitoring equipment.

Verification of the set-up comprised:

– potential interference analysis of the frequency band 1 260-1 300 MHz;
– determination of the nominal E6-signal power at the radar antenna;
– verification of the artificial radar targets.

FIGURE 55

Transmission of the GALILEO E6-signal from Schneeberg

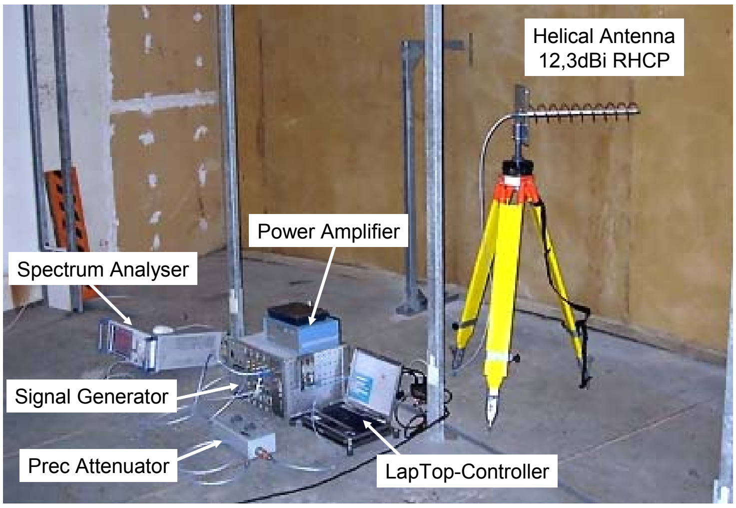

3 Test results

Each measured sequence was named as a “take”. Due to the statistical nature of the P_D the measurement periods (“takes”) had to be of a minimum length to achieve statistically relevant information. Considering the duration of a scan period and the need for many scans the measurement periods were determined as 300 scans (50 min) for low interference power values of −9 dB and −6 dB and 500 scans (85 min) for all values above stepping in 3 dB steps.

Since the radar processor adapts to the noise conditions it was agreed to reset the radar prior to each measurement to avoid influence from one to the next measurement. Each take was time-synchronized with all sites to produce recordings of raw data with time stamps to enable off-line analysis by reproducing conditions of all equipments engaged. Each take comprised a sequence of events as shown in Table 10 and produced one value for P_D.

TABLE 10

Sequence of events for each take

Step	Radar	RTG	Gal-E6	Band condx	Recording	Remarks
1	Reset	Stand-by	Off	Alert	Open files	Prepare
2	Normal Op	Verify xx NM	Off	Open file	Stand-by	Verify Ref P_D
3	Normal Op	Verify xx NM	Set 0 dB + x	Monitor	Recording	Measurement
4	Stop radar	Verify xx NM	Off	Safe file	Safe file	Pause and log

The result of the compatibility measurements performed with the campaign is shown in Table 11.

TABLE 11

Test results by "takes"

Take No.	**Test case**	**E6 ref level/ Att-setting**	**No. of scans**	P_D	**Remarks**
00-v1	max distance/1 m^2	No signal	500	99.0%	Determination of radar reference P_D
01-v2	max distance/1 m^2	−9 dB	300	99.6%	Test had to be repeated due to signals on the frequency (v2 was ok)
02-v2	max distance/1 m^2	−6 dB	300	99.6%	Test had to be repeated due to signals on the frequency (v2 was ok)
03-v1	max distance/1 m^2	−3 dB	500	93.5%	
04-v1	max distance/1 m^2	0 dB	500	74.8%	**25.2% degradation**
05-v2	max distance/1 m^2	3 dB	500	68.0%	Repeated because of critical values
06-v1	max distance/1 m^2	6 dB	300	X	P_D drops dramatically

However, for a better comprehension of the results the conditions under which this behaviour may occur are repeated as follows:

The shown impact on radar performance can only occur under worst-case conditions, i.e. when:

1) the target is at the maximum instrumented distance of the radar;

2) the target has a radar cross section of 1 m^2 (e.g. size of a Cessna);

3) the target is in direct line of view with the GALILEO "satellite";

4) interference from other sources (transmissions from other radars, other services) is not present;

5) one satellite is in view. (*Note: due to the constellation geometry only one GALILEO satellite at any time can be in view of the instantaneous radar beam. See § 2.2.*)

However, this worst-case condition can only occur in a maximum 0.2% of time – equivalent to 173 sec per 24 h day as shown in § 6.3.

Up to a maximum of six satellites is visible in the radar's 360° azimuth scan. This worst-case scenario only applies in the cells were these satellites dwell. Any other of the 3 000 cells is not affected.

FIGURE 56

Detection probability probability of detection vs. GALILEO E6 signal power level

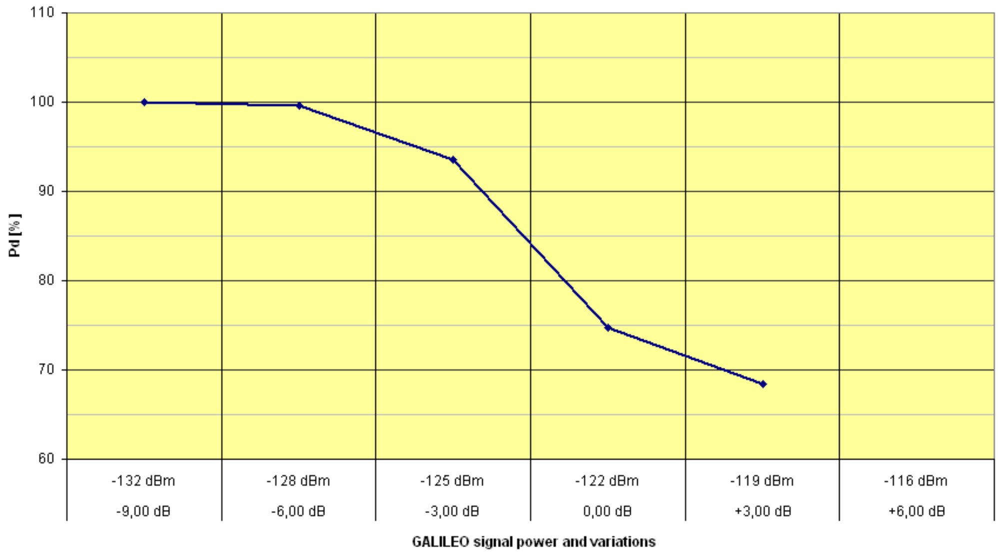

It is also important to note that the conditions at any other geometrical point or moment in time are significantly better than under the shown worst-case conditions, where all above noted conditions must occur simultaneously before the impact will operationally be perceived. Taking even the simplified radar antenna diagrams in Figs 1 and 2 (for example) into account, it can be seen that the radar antenna gain outside bore sight drops by at least 25 dB. It can be seen in the diagram of Fig. 56 that a drop in the interfering RNSS-signal of 6 dB will already return the P_D to 100%.

As shown before, the measured worst-case conditions can only occur for a few seconds, aggregating to a total of 173 seconds over an entire 24 h day.

4 Conclusion

This Report provides the results from a measurement campaign investigating the RF compatibility of a typical primary surveillance radar in the RDS and the transmissions of the GALILEO E6-signal in the RNSS in the frequency band 1 260-1 300 MHz. The radar used is considered representative for more than 120 similar installations worldwide.

The World Radiocommunication Conference (WRC-2000) resolved to allocate RNSS on a co-primary basis to the frequency band 1 260-1 300 MHz. Resolution **608 (WRC-03)** resolved on equal access conditions for all systems in the RNSS allocation between 1 215-1 300 MHz. Resolution 608 provides "*that no constraints in addition to those in place prior to WRC-2000* (...) *shall be placed on the use of RNSS* (*space-to-Earth*) *frequency assignments in the frequency band 1 215-1 260 MHz brought into use until 2 June 2000*". Recommendation ITU-R M.1461 provides a methodology of determining the RF-interference by using an *I*/*N* criterion. For the group of surveillance radars in the frequency band Recommendation ITU-R M.1463 recommends an *I*/*N* ratio of better than −6 dB to protect radar receiver. This value is considered too formalistic as it does not reflect the real operational impacts on a modern radar system.

The German Regulatory Agency (BNetzA) in close cooperation with the German Federal Armed Forces, the Air Force respectively and industry performed a measurement campaign to determine the radio-frequency compatibility of the GALILEO-E6 signal with an operational military radar. The campaign group determined in line with the considerations of the ITU-R WP 8B (former 5B) discussions a model scenario that describes a representative worst-case scenario as follows:

A reference target with a radar cross-section of 1 m^2 is virtually positioned at the maximum instrumented radar range by an active radar target generator (RTG) while the RNSS-signal arrives at the specified representative RF-power level straight in line from behind the target. Test objective is to determine the P_D over statistically relevant periods under varying power level conditions.

One key objective of the campaign was to investigate more appropriate sharing criteria for the definition of "harmful" interference for the operation of radar systems, as radar systems *per se* have options to mitigate or neutralize the impact of noise like interference. It was the other main objective of the campaign to determine grade and statistics under worst-case interference conditions that take the fast growing digital signal processing capabilities of modern radar systems into account.